CALCULATION OF POTENTIAL FLOW ABOUT ARBITRARY BODIES

J. L. HESS and A. M. O. SMITH

Douglas Aircraft Company, Aircraft Division, Long Beach, California

PRINCIPAL NOTATION

A_{ij} normal component of velocity induced at the control point of the ith surface element by a unit value of source density on the jth surface element.

C_p pressure coefficient, Eq. (1.2.11).

E complete elliptic integral of the second kind.

F prescribed normal velocity on boundary surface.

I_{nm} moments of a plane quadrilateral about its centroid.

i, j subscripts denoting quantities associated with the ith and jth surface elements, respectively.

K complex two-dimensional source strength; also complete elliptic integral of the first kind.

N number of surface elements used to approximate a body surface.

$\vec{n}$ unit normal vector to a surface or surface element; as a scalar, distance normal to a surface.

P point in space where potential and velocity are evaluated.

p point on boundary surface where potential and velocity are evaluated; also static pressure.

PV denotes principal value of an integral.

q point where source is located, especially a point on the boundary surface.

R radial coordinate denoting distance from the axis of a cylindrical coordinate system.

r distance between two points in three-dimensional space, especially between a point where a source is located and a point where potential and velocity are evaluated.

r_o distance of a point from the centroid of a quadrilateral.

S denotes the boundary surface about which flow is calculated; also cascade spacing.

B

s	arc length.
T	velocity tangent to a two-dimensional body or an axisymmetric body in axisymmetric flow.
T_2	cross flow velocity component tangent to the profile curve of an axisymmetric body in the xy-plane (Fig. 4).
T_3	circumferential cross flow velocity component on the body surface parallel to the y-axis in the xz-plane (Fig. 4).
V	fluid velocity.
V_{ij}	velocity induced at the control point of the ith surface element by a unit value of source density on the jth surface element.
W, w	complex two-dimensional fluid velocity.
x, y, z	Cartesian coordinates; as subscripts denote velocity components parallel to the coordinate axes; z also used as a complex variable.
α	angle of attack.
β	slope angle of a curve with respect to the positive x-axis; also an eigenvalue of the iteration matrix.
θ	circumferential or polar angle about the axis of a cylindrical coordinate system.
λ	asymptotic convergence factor of an iterative process.
ν	g/V_∞^2 where g is acceleration of gravity.
ξ, η	Cartesian coordinates in the xy-plane of a point where a source is located; η also denotes location of a free surface.
σ	surface source density.
Φ_{ij}	potential induced at the control point of the ith surface element by a unit value of source density on the jth surface element.
φ	velocity potential
∞	subscript denoting quantities associated with the onset flow.

1. INTRODUCTION

1.1 Scope

For the past ten years the authors and their colleagues at the Douglas Aircraft Company have been engaged in the development of a very general method for calculating. by means of an electronic computer, the incompressible potential flow about arbitrary body shapes.[1-8] The method utilizes a distribution of singularity over the body surface and computes this distribution as the solution of an integral equation. Specifically, a source density distribution is obtained as the solution of a Fredholm integral equation of the second kind. The strength of this approach is its generality. Once potential flow is hypothesized no further simplifying assumptions need be introduced. In particular, bodies are not required to be slender, and perturbation velocities are not required to be small. The method is numerically

exact in the sense that any degree of accuracy may be obtained. Good agreement with real flow is also obtained.

The various extensions of the method that have been developed over the years have continally increased the number of flow situations that can be calculated. The principal extensions concern the geometry of the body or bodies about which the flow is to be computed. Separate routines have been constructed for two-dimensional shapes, axisymmetric shapes, and fully three-dimensional shapes. Other extensions include nonuniform flows, unsteady flows, added mass, and two-dimensional free surface effects. The process of extending the basic approach is far from complete. Current investigations include such problems as acoustic scattering, two-dimensional unsteady lift, and steady-state temperature distributions.

It is the main purpose of the present article to describe the work outlined above, rather than to review all current effort in the field. However, alternative methods, both approximate and exact, are also discussed. At least brief mention is made of all work of which the authors are aware that is based on the idea of a singularity distribution over the boundary surface, as opposed to a distribution on an infinitesimally thin lamina.

Sections 1 and 2 present the basic theory. The method of solution is described in Sections 3, 4, and 5, and is compared with other methods in Section 6. Sections 7, 8, and 9 present examples of the calculations and compare them with both theory and experiment, to exhibit the wide variety of flows to which the method has been successfully applied. Finally, extensions to other physical problems are discussed in Section 10.

1.2 Definition of Potential Flow and Its Usefulness

The problem under consideration here is that of the potential flow of an incompressible, inviscid fluid. Let $\vec{V}$ denote the fluid velocity at any point, p the fluid pressure, and ρ the constant fluid density. If the viscosity is set equal to zero and the density is taken as constant, the general Navier–Stokes equations reduce to the well-known Eulerian equation of motion

$$\frac{\partial \vec{V}}{\partial t} + (\vec{V} \cdot \text{grad})\ \vec{V} = -\frac{1}{\rho}\,\text{grad}\,p \qquad (1.2.1)$$

and the equation of continuity becomes

$$\text{div}\,(\vec{V}) = 0. \qquad (1.2.2)$$

In Eq. (1.2.1) all body forces (such as gravity) have been assumed to be conservative, and their potentials have been absorbed in the pressure. Equations (1.2.1) and (1.2.2) hold in the field of flow, that is, the region exterior (or interior) to the boundary surfaces, for example, exterior to a body immersed in the fluid. This region, the region of flow, will be denoted R' (see Fig. 1).

To these equations must be added certain boundary conditions. Attention will be restricted here to the so-called direct problem of fluid dynamics. Specifically, the locations of all boundary surfaces are assumed known, possibly as functions of time, and the normal component of fluid velocity is
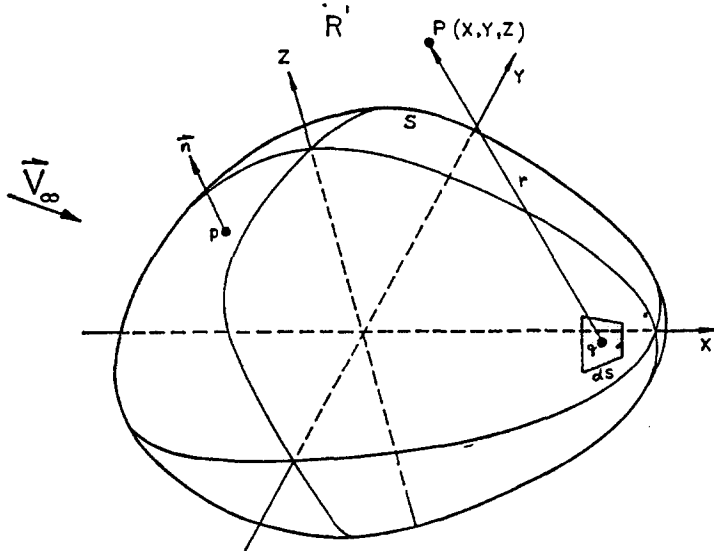

FIG. 1. Flow about a three-dimensional body surface.

prescribed on these boundaries. In the general case there may be several bodies moving with respect to each other. But the entire boundary will be denoted by S (S is thus the boundary of the region R'), and the boundary condition will be written as

$$\vec{V} \cdot \vec{n}\,|_S = F, \tag{1.2.3}$$

where $\vec{n}$ is the unit outward normal vector at a point of S, and F is a known function of position on S and possibly also a known function of time. For the exterior problem a regularity condition at infinity must also be imposed.

The above equations do not define a potential flow, which is a consequence of the condition of irrotationality. The usual procedure in deriving the equations of potential flow is to assume that the velocity field V is irrotational and that it can therefore be expressed as the negative gradient of a scalar potential function Φ. This is true of the overwhelming majority of situations to which the present method is applicable. In particular, it includes all flows that can be generated from rest by the action of conservative body forces or by the motion of the boundaries. However, a slightly

more general class of flows will be considered here. The velocity field $\vec{V}$ is expressed as the sum of two velocities:

$$\vec{V} = \vec{V}_\infty + \vec{v}. \tag{1.2.4}$$

The vector $\vec{V}_\infty$ is the velocity of the onset flow, which is defined as the velocity field that would exist in the fluid if all boundaries ceased to exist or—what is the same thing—if all boundaries became simply transparent with regard to fluid motion. The vector $\vec{v}$ is the disturbance velocity field due to the boundaries. The velocity $\vec{v}$ is assumed to be irrotational, but $\vec{V}_\infty$ is not so restricted. Accordingly, $\vec{v}$ may be expressed as the negative gradient of a potential function φ, that is,

$$\vec{v} = -\operatorname{grad}\varphi. \tag{1.2.5}$$

Since $\vec{V}_\infty$ is the velocity of an incompressible flow, it satisfies Eq. (1.2.2), and thus $\vec{v}$ does also; that is,

$$\operatorname{div}(\vec{v}) = 0. \tag{1.2.6}$$

Using $\vec{v}$ from (1.2.5) in (1.2.6) then gives the expected result: the potential φ satisfies Laplace's equation,

$$\nabla^2\varphi = 0 \tag{1.2.7}$$

in the region R'. The boundary conditions on φ arise from (1.2.3), (1.2.4), and (1.2.5) in the form

$$\operatorname{grad}\varphi \cdot \vec{n}|_S = \frac{\partial\varphi}{\partial n}\bigg|_S = \vec{V}_\infty \cdot \vec{n}|_S - F. \tag{1.2.8}$$

In the usual exterior problem the regularity condition is

$$|\operatorname{grad}\varphi| \to 0 \tag{1.2.9}$$

at infinity. Certain special cases may also arise. Equations (1.2.7), (1.2.8), and (1.2.9) comprise a well-set problem for the potential φ, and it is this problem that the method of this article is designed to solve.

The onset flow $\vec{V}_\infty$ must be such that the disturbance velocity $\vec{v}$ is a potential flow. In the usual case, when $\vec{V}_\infty$ is also a potential flow, this condition is obviously satisfied. It is also satisfied in a small number of other cases, for example, that of a two-dimensional flow whose onset flow is a uniform shear. Here $\vec{V}_\infty$ has a constant vorticity, and the shifting of the streamlines due to

the presence of the boundaries cannot cause a change of vorticity at any point of the field.

The essential simplicity of potential flow derives from the fact that the velocity field is determined by the equation of continuity (1.2.6) and the condition of irrotationality (1.2.5). Thus the equation of motion (1.2.1) is not used, and the velocity may be determined independently of the pressure. Also the time, t, enters only as a parameter in (1.2.8); therefore the instantaneous velocity is obtained from the instantaneous boundary condition; that is, all problems are essentially steady with respect to determination of the velocity. Once the velocity field is known, the pressure is calculated from (1.2.1). The only cases of interest are those for which (1.2.1) can be integrated to give one of the forms of the Bernoulli equation. When $\vec{V}_\infty$ is a potential flow, so that the combined velocity field is $\vec{V} = -\,\mathrm{grad}\,\Phi$, then (1.2.1) integrates to

$$\frac{p}{\rho} = P(t) - \tfrac{1}{2}|\vec{V}|^2 + \frac{\partial \Phi}{\partial t}, \qquad (1.2.10)$$

where $P(t)$ is independent of position in the field. In most applications the flow is steady, and the onset flow is a uniform stream, that is, $\vec{V}_\infty$ is a constant vector. Under these circumstances (1.2.10) can be written in terms of the pressure coefficient C_p as

$$C_p = \frac{p - p_\infty}{\tfrac{1}{2}\rho|\vec{V}_\infty|^2} = 1 - \frac{|\vec{V}|^2}{|\vec{V}_\infty|^2}, \qquad (1.2.11)$$

where p_∞ is the pressure at infinity. For other situations, for example, cases of rotating coordinate axes and steady flows with vorticity, other expressions are used to calculate the pressure.[9]

The problem defined by (1.2.7), (1.2.8), and (1.2.9) is seen to be a classic Neumann problem of potential theory. But the fluid-dynamics problem has certain special features that distinguish it from the fully general Neumann problem. These features greatly influenced the development of the method of solution described in subsequent chapters. In particular, the usual problem is the exterior one, so that the domain of the unknown φ is infinite in extent; but often the solution is of interest only on the boundaries. Also, usually only a few onset flows and surface conditions are of interest, so that the ordinary problem consists of the same boundary conditions for a variety of boundary shapes, as opposed to a variety of boundary conditions for the same boundary shape.

The above formulation is quite general, including as it does cases of unsteady nonuniform onset flows, ensembles of bodies with nonrigid surfaces moving with respect to each other, internal flows, and area suction on the

boundaries. Nevertheless, certain classes of potential-flow problems are excluded. The most important exceptions are problems for which the location of part of the boundary is unknown. Examples are the so-called inverse problem of fluid dynamics, in which it is desired to calculate the shape of a boundary having a given surface velocity distribution, and the problem of a steady three-dimensional lifting body, which has a trailing-vortex wake of unknown position. The method of solution described in this article can attack such problems only by repeated application using assumed boundary locations at each stage. Problems with distributed sources in the flow field lead to Poisson's equation rather than to Laplace's, and the present method is not well adapted to such problems except when particular solutions can be determined. On the other hand, other classes of problems not included in the above formulation can be solved by extensions of the present method. These include problems whose boundary conditions are different from (1.2.8), for example, steady-state temperature distributions for which the potential itself is prescribed on the boundary, and certain fluid flows in the presence of a free surface where one of several linear boundary conditions is applied along the undisturbed position of the free surface. Energy considerations dictate the requirement that in unsteady, two-dimensional lifting cases vorticity must be shed from the trailing edge of the airfoil in question. This problem can be handled by applying the present method step-by-step in time and calculating the location of the trailing vorticity. (Two-dimensional, steady lifting cases are included in the formulations (1.2.7), (1.2.8), and (1.2.9) by the use of circulatory onset flows.) Finally, the method can be generalized to solve other simple, linear, homogeneous, elliptic partial differential equations.

Prospective users of a flow-calculation method are rarely interested in whether or not an accurate solution of an idealized problem can be obtained, but are concerned with how well the calculated flow agrees with the real flow. In the present instance, the crucial question is: under what circumstances does the neglect of viscosity and compressibility lead to usable results? This matter is discussed more fully in Section 8, where a considerable number of comparisons with experiment are given. The conclusions of that section will be anticipated here. The neglect of viscosity is justified except at points in or very near regions of catastrophic separation, for example, wakes. Local regions of separation and reattachment do not normally invalidate the calculations. On the types of bodies of interest in applications, even when catastrophic separation is present, the calculations are valid a moderate distance forward of the separation point. Neglect of compressibility is justified for all flows where the local Mach number does not exceed a value of approximately one-half. By suitably adjusting the calculations, the validity can be extended up to a local Mach number of unity. That is, the adjusted calculated flow agrees with real flow as long as there are no supersonic

regions. The above conclusions refer to calculated fluid velocity and pressure. Obviously, drag forces are never predicted correctly. The rather surprising range over which potential flow can be used to predict real flow accounts for its importance and the interest there has been in it over the years.

1.3 *Exact Analytic Solutions*

Despite the fact that Laplace's equation is one of the simplest and best known of all partial differential equations, the number of useful exact analytic solutions is quite small. The difficulty of course lies in satisfying the boundary conditions, and the direct problem of potential flow, as defined by (1.2.7), (1.2.8), and (1.2.9), can be solved analytically only for an extremely limited class of boundary surfaces S. There are also indirect solutions, which form a different set.

In axisymmetric and three-dimensional cases, the direct problem of potential flow can be solved analytically only by the technique of separation of variables. For this technique to be applicable, the boundary must be a coordinate surface of one of the special orthogonal coordinate systems for which Laplace's equation can be separated into ordinary differential equations. Separability conditions are discussed in many standard works.[10, 11] There are two kinds of separability: simple separability and the so-called "R-separability", in which the solution is assumed to be a product of functions of the individual coordinates divided by a "modulation factor" R that is a known function of the coordinates. Laplace's equation is simply separable in eleven coordinate systems, which are all specializations or limiting cases of ellipsoidal coordinates. Solutions for these systems are relatively easy to obtain and are all well known. It is quite different with the R-separable systems, of which eleven are given by Moon and Spencer.[11] Solutions for these systems are considerably more difficult to obtain. It appears that, at least for the case of axisymmetric flow, it might be possible to obtain analytic solutions for a few of the R-separable coordinate systems, for example, toroidal coordinates and bispherical coordinates. However, as far as can be determined, no such solutions have actually been calculated without the use of approximations. The only exact analytic solution of the direct problem of potential flow about a closed axisymmetric or three-dimensional body is that for the general ellipsoid and its specializations. A few other solutions that use the other coordinate surfaces of ellipsoidal coordinates are also available, for example, flow through certain apertures. A small number of axisymmetric solutions may possibly be generated in the future from R-separable coordinate systems.

In two-dimensional cases Laplace's equation is simply separable in all orthogonal coordinate systems. This technique is not commonly used, however, because in two dimensions the direct problem of potential flow (or any

problem governed by Laplace's equation) can be replaced by the problem of finding a suitable conformal transformation of the boundary. The use of this latter method has resulted in a considerable number of useful potential-flow solutions. But the limits on human ingenuity are such that these solutions comprise a quite restricted class.

There is also a fairly large number of two-dimensional and axisymmetric solutions available from indirect methods. In such approaches, first suggested by Rankine in 1871, a set of known singularities is hypothesized to exist in the fluid, usually in the presence of an onset flow. The singularities most often used are point sources, line sources, doublets, and vortices. For these, the fluid velocity and pressure at any point can easily be obtained. For two-dimensional and axisymmetric flows, the total stream function of the singularities and the onset flow may be utilized to calculate streamlines, any one of which may then be considered to be a boundary surface. A similar procedure could be followed in three dimensions, but it would be considerably more difficult, because of the absence of a simple stream function. These methods do not solve the direct problem of potential flow, because they do not begin with a prescribed boundary surface but instead accept whatever boundary results from the singularity distribution.

It is clear that the variety of boundary shapes for which the exact analytic solutions can be obtained is far too limited to be of much use in practical applications. More general procedures are required. The chief value of analytic solutions is to evaluate the accuracy of approxmiate solutions or of exact numerical methods.

1.4 *Approximate Solutions*

A distinction must be made between approximate solutions and exact numerical methods. In the latter the analytical formulation, including all equations, is exact, and numerical approximations are introduced for purposes of calculation. Examples of numerical approximations are numbers having a finite number of decimal places and integrals that are evaluated by quadrature formulas. Exact numerical methods have the property that the errors in the calculated solution can be made as small as desired, by sufficiently refining the numerical calculations. In contrast, approximate solutions introduce analytical approximations into the formulation itself and thus place a limit on the accuracy that can be obtained in a given case regardless of the numerical procedures used.

Because exact analytic solutions are scarce and exact numerical methods are generally beyond the capability of hand computation, approximate solutions have in the past received most of the attention of investigators in the field of potential flow. Many approaches have been formulated. Some are analytic in that the general solution can be written in simple closed form, and

others are numerical in that considerable computation is required to obtain the solution for each specific case. It is not the intention of this article to discuss approximate solutions at length. Thwaites[12] presents a comprehensive review. The common property of all approximate solutions is that restrictions are placed on the type of body or boundary surface about which the flow can be computed. Moreover, it is not always clear whether or not a particular approximate method is valid for a given body.

A large and well-known class of approximate solutions uses one or both of the following assumptions: (a) the body is slender, with small local surface slope; (b) the perturbation–velocity components due to the body are small with respect to the uniform stream that is the onset flow. Certain restrictions on the body are evident in the assumptions. Other restrictions arise in practice. For example, the curvature must not vary too rapidly along the surface. Many thin bodies are beyond the capability of these methods, for example, a slender missile-type body with corners and flares. Van Dyke[13] considers in detail two perturbation methods that contain several well-known procedures as special cases. He states: "Therefore no precise statements can be made as to when either of them [the two methods] can be applied."

Another type of approximate solution utilizes a distribution of singularities interior to the body surface. For example, the singularities are normally placed along the chord or camber line for two-dimensional airfoils, along the axis of symmetry for axisymmetric bodies, and in a plane for three-dimensional shapes. Various types of singularities are used, for example, sources, dipoles, vortices, etc., both discrete and distributed. The locations and general properties of the singularities are assumed, and their strengths are determined so that boundary conditions are satisfied in some sense on the body surface. In the limit of thin bodies, these methods can in many cases be shown to be equivalent to those of the previous paragraph. Methods based on interior singularity distributions are not limited to slender bodies. A prolate spheroid in a uniform stream parallel to the axis of symmetry can be exactly represented by a source distribution of linearly varying strength located along the axis of symmetry between the foci. It is nevertheless valid to term this method approximate, since general shapes cannot be exactly represented by internal singularities. The idea was first introduced by von Kármán,[14] who considered axisymmetric shapes in axisymmetric flow and represented them by a source distribution along the axis of symmetry. He states: "This [representation] is possible only in the exceptional case when the analytical continuation of the potential function, free from singularities in the space outside the body, can be extended to the axis of symmetry without encountering singular spots." Clearly, such a condition could never be guaranteed in a practical application. A slender axisymmetric ellipsoid-cylinder, which has a curvature discontinuity, would presumably not possess

this property. What degree of accuracy can be obtained in the general case is not known.

Approximate solutions are therefore unsatisfactory for two reasons. First, they are obviously inapplicable in many cases, such as two bodies in close proximity (airfoil with slat), many internal flows, annular inlets, thick or bumpy bodies, and many nonuniform flows. Second, their validity in many cases is not predictable, and the accuracy of the computed solutions is unknown. These facts lead to consideration of exact numerical methods of solution.

2. REDUCTION OF THE PROBLEM TO AN INTEGRAL EQUATION FOR A SOURCE-DENSITY DISTRIBUTION ON THE BODY SURFACE

The exact solution of the direct problem of potential flow for arbitrary boundaries can be approached in a variety of ways, all of which must finally become numerical and make use of a computing machine. The use of a finite-difference approximation of the Laplacian operator naturally suggests itself, as does the use of a form of Green's function. More efficient, however, are methods based on the reduction of the problem to an integral equation over the boundary surface. Many different integral equations can be obtained by the use of Green's theorem, and several other equations can also be derived. Some discussion of alternative methods is contained in Section 6. In this section, discussion will be restricted to the method of this article, which is based on an integral equation for a source-density distribution on the surface of the body or bodies about which the flow is being computed.

The problem considered is that defined by (1.2.7), (1.2.8), and (1.2.9). A sketch illustrating the situation for a single three-dimensional body is shown in Fig. 1. Consider a unit point source located at a point q whose Cartesian coordinates are x_q, y_q, z_q. At a point P whose coordinates are x, y, z the potential due to this source is

$$\varphi = \frac{1}{r(P,q)},\tag{2.1}$$

where $r(P, q)$ is the distance between P and q, namely,

$$r(P, q) = \sqrt{[(x - x_q)^2 + (y - y_q)^2 + (z - z_q)^2]}.\tag{2.2}$$

The designation "source" is employed in accordance with customary fluid-dynamics usage. The potential (2.1) gives rise to a velocity radially outward in all directions from the point q, and thus the point q may be thought of as the location of a "source" of fluid. However, this physical interpretation is not important to the method. It is sufficient to say that the solution is built up of elementary potentials of the form (2.1), without specifying their

nature. The potential in (2.1) satisfies (1.2.9) and satisfies (1.2.7) at all points except the point q. Because of the linearity of the problem, the potential due to any ensemble of such sources or any continuous distribution of them that lies entirely interior to or upon the boundary surface S satisfies Eq. (1.2.9) and satisfies Eq. (1.2.7) in the region R' exterior to S. Of particular interest is the potential of a continuous source distribution on the surface S. If the local intensity of the distribution is denoted by $\sigma(q)$, where the source point q now denotes a general point of the surface S (see Fig. 1), then the potential of the distribution is

$$\varphi = \oiint_S \frac{\sigma(q)}{r(P,q)} \, dS. \tag{2.3}$$

It is shown in basic works of potential theory, for example, Ref. 15, that under very general conditions the disturbance potential of a body in potential flow can indeed be represented in the form (2.3), and it is in this form that it is considered in the present method.

Regardless of the nature of the function $\sigma(q)$, the disturbance potential as given by (2.3) satisfies two of the three equations of the direct problem of potential flow. This function is determined from the requirement that the potential also must satisfy the other equation, (1.2.8), which expresses the normal-velocity boundary condition on the surface S. Applying the boundary condition (1.2.8) as well as subsequently evaluating fluid velocity on the surface, requires evaluating the limits of the spatial derivatives of (2.3) as the point P approaches a point p on the surface S. Care is required because the derivatives of $1/r(P,q)$ become singular as the surface is approached. A rigorous development of the limiting process is given by Kellogg.[15] The details will not be pursued here, but the nature of the limits of the normal and tangential derivatives of φ, that is, the normal and tangential fluid velocities, will be illustrated by an example.

Consider the two-dimensional body whose profile curve is shown in Fig. 2. The coordinate axes, x and y, have been placed in such a way that the curve is tangent to the x-axis at the origin. An integration in the z-direction can be performed that reduces the double integral of (2.3) to a single integral. Also, for illustrative purposes the source density σ is set equal to unity. The x and y velocity components at a point P located a distance h up the positive y-axis are (see Section 4.1 for a more complete discussion)

$$V_x = -\frac{\partial \varphi}{\partial x} = -2 \int \frac{x_q}{x_q^2 + (h - y_q)^2} \, ds$$

and

$$V_y = -\frac{\partial \varphi}{\partial y} = 2 \int \frac{h - y_q}{x_q^2 + (h - y_q)^2} \, ds \tag{2.4}$$

where x_q and y_q are the coordinates of a general point q on the profile curve and s denotes arc length along the profile curve. Obviously, as P approaches the surface, V_x becomes the tangential component of velocity and V_y the normal component. The integrands of (2.4) are shown in Fig. 2 for various distances h of the point P from the surface. It can be seen that as h approaches
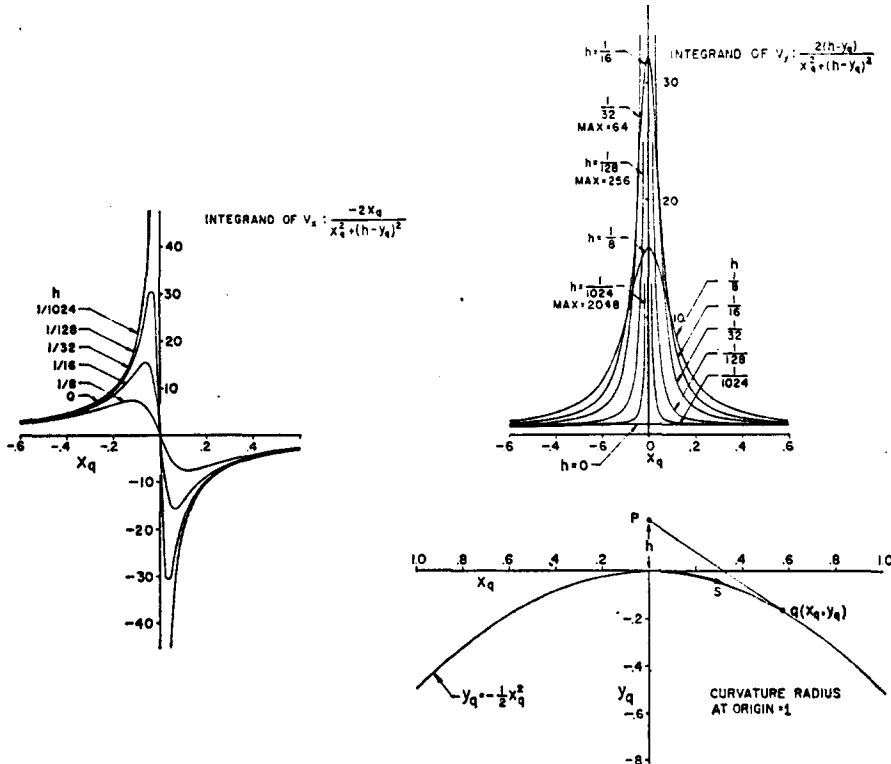

FIG. 2. Influence on the velocity components at points in space of a source density of unit strength located on a two-dimensional surface whose profile curve is a parabola having a unit value of curvature radius at the origin.

zero, the integrand of V_x approaches a function whose behavior near the origin is similar to $-1/s$; that is, the integrand becomes positively infinite for small negative s or x_q and negatively infinite for small positive s or x_q. Thus the integral for tangential velocity must be evaluated as a principal value; that is, the positive and negative infinities are allowed to "cancel out". As h approaches zero, the integrand for V_y approaches a function consisting of a Dirac delta function (an infinite value of infinitesimal width whose integral is finite) plus a function that is well behaved and whose value at the

origin is in fact finite and proportional to the local curvature of the profile curve. Thus, in the limit, the integral for normal velocity consists of a term outside the integral plus a term whose integrand is well behaved. Although the example here is two-dimensional, the conclusions are true in general. In three dimensions the integral for surface tangential velocity has a singular integrand and must be evaluated as a principal value. The normal velocity consists of a term outside the integral plus an integral that can be evaluated by ordinary means. In three dimensions the integrand in the expression for normal velocity is not finite, but it is integrable.

In accordance with the procedure presented by Kellogg,[15] the disturbance potential as given by (2.3) is differentiated, and the boundary condition (1.2.8) applied to it by allowing the point P to approach a point p on the surface S. The result is the following integral equation for the source-density distribution $\sigma(p)$:

$$2\pi\,\sigma(p) - \oint\!\!\!\oint_S \frac{\partial}{\partial n}\left(\frac{1}{r(p,q)}\right)\sigma(q)\,\mathrm{d}S = -\,\vec{n}(p)\cdot\vec{V}_\infty + F. \qquad (2.5)$$

In this equation, $\partial/\partial n$ denotes differentiation in the direction of the outward normal to the surface S at the point p, and the unit outward normal vector has been written $\vec{n}(p)$ to show explicitly its dependence on location. The solution of (2.5) is the central problem of the present method.

Equation (2.5) is a Fredholm integral equation of the second kind over the boundary surface S. The term $2\pi\,\sigma(p)$ arises from the delta function that is brought in by the limiting process of approaching the boundary surface, as illustrated by the above example. The kernel of the integral equation, $-\partial/\partial n\,[1/r(p,q)]$, is the outward normal velocity at the point p due to a unit point source at the point q. This kernel depends only on the geometry of the surface S. The specific boundary conditions, that is, onset flow, suction velocity, etc., enter (2.5) only on the right side. This fact is useful in applications, since it means that for a given body shape several different flows may be computed simultaneously.

The theory of the solution of (2.5) is discussed extensively by Kellogg,[15] and fundamental existence and uniqueness theorems are presented. The conditions under which a solution can be obtained are very general. The surface S need not be slender or analytic. In fact, for the problem of flow exterior to a given surface, S may consist of several disjoint surfaces. The right side is likewise practically unrestricted. In particular, since only $\vec{V}_\alpha$ enters (2.5), it is not absolutely essential that this velocity field be derivable from a potential function, although of course the disturbance velocity field must be a potential flow. Both $\vec{V}_\alpha$ and F may vary with position. Internal flows as well

as external may be considered. There is one restriction on (2.5). The existence proof of Ref. 15 requires that the prescribed boundary value, that is, the right side of (2.5), be a continuous function of position on the surface. Because of the presence of $\overline{n}(p)$, this means that in general the surface S must have a continuous normal vector. Thus boundaries with corners are excluded from the existence proof. In practice, however, it has been found that the present method does give correct results near convex corners, where the surface velocity is in general infinite. For concave corners the method has difficulty, especially if the corner is a stagnation point of the flow. For some onset flows or for corners of small turning angle, the calculated results are sufficiently accurate for most purposes. Other situations require the concave corner to be rounded in order to obtain an accurate solution. (In any real flow it is automatically rounded of course by the boundary layer.)

For a known boundary surface S, the kernel of (2.5) can be calculated in a straightforward manner, and the equation is a linear one for the unknown function σ. This procedure is not well suited to the solution of problems for which all or part of the boundary has an unknown location, for example, the so-called inverse problem of potential flow, in which the surface velocity distribution is prescribed but not the shape of the boundary. In such problems the kernel cannot be evaluated. If the coordinates of the boundary were considered as unknowns in the kernel, the resulting equation would be nonlinear. The only possibility of using the present method for problems having boundaries with unknown locations is to assume the locations of all boundaries, solve the resulting direct problem, and then repeat the process after adjusting the boundaries by "cut and try" until all conditions are satisfied.

For three-dimensional bodies (2.5) is a two-dimensional integral equation. For two-dimensional and axisymmetric bodies, one integration can be performed in advance, and (2.5) is thus reduced to a one-dimensional integral equation. This reduction is possible for axisymmetric bodies even if the flow itself is not axisymmetric, for example, flow at an angle of attack. This feature accounts for the efficiency of the integral-equation methods. The dimensionality of the problem is reduced by one: from three to two for three-dimensional bodies and from two to one for two-dimensional and axisymmetric bodies. Moreover, for exterior flows the domain of the function to be found is reduced from an infinite one, the exterior flow field, to a finite one, the body surface.

Equation (2.5) is an integral equation of the second kind, for which the unknown function appears outside the integral as well as inside. Some other integral-equation methods for solution of potential-flow problems lead to equations of the first kind, for which the unknown function appears only in the integral. Equations of the second kind have many advantages, both

theoretical and practical. Existence and uniqueness proofs are relatively abundant for equations of the second kind, but they are scarce for equations of the first kind. Equations of the first kind frequently occur that have either no solution or infinitely many solutions. Numerically, integral equations of the second kind are considerably more tractable. For example, if the integral equation is approximated by a set of linear algebraic equations, as it is in the present method, the presence of the term outside the integral insures that in general the diagonal entries of the resulting coefficient matrix will be much larger than any off-diagonal entries. Since an equation of the first kind lacks such a term, the diagonal entries of the approximating coefficient matrix are not necessarily larger than the other entries. This difference can be crucial numerically if iterative matrix-solution methods are used.

The two terms on the left side of (2.5) have a simple interpretation. The term $2\pi\,\sigma(p)$ is the contribution to the outward normal velocity at a point p on the boundary of the source density in the immediate neighborhood of p. The integral term represents the contribution of the source density on the remainder of the boundary surface to the outward normal velocity at p. The feeling is frequently expressed that local effects should dominate and that the integral term in (2.5) should thus be much less important than the term $2\pi\,\sigma(p)$. This situation can be true only if the particular nature of the function $\sigma(p)$ causes the integral largely to cancel itself, and it is not due to an inherent difference in size between the two terms. To illustrate the magnitude of these terms, the source density will be assumed to have a constant value of unity over the boundary surface S. The normal velocity in the direction exterior to S at a point p due to this source distribution is given by the left side of (2.5) as

$$[V_n(p)]_{\sigma=1} = 2\pi - \oiint\limits_{S} \frac{\partial}{\partial n}\left(\frac{1}{r(p,q)}\right) dS. \qquad (2.6)$$

If this expression is integrated over the entire closed surface S, the result is the total velocity flux outward from S due to the source distribution. From the definition (2.1) it can be readily shown that the total velocity flux due to a unit point source is 4π. Thus the total flux due to a unit source distribution on S is 4π times the total surface area of S. If (2.6) is integrated over S, the local contribution given by the first term on the right is obviously 2π times the total surface area of S. Thus the integral over S of the second term on the right side of (2.6) is exactly equal to that of the first term. Accordingly, for a unit source-density distribution the average over all points p of S of the local contribution to the normal velocity is identical with the average of the contribution of the remainder of the surface S. (If the normal velocity in the direction interior to S were integrated, conservation of fluid would require the result to vanish. Thus in this case the average values of the two

terms of (2.6) are equal in magnitude but of opposite sign.) The conclusion regarding the approximating matrix mentioned in the previous paragraph is that although the diagonal entries are all larger than any off-diagonal entries, the sum of all diagonal entries is approximately equal to the sum of all off-diagonal entries. Similarly, it is not necessarily true that the kernel of (2.5) is larger when q is near to p than when it is relatively far away. For example, on a two-dimensional circular cylinder the kernel is constant all around the circle.

There is a certain difference between the exterior flow problem and the interior flow problem. If the same closed surface is considered, the only difference between the two problems is the reversal of the outward normal direction n and thus the reversal of the sign of the integral term of (2.5). If the boundary surface is convex, the kernel of (2.5) is positive for the exterior problem and negative for the interior problem. This is evident from the physical interpretation of the kernel. For the exterior problem, the integral equation is determinative in that if the right side of (2.5) is zero, the only solution is $\sigma = 0$; that is, no nonzero source distribution gives rise to zero normal velocity everywhere on the boundary. Thus the solution of the exterior problem exists and is unique, and no difficulties are encountered in solving the equation. For the interior problem the integral equation (2.5) is indeterminative; that is, there is a source distribution, not identically zero, that gives zero normal velocity everywhere on the boundary.* Clearly such a source distribution gives zero fluid velocity everywhere within the boundary For example, a constant source density on a circular cylinder or sphere satisfies this condition. Thus a source-density distribution for the interior problem exists only if the right side of (2.5) satisfies a certain condition, and if it does exist, it is not unique. The condition required of the right side is that its integral over the boundary must vanish. This simply means that the total flux across the boundary must be due to the onset flow, for example, due to interior sources. The surface source density distribution does not contribute to the flux. This is certainly a physical requirement for flow of an incompressible fluid. If any solution σ can be found, the nonuniqueness is not physically significant, since it means only that to any solution may be added a source distribution that gives rise to no interior velocity. If the integral equation is approximated by a set of linear algebraic equations, the coefficient matrix for the interior problem is either singular or nearly singular, depending on the details of approximation. In the present method the matrix is nearly singular, and nothing unusual seems to occur in the calculations.

---

* If a set of linear algebraic equations has a non-trivial solution for a zero right side the coefficient matrix is said to be singular. Since the word singular has a different meaning for an integral equation, the word indeterminative is used here to describe this condition, and the word determinative is used to describe the opposite situation when there is no non-trivial solution for a zero right side.

c

3. THE METHOD OF SOLUTION

3.1 *General Remarks*

The method chosen for the numerical solution of the integral equation
(2.5) was dictated, to a considerable extent, by the fact that the boundary
surface S, which is the domain of integration, is completely arbitrary. In
particular, this means that the integration must be performed numerically
rather than analytically. The result is that methods that approximate the
kernel or the unknown function by a series of suitably chosen functions are
not very attractive. Two approaches present themselves. The equation may
be attacked directly as an integral equation by using an iterative procedure
appropriate for Fredholm integral equations. Alternatively, the integral
equation may be approximated by a set of linear algebraic equations, which
are solved by any of the usual techniques. Although the two approaches differ
conceptually, in practice the distinction is rather obscure. In the former,
the integral is evaluated by some form of approximate quadrature, and the
process is iterated. In the latter, an approximate quadrature is used to
obtain a set of linear equations, which may then be solved by iteration. It
is possible to construct examples for which the two approaches lead to
identical sequences of numerical operations. For either approach an approxi-
mate integration procedure must be selected from among the large number of
available quadrature formulas. Here again, the fact that the boundary is
arbitrary affects the situation. This surface must be approximated in some
manner for the computer, and the manner of approximating the surface is
bound up with the approximate integration procedure, as it is with the entire
method of solution.

The present method of solution was selected largely because of its con-
ceptual simplicity. It was felt that resort should be made to a complicated
method only after a simple method had proved too inaccurate or too time
consuming. Such has not been the case. Although experience has indicated
that certain modified approaches might yield improvements in speed or
accuracy, the prospective gains have so far appeared too small to justify the
effort.

The approach adopted consists of approximating (2.5) by a set of linear
algebraic equations. This is accomplished in the following manner. The
boundary or body surface S about which the flow is to be computed is
approximated by a large number of surface elements, whose characteristic
dimensions are small compared to those of the body. Over each surface
element the value of the surface source density is assumed constant. This
reduces the problem of determining the continuous source density function σ
to that of determining a finite number of values of σ, one for each of the
surface elements. The contribution of each element to the integral in (2.5) can

be obtained by taking the constant but unknown value of σ on that element out of the integral and then performing the indicated integration of known geometric quantities over the element. Requiring (2.5) to hold at one point of the approximate body surface, that is, requiring the normal velocity to take on its prescribed value at one point, gives a linear relation between the values of σ on the elements. On each element a control point is selected where (2.5) is required to hold. This gives a number of linear equations equal to the number of unknown values of σ. The coefficient matrix consists of the normal velocities induced by the elements at each other's control points for unit values of source density. Once the linear equations have been solved, flow velocities and potential may be calculated at any point by summing the contributions of the surface elements and that of the onset flow. Usually, velocities and pressures on the body surface are of greatest interest. Because of the manner in which the solution has been effected, these must be evaluated at the control points, that is, at the same points where the normal velocity was made to assume its prescribed value.

3.2 *Approximation of the Body by Surface Elements*

The basic input to the computer program consists of the specification of (1) the body surface about which the flow is to be computed, (2) the onset flow if this is not a uniform stream, and (3) the prescribed normal velocity on the surface if this is not zero. The specifications of the last two of these are straightforward, and in most cases are not even required. Of several possible ways of specifying the body surface, the only one seriously considered consists in defining the body by means of the coordinates of a set of points distributed over the surface. Specifications of the surface that rely on analytic expressions or require surface slopes and curvatures may simplify the calculations, but such information is rarely available in practical cases. The choice of input points rests with the user of the method. They may, for example, be taken from drawings. The numerical significance of the coordinates of the input points must be sufficient to guarantee the accurate computation of surface slopes. Because the input points are used to form the approximating surface elements, their distribution and total number determine the accuracy of the resulting calculations.

Figure 3 shows the surface elements used to approximate various types of bodies. For two-dimensional and axisymmetric body shapes, only a single profile curve need be defined by input points. This curve is assumed to lie in the xy-plane, and the x-axis is always taken as the symmetry axis for axisymmetric bodies. For closed two-dimensional bodies, a complete closed curve is specified by input points, and an axisymmetric closed body is specified by input points lying on the half of the contour in the half-plane $y \geqslant 0$. These points are connected by straight-line segments, and the profile curve is

approximated by an inscribed polygon. The surface elements for two-dimensional bodies are thus thin, infinite plane strips, and those for axi-symmetric bodies are frustums of cones having small slant heights. It should be mentioned that this representation is used for axisymmetric bodies even for certain cases when the flow is not axisymmetric, but varies circumferentially in a known way, for example, the case of cross flow about an axisymmetric body in a uniform stream perpendicular to the body's symmetry axis. For such cases the subsequent calculations are different from those for the axisymmetric case, but the input is identical, and the calculations are carried out without resort to fully three-dimensional techniques. For truly three-dimensional bodies, the input points must be distributed over the entire surface. These points are associated in groups of four and used to form plane quadrilateral surface elements (see Fig. 3). The plane of the element is
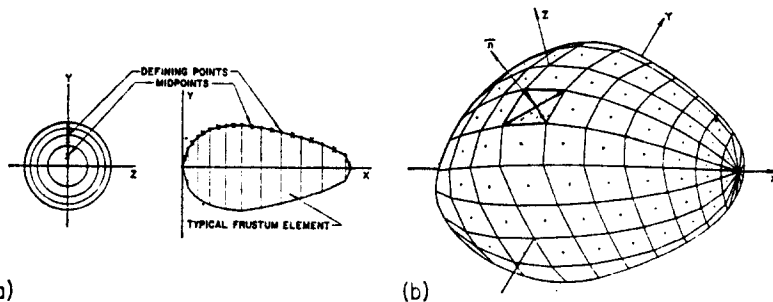
FIG. 3. Approximation of the body surface by elements. (a) Two-dimensional and axisymmetric bodies. (b) Three-dimensional bodies.

equidistant from the four input points used to form it, and its unit normal vector $\vec{n}$ is the normalized cross-product of two "tangential" vectors each of which is obtained by subtracting the coordinates of two of the four input points. The corners of the quadrilateral are projections of the four input points into the plane of the element. In forming these elements, most input points are used in the formation of four elements, so that the number of input points required is only slightly larger than the number of resulting elements. The details of the input and element-formation procedure for three-dimensional bodies are given in the report form of Ref. 3.

For all body geometries, the order in which the points defining the surface are input determines which direction is considered the "outer" normal direction and thus determines on which side of the surface the flow is computed. For example, points defining a two-dimensional or axisymmetric body are input sequentially along the profile curve, and the flow field is considered to lie to the left with respect to the direction from any input point

to the next one in the sequence. In the case of exterior flow about a single closed contour, the defining points are input in clockwise order about the contour. If an interior flow is desired, the points are input in counterclockwise order. If an exterior flow is calculated, the interior flow is normally not meaningful and vice versa. The order of the input points determines a preferred tangential direction along the profile curve. As described in Section 3.5, the sign of calculated tangential velocities indicates whether the velocity is in the direction determined by the order of the input points or in the opposite direction. The order of the input points is also used to prescribe the slope angle of the profile curve, which may be in any of the four quadrants, that is, may vary from $-\pi$ to $+\pi$. For fully three-dimensional cases, the outward normal is determined by the same principle as that used for two-dimensional cases. The procedure employed is, however, somewhat more lengthy to explain (see the report form of Ref. 3).

On each element a control point is selected at which the normal velocity boundary condition is to be satisfied. For two-dimensional and axisymmetric bodies, the control points are the midpoints of the line segments joining the input points that define the profile curve. This is the obvious choice for two-dimensional bodies and seems to be a reasonable choice for axisymmetric bodies, although there is some question. For the quadrilateral elements used to approximate three-dimensional bodies, the proper choice of the control point is not at all obvious. It seems evident that the control point for a rectangular element should be the center, but there are many possible definitions that reduce to the center for a rectangular element. On each quadrilateral element there is one point at which a constant source density on that element gives rise to no velocity in the plane of the element; that is, there is a point at which the effect of the element is entirely normal. It was decided to use this point as the control point, although subsequent results indicated that the centroid of the area of the quadrilateral is an equally good choice. These two points are not necessarily near each other if the element is not approximately rectangular.

It should be emphasized that for all body geometries the surface elements are simply devices for effecting the numerical solution of the integral equation (2.5). They essentially define integration increments and normal directions at points of the surface. In particular, the polygonal or polyhedral bodies shown in Fig. 3 have no direct physical significance. The flows eventually computed are not those about these bodies. It is only at the control points that the normal velocity assumes its prescribed value. For example, if the normal velocity is prescribed as zero, it is in general nonzero at all points of the element except the control point; that is, the element "leaks". At the edges of the elements the velocity approaches infinity because of the discontinuity of the source density and/or the discontinuity in slope, but the approach to infinity is not that associated with corner flows. The computed

flow has significance only at the control points themselves and at points off the body surface.

From the manner in which quadrilateral elements are formed in three-dimensional cases, it is evident that in general the edges of adjacent elements are not coincident; that is, there are small "openings" between the elements. In view of the discussion in the previous paragraph, this is a matter of small concern. Any errors due to this source are of higher order than, and are negligible compared to, those due to the basic approximation of the body surface by plane elements over each of which the source density is constant. The important thing is that the "width" of the openings, as measured by the distance that the four input points must be projected to put them in the plane of the element, be small compared to the dimensions of the element, and this is guaranteed by the method of element formation for any reasonable distribution of input points. The use of triangular surface elements, as suggested by Levy,[16] eliminates these openings; but this does not seem worth while, since such elements are considerably more awkward for the user. In particular, quadrilateral elements are very well suited to the frequently occurring case when points of the body surface are known only along plane curves at certain fixed values of one of the coordinates, for example, "section data". However, since a triangle is a special case of a quadrilateral, the present method can be used to generate plane triangular surface elements if desired. The required number of input points is still only slightly larger than the resulting number of elements.

The accuracy of the calculation is determined by the number and distribution of the elements used to approximate the body surface. It often turns out in practice that for satisfactory accuracy a considerably larger number of elements should be used than the number of points at which it is desired to calculate velocities and pressures. For exterior flows about simple, smooth axisymmetric bodies and about nonlifting two-dimensional bodies, 60 to 80 elements are usually sufficient. Lifting two-dimensional airfoils require more elements—100 or more, depending on the shape. Complicated surfaces, multiple bodies, and many internal flows may need more than 200 elements in two-dimensional and axisymmetric cases. Three-dimensional bodies of course require considerably larger numbers of elements. Only the simplest shapes can be calculated with less than 200 elements. In practical applications, useful results have been obtained for fairly complicated shapes—including multiple bodies—with numbers of elements between 500 and 1000. Because of the input required, the long computing times, and the machine storage limits, most users accept lesser accuracies in three-dimensional cases than in two-dimensional or axisymmetric cases.

The proper distribution of elements over the body surface is largely a matter of intuition and experience. Anyone familiar with the general properties of low-speed flow can immediately formulate a fairly good distribution

for the large majority of body shapes. A small amount of experimentation is sufficient to give such a person considerable additional "feel" for the proper distribution. Elements should be concentrated in regions where the body geometry—slope or curvature—changes rapidly with position, or where the flow properties, particularly the source density, are expected· to vary rapidly. For example, elements should be concentrated in all high-curvature regions, near exterior corners (especially the trailing edge of an airfoil), and—in cases of two bodies near each other—along the portions of their surfaces that face each other. Elements should not be concentrated near unrounded concave corners; but if the corner is extreme enough to require rounding, a very great concentration of elements is necessary in that region. In regions where neither the geometric properties of the body nor the flow properties vary rapidly with position, elements may be distributed more sparsely. It should be remarked that if several small elements are in the vicinity of a large one, the accuracy is that associated with the large element. The foregoing is therefore an inefficient distribution, since no additional accuracy results from the additional number of small elements. The size of elements should change gradually between regions of concentration and regions where the distribution is sparse. The characteristic dimensions of an element should usually be no more than 50 per cent greater than those of adjacent elements.

There is one special device that can be used only for two-dimensional cases. If there are two body contours that can be obtained from each other by an analytically known conformal transformation, then the potential flow about one body can be calculated analytically from the potential flow about the other. Therefore it is possible to obtain increased computational speed and accuracy by means of a prior adjustment of the body shape. A very complicated shape can often be transformed by a simple conformal mapping into a smooth shape, for which the flow can be accurately calculated with a comparatively small number of elements. In particular, it is easy to find transformations that remove all corners. For any body a number of such transformations are possible.

3.3 The Effects of the Elements at Each Other's Control ·Points. Matrices of Influence Coefficients

3.3.1 General remarks. Once the body surface has been approximated by elements of the appropriate type, the elements are ordered sequentially and numbered from 1 to N, where N is the total number of elements. The exact order of the sequence is immaterial. It is simply a logical device for keeping track of the elements during the computational procedure. Reference will accordingly be made to the ith element and the jth element, where the integers i and j denote the positions of the elements in the sequence.

Assume for the moment that the surface source density on the jth element

has the constant value of unity. Denote by Φ_{ij} and $\vec{V}_{ij}$ the potential and velocity, respectively, that are induced at the control point of the ith element by a unit source density on the jth element. The formulas for the induced potential and velocity form the basis of the present method of flow calculation. They are obtained by integrating over the element in question the formulas for the potential and velocity induced by a unit point source and thus depend on the location of the point at which the potential and velocity are being evaluated and also on the geometry of the element. Since there is no restriction on the location of the control point of the ith element with respect to the jth element, the formulas for Φ_{ij} and $\vec{V}_{ij}$ are those for the potential and velocity induced by an element at an arbitrary point in space. The dependence of the formulas on the geometry of the element means that there are three distinct sets of formulas for Φ_{ij} and $\vec{V}_{ij}$, corresponding to the three different types of elements that are appropriate for use with two-dimensional bodies, axisymmetric bodies, and fully three-dimensional bodies, respectively. The axisymmetric case is further subdivided into the case where the flow is also axisymmetric and the case where the flow is not axisymmetric but has a known variation with circumferential position, for example, the so-called cross flow over an axisymmetric body. Specific formulas for the potential and velocity induced by an element are given in Section 4 for the various body geometries. This section describes their general nature and use.

3.3.2 *Three-dimensional flow.* For the plane quadrilateral elements used to approximate three-dimensional bodies, the unit-point-source formulas for potential and velocity can be integrated analytically over an element. This is most conveniently done by using a coordinate system in which the element itself lies in a coordinate plane, and thus coordinates of points and components of vectors must be transformed between the reference coordinate system in which the body surface is input and an "element coordinate system" based on the element in question. The analytic integration over the element produces rather lengthy formulas, whose evaluation is time consuming. To conserve computing time, the effect of an element at points sufficiently far from the element is calculated approximately. This is accomplished by means of a multipole expansion. In fact, if the point in question is farther from the centroid of the element than four times the maximum dimension of the element, the quadrilateral source element may be replaced by a point source of the same total strength located at its centroid. With the accuracy criteria adopted, errors due to the use of the multipole expansion or point-source formulas are apparently small compared with those arising from the basic approximation of the body surface by plane elements having

constant values of source density. The use of these alternative formulas therefore involves no loss of accuracy at all in the overall calculation.

When this phase of the calculation has been completed, the result consists of the $N \times N$ matrices Φ_{ij} and $\vec{V}_{ij}$ that give the potentials and velocities induced by the elements at each other's control points for a unit source density. The vector matrix $\vec{V}_{ij}$ is

$$\vec{V}_{ij} = X_{ij}\,\vec{i} + Y_{ij}\,\vec{j} + Z_{ij}\,\vec{k}, \qquad (3.3.1)$$

where $\vec{i}, \vec{j}, \vec{k}$ are the unit vectors along the axes of the reference coordinate system in which the body surface is input, and the scalar matrices X_{ij}, Y_{ij}, Z_{ij} are simply the components of $\vec{V}_{ij}$. The normal velocity induced at the control point of the ith element by a unit source density on the jth element is

$$A_{ij} = \vec{n}_i \cdot \vec{V}_{ij}, \qquad (3.3.2)$$

where $\vec{n}_i$ is the unit normal vector to the ith element. The five matrices Φ_{ij}, X_{ij}, Y_{ij}, Z_{ij}, and A_{ij} do not necessarily have any zero entries. The number of elements used in three-dimensional cases is large enough for the handling of the amount of numerical data represented by these matrices to be a considerable problem.

It should be mentioned that the $i = j$ case does not require special handling. Because the integration over an element is done analytically for nearby points, problems of infinite integrands or principal-value integrals, which might be expected from the discussion of Section 2, fail to materialize. The velocity induced by an element at its own control point has a magnitude of 2π and is directed along the element's normal vector.

If the body has one or more symmetry planes that are also planes of symmetry or antisymmetry of the flow field these may be accounted for automatically. Only the nonredundant portion of the body surface is approximated by surface elements. Once the potential and velocity induced at the control point of the ith element by the jth element has been computed, the jth element is reflected in each symmetry plane and the calculation repeated. The effects of the reflected elements at the control point of the ith element are either added to or subtracted from the effect of the jth element itself, depending on whether the pertinent plane is one of symmetry or antisymmetry. Thus, although potentials and velocities induced by elements all over the body surface must be computed, they are computed only at control points on the nonredundant portion and are added, so that the matrices Φ_{ij} and $\vec{V}_{ij}$ have an order equal to the number of elements describing the nonredundant portion of the body surface.

3.3.3 *Two-dimensional and axisymmetric flow.* For two-dimensional flow
and for axisymmetric flow, one integration can be performed in advance: an
integration to infinity in both directions normal to the profile curve for the
two-dimensional case and an integration in the circumferential direction at a
fixed radial distance and fixed axial location for the axisymmetric case. The
integration does not depend on the approximation of the body by elements;
it is possible solely because the source density does not vary in the direction
of integration. Thus instead of considering as elements infinite strips or
frustums of cones over which the unit-point source formulas are to be
integrated, the elements may be considered to be the line segments joining
the input points along the profile curve (Fig. 3a). The formulas that must be
integrated over these line segment elements are not, of course, those for the
simple point source but those for the integral of the point source in the
proper direction. The singularity whose effect is integrated over a line-
segment element is an infinite line source of unit strength for the two-dimen-
sional problem and a ring source of unit strength for the axisymmetric
problem.

In two dimensions, the necessary integration over a line-segment element
can be performed analytically. Again, this is most conveniently done by
using a coordinate system based on the element. Since computing times for
two-dimensional flows are rather small, the effects of all elements on each
other's control points are computed from the formulas produced by the
analytic integration. No approximate formulas are used. Just as in three
dimensions, no trouble is encountered for the case $i = j$. The velocity induced
by an element at its own control point has a magnitude of 2π and a direction
normal to the element.

The ring source that is appropriate for use with axisymmetric flows gives
rise to a potential and a velocity at a point in space that may be expressed
in terms of complete elliptic integrals. These expressions cannot be integrated
analytically over a line-segment element, and resort must be made to numerical
integration. The numerical-integration scheme used to calculate the effect of
an element at a point in space uses a variable number of ordinates to effect
the integration. The farther away the point in question lies from the element,
the smaller is the number of ordinates used. Thus a saving in computing
time is obtained with no loss in overall accuracy. The case $i = j$ does require
special handling to numerically calculate the principal value of the relevant
integrals. The velocity induced by an element at its own control point has
both a normal and a tangential component, whose magnitudes cannot be
predicted in advance.

For both two-dimensional and axisymmetric flows, the results of this
phase of the calculation are the $N \times N$ matrices Φ_{ij} and $\vec{V}_{ij}$. The vector
$\vec{V}_{ij}$ has only two components

$$\vec{V}_{ij} = X_{ij}\,\vec{i} + Y_{ij}\,\vec{j}. \tag{3.3.3}$$

For the axisymmetric case, the component Y_{ij} represents a radial component of velocity rather than a y-component. However, since all quantities are independent of circumferential location, it is sufficient to consider only the xy-plane. It is more convenient to resolve $\vec{V}_{ij}$ into normal and tangential components rather than x- and y-components. Let $\vec{n}_i$ and $\vec{t}_i$ be the unit outward normal vector and unit tangential vector to the ith element, respectively. The direction of $\vec{t}_i$ is given by the order of the input points; that is, $\vec{t}_i$ is tangent to the profile curve in the clockwise sense for exterior flow about a single closed body. Then with the definitions

$$A_{ij} = \vec{n}_i \cdot \vec{V}_{ij} \quad \text{and} \quad B_{ij} = \vec{t}_i \cdot \vec{V}_{ij}, \tag{3.3.4}$$

$\vec{V}_{ij}$ can be written as

$$\vec{V}_{ij} = A_{ij}\,\vec{n}_i + B_{ij}\,\vec{t}_i \tag{3.3.5}$$

The scalar quantities A_{ij} and B_{ij} are the outer normal and clockwise tangential components, respectively, of the velocity induced at the control point of the ith element by a unit source density on the jth element. In two-dimensional and axisymmetric cases there are only three matrices, Φ_{ij}, A_{ij}, and B_{ij}. Since the number of elements used in these cases is considerably smaller than that used in the three-dimensional case, the manipulation of these matrices is not a major problem.

3.3.4 Cross flow about an axisymmetric body.

In order to perform the circumferential integration in the case of an axisymmetric body, it is not necessary that the source density be constant in that direction. It is sufficient that the source density vary with circumferential location in a known way. The most important situation of this type is that of the cross flow about an axisymmetric body immersed in a uniform stream perpendicular to the axis of symmetry of the body. Because of the linearity of the problem, this flow may be combined with the axisymmetric flow about the same body to give the flow at any angle of attack. For the pure cross flow it can be shown[2] that the velocity potential and source density are both proportional to the cosine of the circumferential angle, where this angle is measured from the direction of the uniform stream. If the uniform stream is assumed to be parallel to the y-axis, the situation is as shown in Fig. 4. Any point in space lies in a plane through the symmetry axis (x-axis) at an angle θ to the xy-plane. The velocity at this point may be resolved into two components parallel to this plane plus one component normal to it. The two velocity components parallel to the plane and the potential itself are proportional to

cos θ and are thus characterized by their values at the point in the xy-plane having the same axial and radial location as the point in question. The velocity component normal to the plane containing the point and the symmetry axis is proportional to sin θ and is thus characterized by its value at the point in the yz-plane having the same axial and radial location.
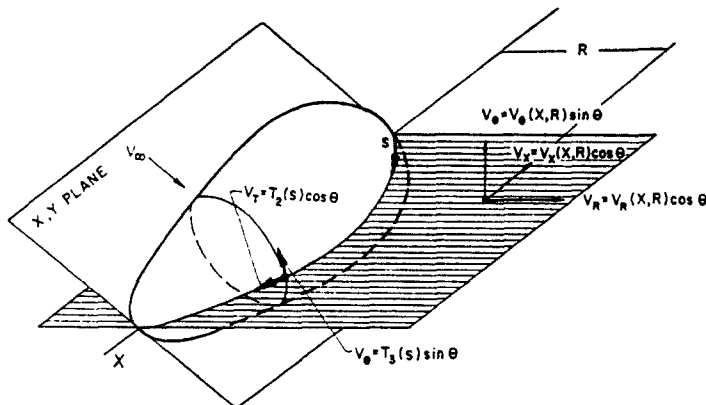

FIG. 4. Circumferential variation of velocity components for cross flow about an axisymmetric body.

The present method of solution approximates the body surface in the same way that it does for axisymmetric flow. The source density on each element is assumed to be constant in the axial and radial directions and to be proportional to cos θ. The formulas for the potential and velocity due to a point source are integrated circumferentially. The results are corresponding formulas for a ring source whose strength varies as the cosine of the circumferential angle. These expressions are remarkably similar to those for a constant-strength ring source, and many of the expressions and functions that must be evaluated are common to both. The ring-source expressions are integrated numerically over the line-segment elements in the same way as they were for axisymmetric flow. The results are Φ_{ij} and $\overrightarrow{V_{ij}}$, the potentials and velocities induced at the control points by the elements per unit value of source density. Here is meant unit value of source density on the line segment in the xy-plane. The vector $\overrightarrow{V_{ij}}$ has exactly the form given by (3.3.3), (3.3.4), and (3.3.5), although the numerical values are of course different. The control points are in the xy-plane, and Φ_{ij}, A_{ij}, and B_{ij} represent potential, normal velocity, and tangential velocity, respectively, in this plane. To find the potential or velocity components normal and tangential to the meridian curve at any other circumferential location, these quantities must be multiplied by cos θ.

It remains to compute the circumferential component of velocity. Let Θ_{ij} be the circumferential velocity induced by the jth element at a point obtained from the control point of the ith element by rotating it 90° circumferentially into the xz-plane. From the preceding discussion it is seen that this value characterizes the circumferential velocity at that axial and radial location. This quantity is related to Φ_{ij} by

$$\Theta_{ij} = \frac{1}{\bar{y}_i} \, \Phi_{ij}, \qquad (3.3.6)$$

where $\bar{y}_i$ is the y-coordinate or radial coordinate of the control point of the ith element. Only one of these matrices need be evaluated, and it is Θ_{ij} that is computed. The close relationship (3.3.6) between the characteristic values of circumferential velocity and potential holds in general—not just for the effect of a single surface element. However, the two have different circumferential variations. The potential varies as $\cos\theta$, and the circumferential velocity varies as $\sin\theta$.

The treatment described in this subsection can also be used for the case of a body rotating about a line perpendicular to and intersecting its axis of symmetry, since the variation of all quantities with circumferential location is identical. The only difference is the onset flow.

3.3.5 *Special two-dimensional applications. Cascades and hydrofoils.* It is clear that the use of a simple point-source singularity as a basis is not essential to the present method. All the foregoing began with the point source, but in the two-dimensional and axisymmetric cases what was finally integrated over the line-segment elements were the effects of line and ring sources. This idea can be generalized much further. Instead of the point-source potential given by (2.1), the solution can be built up by superposition of the potentials of a wide variety of elementary singularities, which to be useful should satisfy all conditions of the problem except the condition on the boundary surface S. Thus if (1.2.7) and (1.2.9) were replaced by other conditions, new elementary singularities could be used, and the kernel of the integral equation (2.5) would then be derived from these singularities. Two such applications are discussed in this article. The first is the flow about an infinite two-dimensional cascade, an infinite set of identical bodies displaced successively a fixed distance parallel to a straight line. To reduce this problem to one for a single body surface, the proper elementary singularity is an infinite series of equal line sources spaced equally along a straight line. The required summation of effects can be accomplished analytically. The second problem is that of a two-dimensional body performing steady translation in the presence of a free surface, for example, a hydrofoil. The potential of the proper elementary singularity, whose analytic expression is quite complicated, satisfies a condition on the free surface and a radiation condition at infinity. For both

these problems, the procedure is exactly the same as that described above for the ordinary two-dimensional case. Matrices Φ_{ij} and $\vec{V}_{ij}$ are obtained, and the latter has the form given by (3.3.3), (3.3.4), and (3.3.5). The only difference lies in the specific expressions that are integrated over the line-segment elements.

3.4 *Approximation of the Integral Equation by a Set of Linear Algebraic Equations*

In all the cases discussed in the previous section, one result of the calculation is the matrix A_{ij}, whose entries are the normal velocities induced by the elements at each other's control points for unit values of source density. To obtain actual normal velocities, the entries of A_{ij} must be multiplied by the proper values of the source density σ. In particular, the quantity

$$\sum_{j=1}^{N} A_{ij}\, \sigma_j \tag{3.4.1}$$

is the normal velocity at the control point of the ith element due to the complete set of surface elements. Clearly, (3.4.1) is the approximation of the normal velocity associated with the disturbance potential of the body surface. To obtain the prescribed normal velocities at the control points of all elements, (3.4.1) must be set equal to the proper value as given by (1.2.8) for every value of i. The result is

$$\sum_{j=1}^{N} A_{ij}\, \sigma_j = -\,\vec{n}_i \cdot \vec{V}_{\infty_i} + F_i, \qquad i = 1, 2, \ldots, N. \tag{3.4.2}$$

Equation (3.4.2) is a set of linear algebraic equations for the values of source density on the surface elements. This set of linear algebraic equations is the desired approximation of the integral equation (2.5). Notice that the onset flow velocity $\vec{V}_\infty$ and the prescribed resultant normal velocity F have been subscripted with i to denote explicitly the fact that these quantities may vary over the body surface.

Methods of solving (3.4.2) for the set of source densities σ_j are discussed in Section 5. Both direct and iterative methods are used. Normally, an iterative solution is used for three-dimensional flows and a direct solution is used for all other cases. In the usual case, the onset-flow velocity $\vec{V}_\infty$ is simply a constant vector of unit magnitude, and the prescribed normal velocity F is zero. In such a case, the points on the body surface are the only input to the method. Nonuniform onset flows must in general be input by specifying the onset-flow velocity components at the control points of the elements. However, certain frequently occurring flows can be generated automatically. The most important is the circulatory onset flow due to a known distribution

of interior vorticity that is used for two-dimensional lifting airfoils. The rotational onset flow appropriate for rotating bodies can also be generated. For any fixed, impermeable ensemble of bodies in steady flow, the function F is zero. It is required for cases of area suction and certain unsteady flows, including the case of two bodies moving with respect to each other.

For a given type of flow—two-dimensional, axisymmetric, or three-dimensional—it is evident from the description of the previous section that the matrix A_{ij} (and all other computed matrices) depends only on the geometry of the body surface and is independent of the onset flow or prescribed normal velocity. A two-dimensional body has only one A_{ij} for all flows. The same is true for a three-dimensional body if symmetry is not utilized or if all onset flows have the same symmetry. An axisymmetric body has one A_{ij} for all axisymmetric flows and another for all cross flows. Various onset flows or normal-velocity conditions simply provide different right sides for the equations (3.4.2). Solutions for several onset flows to the same body are often desired. For example, the flow about a two-dimensional lifting airfoil at any lift coefficient can be obtained from three basic flow solutions: those due to each of two uniform streams at right angles to each other and that due to a circulatory onset flow that corresponds to a pure circulation about the airfoil. If more than one airfoil is simultaneously present, there is more than one independent circulatory onset flow. Since only one matrix is involved, solutions for various onset flows are efficiently obtained at the same time. If a direct solution method is used for (3.4.2), the time required to solve for several onset flows is scarcely greater than that required for one. Of course, a complete set of values of source density σ_j is obtained for each flow.

3.5 Computation of the Flow Quantities of Interest

Once the values of the source density σ_j have been obtained as the solution of (3.4.2), all other flow quantities of interest can be obtained by relatively rapid direct calculation. The chief interest in most cases is in the flow on the body surface. Flow quantities on the body surface are computed only at the control points of the elements, by use of the matrices described in Section 3.3.

In three-dimensional cases, the potential and velocity at a control point on the body surface are calculated from

$$\left.\begin{aligned}
\varphi_i &= \sum_{j=1}^{N} \Phi_{ij}\, \sigma_j \\[2mm]
\vec{V}_i &= \sum_{j=1}^{N} \vec{V}_{ij}\, \sigma_j + \vec{V}_{\infty i}
\end{aligned}\right\} \quad i = 1, 2, \ldots, N. \qquad (3.5.1)$$

The velocity $\vec{V}_i$ at each control point is given in terms of its components along the axes of the reference coordinate system in which the body is input.

In actual computation, the scalar matrices X_{ij}, Y_{ij}, and Z_{ij} are multiplied by σ and summed. Notice that φ_i is the perturbation potential due to the body surface, and $\vec{V_i}$ is the total velocity, including the effects of the onset flow. For the majority of applications these are the desired forms. Perturbation velocities may be calculated if desired. The components of $\vec{V_i}$ are used to compute velocity magnitude and then pressure coefficient from (1.2.11). The latter quantity has meaning only for a uniform onset flow.

In two-dimensional and axisymmetric cases the perturbation potential and tangential velocity at a control point of an element are calculated from

$$\left. \begin{array}{l} \varphi_i = \sum\limits_{j=1}^{N} \Phi_{ij}\, \sigma_j \\[2em] T_i = \sum\limits_{j=1}^{N} B_{ij}\, \sigma_j + \vec{t_i} \cdot \vec{V}_{\infty_i} \end{array} \right\} \quad i = 1, 2, \ldots, N . \qquad (3.5.2)$$

Again the velocity is a total velocity, and the potential is a perturbation. The sign of T_i is positive if this velocity is clockwise with respect to the profile curve of the body and negative if it is counter clockwise. The tangential velocity T_i is the only velocity component, and the pressure coefficient is calculated from it in the usual way. For the special two-dimensional applications of cascades and hydrofoils the tangential surface velocity is calculated as shown in (3.5.2), but the potential is not calculated.

For the case of cross flow about an axisymmetric body, the velocity component tangential to the profile curve of the body at a control point is calculated from (refer to Fig. 4 for definition of velocity components)

$$T_{2_i} = \sum\limits_{j=1}^{N} B_{ij}\sigma_j + \vec{t_i} \cdot \vec{V}_{\infty_i}, \qquad i = 1, 2, \ldots, N . \qquad (3.5.3)$$

This also represents a clockwise velocity. The velocity component tangent to a meridian curve of the body at any circumferential angle θ is $T_{2_i} \cos \theta$. The circumferential component of velocity at a point obtained by circumferentially rotating a control point 90° into the xz-plane is given by

$$T_{3_i} = \sum\limits_{j=1}^{N} \Theta_{ij}\, \sigma_j + \vec{j} \cdot \vec{V}'_{\infty_i}, \qquad i = 1, 2, \ldots, N . \qquad (3.5.4)$$

where $\vec{j}$ is the unit vector parallel to the y-axis and $\vec{V}'_{\infty_i}$ is the onset-flow velocity evaluated at the rotated location of the control point. Circumferential velocity components at other values of θ are $T_{3_i} \sin \theta$. Both of the velocity components (3.5.3) and (3.5.4) may be obtained as perturbation velocity components if desired. The perturbation potential at a control point is

$$\varphi_i = \bar{y}_i \,(T_{3_i} - \vec{j} \cdot \vec{V}'_{\infty_i}), \qquad i = 1, 2, \ldots, N . \qquad (3.5.5)$$

where $\bar{y}_i$ is the y-component or radial component of the control point. [If T_{3_i} is computed as a perturbation velocity component, nothing is subtracted from $\bar{y}_i T_{3_i}$ in (3.5.5)].

Flow quantities may be computed at points off the body surface for all flow geometries. The coordinates of an off-body point are input and used to obtain quantities Φ_{ij} and $\vec{V}_{ij}$ for $j = 1, 2, \ldots, N$. These are calculated by the same formulas as those used for calculating induced potential and velocity at a control point of a surface element. It is simply a matter of using the coordinates of the off-body point in place of the coordinates of the ith control point. The potential and velocity at such a point are calculated in the form

$$\varphi = \sum_{j=1}^{N} \Phi_{ij}\, \sigma_j \quad .$$

$$\vec{V} = \sum_{j=1}^{N} \vec{V}_{ij}\, \sigma_j \quad .$$

(3.5.6)

(The use of the subscript i on Φ_{ij} and $\vec{V}_{ij}$ is perhaps misleading in this context, since the computation is at an off-body point, not at the control point of the ith surface element. The subscript has been retained to avoid introducing another symbol for a quantity that is calculated in exactly the same way as it is for points on the body surface. Perhaps i can be thought of here as denoting the ith off-body point.) At off-body points both the potential and velocity are perturbation quantities due only to the effect of the body surface, unless the onset flow is a uniform stream, in which case its effect can be added to the velocity. For all flow geometries, the velocity at off-body points is given by its components along the axes of the reference coordinate system.

In many fluid dynamics applications the potential itself is of no interest. Accordingly, provision has been made for deleting that part of the calculation. This saves computation time and eliminates the storage requirements for one matrix, except for the cross-flow case, in which the potential is calculated from the circumferential velocity. The reduction in computation time is not great, since much of the required calculation is common to Φ_{ij} and $\vec{V}_{ij}$. Also, storage requirements are not an important factor except for three-dimensional cases.

In applications it is often required to calculate certain basic flows and combine them linearly to obtain a particular flow or a set of such flows. The three common cases are: two-dimensional airfoils at prescribed angle of attack or prescribed lift coefficient, inlets at prescribed mass–flow ratio, and axisymmetric bodies at prescribed angle of attack. Provision has been

D

made for automatically combining basic flows. The basic flows for a lifting, two-dimensional airfoil are the nonlifting flows due to uniform streams at 0° and 90° inclination to the airfoil reference line and the flow due to a pure circulation about the airfoil. The latter uses an onset flow due to a known distribution of vorticity interior to the airfoil. Orginally the method used a point vortex of unit strength located at the center of curvature of the airfoil leading edge. It was later found that improved accuracy was obtained by using a vorticity distribution of unit strength over the profile curve of the airfoil. Since the velocity due to a vortex is simply that due to a source rotated 90°, the normal and tangential components of this circulatory onset flow at the midpoints of the elements are found by summing the rows of the matrices B_{ij} and A_{ij}, respectively. The three basic flows for the airfoil are linearly combined to satisfy the Kutta condition at the trailing edge and to give the prescribed angle of attack or lift coefficient. Normally, a set of angles of attack or lift coefficients is prescribed and the corresponding flows generated from the three basic flows. For multiple airfoils, there is a circulatory solution for each airfoil and a Kutta condition at each trailing edge. For inlets, the basic flows are the flows at two distinct mass-flow ratios. They are obtained by blocking the inlet in different ways. The flows for all possible mass-flow ratios can then be obtained as linear combinations of these two. For a closed axisymmetric body in a uniform stream, the two basic flows are the axisymmetric flow and the pure cross flow. For flow due to a uniform stream at an inclination α to the axis of symmetry of the body, the velocity component tangent to a meridian curve at a circumferential angle θ is (dropping the subscript i)

$$T \cos \alpha + T_2 \sin \alpha \cos \theta \qquad (3.5.7)$$

and the circumferential velocity component is

$$T_3 \sin \alpha \sin \theta. \qquad (3.5.8)$$

If the onset velocity is assumed to have a unit magnitude, the surface pressure coefficient is

$$C_p = 1 - (T \cos \alpha + T_2 \sin \alpha \cos \theta)^2 - T_3^2 \sin^2 \alpha \sin^2 \theta \qquad (3.5.9)$$

or

$$C_p = C_{p_0} - TT_2 \sin 2\alpha \cos \theta + \sin^2 \alpha \, (T^2 - T_2^2 \cos^2 \theta - T_3^2 \sin^2 \theta), \qquad (3.5.10)$$

where C_{p_0}, which equals $1 - T^2$, is the pressure coefficient at zero angle of attack. These formulas give velocity and pressure at any α and θ in terms of the basic flow solutions. Although (3.5.10) resembles an expansion for small values of α, this formula is in fact exact for any α.

In hydrodynamic applications, the integral

$$\oiint\limits_{S} \varphi \; \frac{\partial \varphi}{\partial n} \; \mathrm{d}S \qquad\qquad (3.5.11)$$

over the body surface is of interest because it expresses the kinetic energy of the fluid motion. This integral is evaluated numerically by summing the relevant quantities over the surface elements. The results give the added mass in cases of pure translation and the analogous quantity in cases of pure rotation.

Potential flow in the sense of this article is incompressible flow. It seemed valuable, however, to include in the method the ability to account, at least to first order, for the effect of Mach number. Accordingly, for the case of a uniform onset flow the method has the capability of performing a Goethert transformation. The body surface is stretched in the direction parallel to the free stream, the incompressible flow about the resulting body is calculated, and the calculated velocities are transformed in the well-known manner.[17] Although based on a small-perturbation theory, this method has proved quite accurate in a variety of fairly extreme flows, some examples of which are shown in Section 8. In two dimensions, other compressibility corrections are available that adjust incompressible pressures on the body itself (not stretched).[17] In some cases these may be preferable to the Goethert transformation.

3.6 Computation Time

It is not possible to formulate precise general estimates of computing times for the present method, because so many factors are involved. Moreover, such estimates are soon rendered obsolete by changes in computing equipment. It seems useful, however, to present some examples of computation times for typical cases, to illustrate the magnitude of these times and to provide approximate rules for estimating them. All times apply to an IBM 7094 computer, which performs a typical arithmetic operation in about 10 μsec and transfers large amounts of data sequentially from low-speed storage (magnetic tape) to high-speed storage (magnetic core) at an approximate rate of one complete number (36 binary places) every 100 μsec.

For flow about two-dimensional and axisymmetric bodies it is useful to divide the total computing time into two parts: the time required to solve the set of linear algebraic equations and the time for all other calculations, most of which is required to calculate the matrices of induced potentials and velocities. These two times vary in different ways with the number N of elements used to approximate the body surface. The linear algebraic equations are solved by a direct method for two-dimensional and axisymmetric bodies. The time required to effect this solution is approximately proportional to

N^3, and it is independent of the particular body or onset flow that is considered. For $N = 100$, direct solution of the linear algebraic equations requires about 0.6 min. The computation time required for all other lengthy calculations is very nearly proportional to N^2. For ordinary two-dimensional flows with $N = 100$, the time required for the remaining calculation is about one minute; that is, the total time is about 1.6 min. For an axisymmetric body, either in axisymmetric flow or cross flow, the additional calculations require about two minutes if $N = 100$, and the total computation time is about 2.6 min. For an equal number of surface elements a cascade requires roughly the same computing time as a single two-dimensional body, and a hydrofoil requires approximately the same time as an axisymmetric body.

Computing times for a three-dimensional flow can be estimated only very approximately. Estimation is complicated because the method uses (1) the symmetry of the body surface, (2) approximate formulas for calculating the matrices of induced velocities and potentials, and (3) an iterative method for solving the set of linear algebraic equations. The computing time is not exclusively a function of the number of elements N, but it can also be significantly different for different body shapes and onset flows, particularly the time for the solution of the linear equations. Several times as many iterations may be required for convergence in one case as were required for another. Generally, computing time varies as N^2. The magnitude of the time required may be illustrated by an example. A solution for a single flow about a body with one symmetry plane (the common case in applications) and with 650 elements on the nonredundant portion of the body typically requires an hour and a half. Unfavorable cases may require twice this time. A more detailed analysis of the variation of computing time for three-dimensional flows is contained in the report form of Ref. 3 together with several examples, but the specific times quoted apply to obsolete computing equipment.

4. CALCULATION OF THE POTENTIAL AND VELOCITY INDUCED BY A SURFACE ELEMENT AT A POINT IN SPACE

As was stated in Section 3.3, the formulas for the potential and velocity at a general point in space due to a unit source density on a surface element form the basis of the present method of flow calculation. These formulas yield the induced potential and velocity matrices, Φ_{ij} and $\vec{V}_{ij}$, which are used in the manner described in Section 3 to effect a solution. The following sections present the required potential and velocity formulas for the various types of surface elements that are used for different body geometries.

4.1 *Two-dimensional Bodies*

For two-dimensional flows all quantities are independent of the coordinate

z. Thus one integration can be performed in advance both in the expression (2.3) for the potential and in the integral equation (2.5). These surface integrals are reduced to single integrals over the profile curve of the body. As was mentioned previously, this is equivalent to using a line source instead of a point source as the elementary singularity to be integrated over the line-segment elements that approximate the body's profile curve. The potential due to a line source of unit strength is obtained by integrating the point-source potential (2.1), and the corresponding velocity components are obtained by integrating the derivatives of this expression. The integrations for the velocity components are straightforward. Specifically, the velocity components at a point with coordinates *x*, *y*, 0 due to a line source of unit strength at a location $x = \xi$, $y = \eta$, $-\infty < z < \infty$ are

$$V_x = -\frac{\partial \varphi}{\partial x} = \int_{-\infty}^{\infty} \frac{(x - \xi)\, dz}{[(x - \xi)^2 + (y - \eta)^2 + z^2]^{\frac{3}{2}}} = 2\, \frac{x - \xi}{(x - \xi)^2 + (y - \eta)^2}$$

$$(4.1.1)$$

$$V_y = -\frac{\partial \varphi}{\partial y} = \int_{-\infty}^{\infty} \frac{(y - \eta)\, dz}{[(x - \xi)^2 + (y - \eta)^2 + z^2]^{\frac{3}{2}}} = 2\, \frac{y - \eta}{(x - \xi)^2 + (y - \eta)^2}$$

The integration for the line-source potential is more troublesome. Direct integration of (2.1) from $z = -\infty$ to $z = +\infty$ in a manner analogous to the integrations for the velocity components yields an infinite value of potential at all points (*x*, *y*, 0). This difficulty may be overcome by using a limiting process and taking advantage of the fact that a constant may be added to the potential without changing any quantity of physical significance. The potential at (*x*, *y*, 0) due to the line source is taken in the form

$$\varphi = \lim_{L \to \infty} \left[\int_{-L}^{L} \frac{dz}{\sqrt{[(x - \xi)^2 + (y - \eta)^2 + z^2]}} - \ln 4L^2 \right] \quad (4.1.2)$$

The term in brackets is the potential of a line source of length 2*L* to which a constant depending on the length has been added. Performing the indicated operations gives

$$\varphi = \ln \left[\frac{1}{(x - \xi)^2 + (y - \eta)^2} \right], \quad (4.1.3)$$

to which a finite constant may be added. The expressions (4.1.1) and (4.1.3) are the expected two-dimensional results except perhaps for sign and a factor of two.

To obtain the potential and velocity induced by an element at a point in space, expressions (4.1.1) and (4.1.3) must be integrated over a line-segment element. This is most easily done in a coordinate system based on

the element. As is shown in Fig. 5, the line-segment element is taken as lying along the x-axis of the "element coordinate system" with its center at the origin. The positive y-direction is the direction of the outward normal
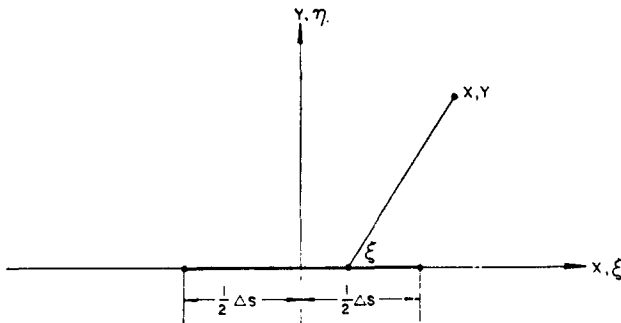
FIG. 5. Integration over a line-segment element for the two-dimensional case.

vector to the element. The length of the segment is denoted Δs to illustrate the fact that this length approximates an arc length along the profile curve of the body. The velocity components at a point $(x, y, 0)$ due to the element are

$$V_x = 2 \int\limits_{-\Delta s/2}^{\Delta s/2} \frac{(x - \xi)\, d\xi}{(x - \xi)^2 + y^2} = \ln \left[\frac{(x + \Delta s/2)^2 + y^2}{(x - \Delta s/2)^2 + y^2}\right],$$

$$\text{(4.1.4)}$$

$$V_y = 2 \int\limits_{-\Delta s/2}^{\Delta s/2} \frac{y\, d\xi}{(x - \xi)^2 + y^2} = 2 \left[\tan^{-1}\left(\frac{x + \Delta s/2}{y}\right) - \tan^{-1}\left(\frac{x - \Delta s/2}{y}\right)\right].$$

If additive constants are neglected, the potential at $(x, y, 0)$ due to the element is

$$\varphi = - \int\limits_{-\Delta s/2}^{\Delta s/2} \ln\left[(x - \xi)^2 + y^2\right] d\xi$$

$$= -x V_x - y\, V_y - (\Delta s/2) \ln \left(\{[x + (\Delta s/2)]^2 + y^2\}\right.$$

$$\left.\{[x - (\Delta s/2)]^2 + y^2\}\right) \quad \text{(4.1.5)}$$

Unlike the three-dimensional case, where it is natural to require the potential to vanish at infinity, there is no obvious choice of additive constant for the expression (4.1.5), which is infinite at infinity.

The inverse tangents in (4.1.4) are to be evaluated in the principal-value range from $-\pi/2$ to $+\pi/2$. The two inverse tangents may be combined by means of the tangent law in the form

$$V_y = 2 \tan^{-1}\left(\frac{y\, \Delta s}{x^2 + y^2 - (\Delta s/2)^2}\right) \quad \text{(4.1.6)}$$

where the inverse tangent is evaluated in the range from $-\pi$ to $+\pi$ by taking into account the individual signs of the numerator and denominator of its argument. In either form it is clear that as $y \to \pm 0$, $V_y \to \pm 2\pi$ if $|x| < \Delta s/2$ and $V_y \to 0$ if $|x| > \Delta s/2$. The midpoint of the line segment is taken as $x = 0$, $y = +0$, and the velocity induced by the element on its own control point has a magnitude of 2π and is directed along the outer normal to the element as indicated in Section 3.3 (V_x is clearly zero for $x = 0$). The velocity component V_x is logarithmically infinite at the ends of the line segment, and the potential is finite everywhere except at infinity.

Since the above formulas are written in a coordinate system based on the element, the coordinates of the point where potential and velocity are to be evaluated must be expressed in this system before these formulas are used. After V_x and V_y are computed, they must be transformed into the reference coordinate system in which the body shape was input, to obtain the components of $\vec{V}_{ij}$ in the form (3.3.3). The computation of φ gives Φ_{ij} directly.

The above formulas can be written more compactly in complex notation. The real notation was used here to show the similarity to the three-dimensional case.

4.2 Axisymmetric Bodies in Axisymmetric Flow

For axisymmetric flows all quantities are independent of circumferential location. Thus, just as in the two-dimensional case, one integration can be performed in advance both in the expression (2.3) for the perturbation potential and in the integral equation (2.5). These surface integrals are reduced to single integrals over the profile curve of the body. As is mentioned
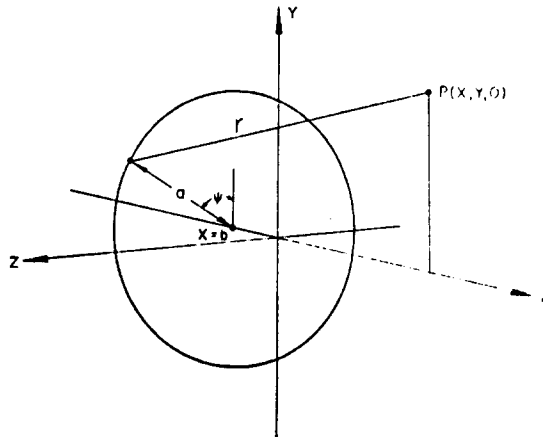
FIG. 6. A ring source of constant strength lying in the plane $x = b$.

in Section 3.3, this is equivalent to using a constant-strength ring source as the elementary singularity to be integrated over the line-segment elements that approximate the profile curve of the body.

The x-axis is taken as the axis of symmetry. Figure 6 illustrates a ring source of radius a lying in the plane $x = b$. If the ring source is assumed to be of unit strength, the potential due to the source at a point $(x, y, 0)$ is

$$\varphi = \int_{-\pi}^{\pi} \frac{a \, d\psi}{r} = 2a \int_{0}^{\pi} \frac{d\psi}{\sqrt{[(x - b)^2 + y^2 + a^2 - 2ay \cos \psi]}} \quad (4.2.1)$$

where ψ is the circumferential angle around the ring source measured from the positive y-axis. The corresponding velocity components are

$$V_x = -\frac{\partial \varphi}{\partial x} = 2a \int_{0}^{\pi} \frac{(x - b) \, d\psi}{[(x - b)^2 + y^2 + a^2 - 2ay \cos \psi]^{\frac{3}{2}}}$$

$$(4.2.2)$$

$$V_y = -\frac{\partial \varphi}{\partial y} = 2a \int_{0}^{\pi} \frac{(y - a \cos \psi) \, d\psi}{[(x - b)^2 + y^2 + a^2 - 2ay \cos \psi]^{\frac{3}{2}}}$$

By a series of substitutions and algebraic manipulations,[1] these formulae may be expressed in terms of complete elliptic integrals. The results are

$$\varphi = \frac{4a \, K(k)}{\sqrt{[(y + a)^2 + (x - b)^2]}},$$

$$V_x = \frac{4a(x - b) \, E(k)}{[(y - a)^2 + (x - b)^2] \sqrt{[(y + a)^2 + (x - b)^2]}} \quad (4.2.3)$$

$$V_y = \frac{2a}{y \sqrt{[(y + a)^2 + (x - b)^2]}} \left[K(k) + \frac{y^2 - a^2 - (x - b)^2}{(y - a)^2 + (x - b)^2} E(k) \right]$$

where $K(k)$ and $E(k)$ are the complete elliptic integrals of the first and second kind, respectively. Their argument is given by

$$k^2 = \frac{4 \, ay}{(y + a)^2 + (x - b)^2}. \quad (4.2.4)$$

These are the equations that must be integrated over a line-segment element.

Consider a typical line-segment element as shown in Fig. 7. For the axisymmetric case no simplification results from using a coordinate system based on the element. The calculation is performed in the reference coordinate system, except that it is convenient to translate the origin of coordinates to the point on the axis of symmetry that lies directly below the midpoint of the segment. The slope angle of the segment with respect to the positive x-axis is denoted by β. Distance along the line segment measured

from the midpoint is denoted by s, and the length of the segment is Δs. The y-coordinate of the midpoint of the segment is designated by y_0. For a point along the line segment the parameters of the ring source are

$$a = y_0 + s \sin \beta,$$

$$b = s \cos \beta \tag{4.2.5}$$

The potential and velocity induced by the element at the point $(x, y, 0)$ are obtained by substituting a and b from (4.2.5) into (4.2.3) and integrating the results with respect to s from $-\Delta s/2$ to $+\Delta s/2$. Since the integration is performed in terms of s, no special handling is required for vertical elements having $\beta = \pi/2$.
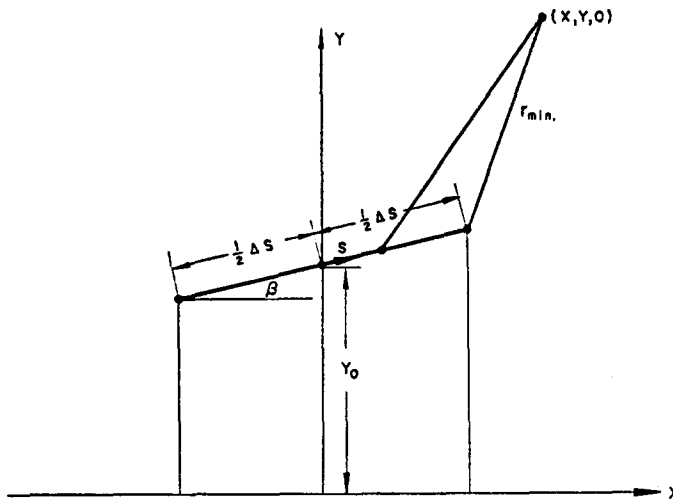
FIG. 7. Integration over a line-segment element for the case of an axisymmetric body.

The required integrations are performed numerically by Simpson's rule. The line segment is divided by equally spaced points into subsegments; that is the element is divided into subelements. The number of subelements is taken as $16 \Delta s/r_{min}$ rounded to the nearest even integer, where r_{min} is the distance from the point $(x, y, 0)$ to the nearer of the endpoints of the line segment. Thus the farther the point in question lies from the element, the fewer the number of subelements used in the calculation. The minimum number of subelements is two. The constant 16 used to select the number of subelements was determined by trial and error to give good results, but other choices are certainly possible.

The above procedure cannot be used for calculating the effect of the element at its own midpoint. The expressions (4.2.3) for the velocity components V_x and V_y are singular for $x = b$, $y = a$. In the translated coordinate system, the midpoint has coordinates $x = 0$, $y = y_0$, and the singularity occurs for $s = 0$. The singularity is of the form $1/s$ and is thus not integrable. The required integrals must be considered principal values. (If expressions (4.2.3) are combined to give velocity components normal and tangent to the element, the expression for normal velocity is logarithmically infinite at $s = 0$ and is thus integrable. However, such an approach does not seem to have any advantage over the one described below.) Evaluation of these is carried out in the following way, some aspects of which are illustrated in Fig. 8. A certain distance d is selected. The portion of the line segment within

INTEGRALS EVALUATED BY
NUMERICAL INTEGRATION USING
ORDINARY SUBELEMENTS

INTEGRALS EVALUATED
BY SERIES EXPANSION
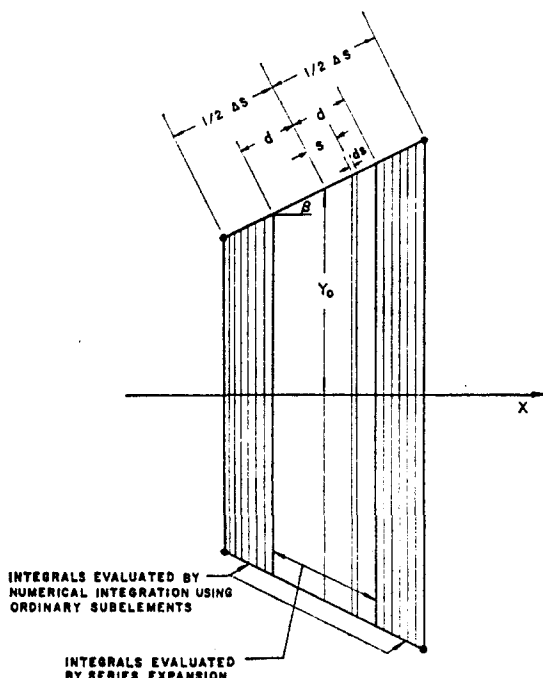
FIG. 8. The singular subelement.

the distance d of the midpoint is designated the singular subelement. The expressions (4.2.3) are expanded in terms of s/y_0, where this quantity is assumed to be small. The result[1, 5] in each case is a term proportional to $1/(s/y_0)$ plus a power series in s/y_0 plus another power series in s/y_0 multiplied by $\ln (s/y_0)$. These expansions are integrated from $s = -d$ to $s = +d$, to obtain the effect of the singular subelement on the midpoint. Since the integration interval is symmetric about $s = 0$ and $1/(s/y_0)$ is an odd function,

the contribution of this term is allowed to cancel out, and thus, effectively, the integrals are evaluated as principal values. All other terms in the expansions are integrable. In each case the result of the integration is a power series in d/y_o plus another power series in d/y_o multiplied by $\ln (d/y_o)$. The contributions of the singular subelement to the potential and velocity at the midpoint are

$$\varphi' = 4y_o \left(\frac{d}{y_o}\right)\left\{\left[1 - \ln\left(\frac{1}{8}\,\frac{d}{y_o}\right)\right] - \frac{1}{144}\left(\frac{d}{y_o}\right)^2\left[2 - 2\sin^2\beta\right.\right.$$

$$\left.\left. + 3(1 + 2\sin^2\beta)\ln\left(\frac{1}{8}\,\frac{d}{y_o}\right)\right] + \ldots\right\},$$

$$V_x' = -\sin 2\beta \left(\frac{d}{y_o}\right)\left\{1 + \frac{1}{144}\left(\frac{d}{y_o}\right)^2\left[13 + 6\sin^2\beta\right.\right.$$

$$\left.\left. + 6\ln\left(\frac{1}{8}\,\frac{d}{y_o}\right)\right] + \ldots\right\},$$

$$V_y' = -2\left(\frac{d}{y_o}\right)\left\{\left[\sin^2\beta + \ln\left(\frac{1}{8}\,\frac{d}{y_o}\right)\right] - \frac{1}{48}\left(\frac{d}{y_o}\right)^2\left[3\cos^2\beta\right.\right.$$

$$\left.\left. - 2\sin^4\beta + 3\ln\left(\frac{1}{8}\,\frac{d}{y_o}\right)\right] + \ldots\right\}. \quad (4.2.6)$$

In computation the above series are terminated after the third-order terms shown. The series for the potential in (4.2.6) has also been obtained by the above procedure. Since the expression (4.2.3) for the potential is only logarithmically infinite at $s = 0$, its expansion in terms of s/y_o does not contain a term proportional to $1/(s/y_o)$.

The contributions of the "ends" of the element, that is, the portions farther from the midpoint than the distance d, to the potential and velocity at the midpoint are evaluated as if these portions were separate elements. That is, expressions (4.2.3) are integrated numerically over these portions in the manner described above.

The selection of the semiwidth d of the singular subelement is the result of a compromise. On the one hand, it is desirable to have d as small as possible, to minimize truncation errors in the series (4.2.6) for the contribution of the singular subelement. On the other hand, it is desirable to have d as large as possible, to reduce errors arising from the use of numerical integration near a singularity. The situation is complicated by the fact that the truncation errors of (4.2.6) depend on the magnitude of d/y_o, while the errors arising from the numerical integration of (4.2.3) over the "ends" of the element depend on the magnitude $1/d$. The troublesome elements are those having a small value of y_o, which occur for example at the nose and tail of simple closed axisymmetric bodies. (Since, as stated in Section 3.2, the

points defining the body profile are restricted to nonnegative values of y in axisymmetric cases, no midpoint can have a zero y-coordinate.) The rule for determining d, which was developed by trial and error, is

$$d = 0.08 \, y_o \quad \text{if} \quad 0.08 \, y_o < \Delta s/2,$$

$$d = \Delta s/2 \quad \text{if} \quad 0.08 \, y_o > \Delta s/2. \tag{4.2.7}$$

Thus for elements near the axis of symmetry, for which y_o and Δs are of the same order of magnitude, the singular subelement is a small fraction of the total element. For elements having a value of y_o large compared to Δs the singular subelement is the entire element, and no contribution of the "ends" of the elements need be calculated.

In the above calculation the midpoint is assumed from the outset to lie on the element. Thus any contribution to the velocity that depends on the limiting process of approaching the surface is not included and must be added separately. As was stated in Section 2, the limiting process of approaching the surface gives rise to a velocity of magnitude 2π (for unit value of the local source density) with direction normal to the local surface. In component form this velocity is

$$V_x'' = -\, 2\pi \sin \beta,$$

$$V_y'' = 2\pi \cos \beta. \tag{4.2.8}$$

Thus in general the velocity components induced by an element at its own midpoint consist of the sum of three contributions: the numerical integration of (4.2.3) over the "ends" of the element, the series (4.2.6) for the effect of the singular subelement, and the components (4.2.8) arising from the limiting process of approaching the surface. The potential induced by an element at its own midpoint consists of the sum of contributions from the first two of these three.

Since a coordinate system based on the element is not used, the above formulas for velocity components induced by an element at the midpoint of any element, including itself, directly yield X_{ij} and Y_{ij}, the components of $\vec{V}_{ij}$ in the reference coordinate system (Eq. (3.3.3)).

When formulas (4.2.3) are used to compute quantities at points off the body surface, special treatment is required for points on the axis of symmetry. It can be seen that V_y is indeterminate for $y = 0$. However, it is clear from symmetry that in this case $V_y = 0$, and this value is simply used instead of the formula for V_y.

4.3 *Axisymmetric Bodies in Cross Flow*

If an axisymmetric body is immersed in an onset flow that is a uniform stream in a direction normal to the body's axis of symmetry, the velocity

potential and source-density distribution are proportional to the cosine of the circumferential angle. There is no other dependence on circumferential location. This fact, which was first stated by Lotz,[18] is discussed at some length in Ref. 2. Here space permits little elaboration on the brief discussion of subsection 3.3.4 and the general illustration of the flow contained in Fig. 4. The fact that the dependence of all quantities on circumferential location is known in advance for all body shapes permits this basically three-dimensional flow to be calculated without resort to fully three-dimensional techniques. In fact, computing times are scarcely greater than those for the case of axisymmetric flow. The same approach may be used for all flows having this circumferential variation. In particular, this includes the case of an axisymmetric body rotating about a line normal to and intersecting its axis of symmetry.

Since circumferential variations are known in advance, this case is similar to that of axisymmetric flow in that an integration in the circumferential direction may be performed in advance and all surface integrals reduced to single integrals over the profile curve of the body. This is equivalent to using a ring source whose strength is proportional to the cosine of the circumferential angle as the elementary singularity to be integrated over the line-segment elements that approximate the profile curve of the body.

Again the x-axis is taken as the axis of symmetry of the body, and the y-direction is the direction of zero value of circumferential angle. For the cross-flow case this means that the uniform onset flow is parallel to the positive y-axis, and for the rotating body the axis of rotation is parallel to the z-axis. Figure 9 illustrates a ring source of radius a lying in the plane $x = b$. The strength of the ring source is $\cos \psi$, where ψ is the circumferential angle around the ring. In computing the potential and velocity induced by this ring source at a point in space with coordinates x, y, z, it is convenient to introduce cylindrical coordinates $y = R \cos \theta$, $z = R \sin \theta$. The potential at this point due to the ring source is

$$\varphi = \int_{-\pi}^{\pi} \frac{a \cos \psi \, d\psi}{r} = \int_{-\pi}^{\pi} \frac{a \cos \psi \, d\psi}{\sqrt{[(x - b)^2 + R^2 + a^2 - 2R a \cos (\theta - \psi)]}} \quad (4.3.1)$$

By a change of variable this can be written

$$\varphi = 2a \cos \theta \int_0^{\pi} \frac{\cos \psi \, d\psi}{\sqrt{[(x - b)^2 + R^2 + a^2 - 2R a \cos \psi]}}. \quad (4.3.2)$$

The equivalence of (4.3.1) and (4.3.2) expresses the fact that a source density that varies as the cosine of the circumferential angle gives rise to a potential that also varies as the cosine of circumferential angle. That the converse of this statement is also true is due to the fact that the statement holds

for all harmonics; that is, a source density that varies as cos $m\psi$ gives rise to a potential that varies as cos $m\theta$ for all integer values of m.
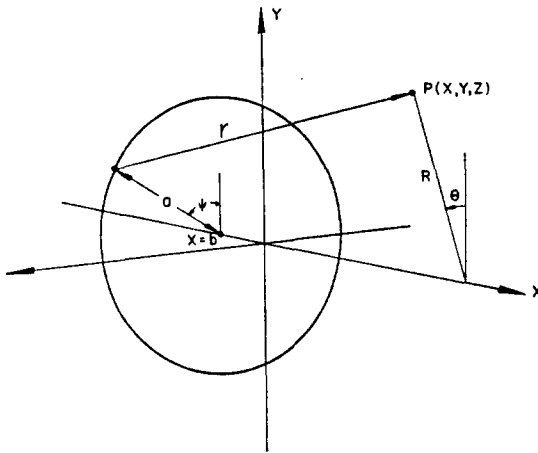
FIG. 9. A ring source whose strength is proportional to the cosine of the circumferential angle.

The axial, radial, and circumferential velocity components at the point (x, R, θ) due to the ring source are

$$V_x = -\frac{\partial q}{\partial x} = 2a\cos\theta \int_0^\pi \frac{(x-b)\cos\psi \, d\psi}{[(x-b)^2 + R^2 + a^2 - 2aR\cos\psi]^{\frac{3}{2}}},$$

$$V_R = -\frac{\partial q}{\partial R} = 2a\cos\theta \int_0^\pi \frac{(R - a\cos\psi)\cos\psi \, d\psi}{[(x-b)^2 + R^2 + a^2 - 2aR\cos\psi]^{\frac{3}{2}}}, \qquad (4.3.3)$$

$$V_\theta = -\frac{1}{R}\frac{\partial q}{\partial \theta} = \frac{2a\sin\theta}{R} \int_0^\pi \frac{\cos\psi \, d\psi}{\sqrt{[(x-b)^2 + R^2 + a^2 - 2aR\cos\psi]}}$$

These expressions explicitly exhibit the circumferential behavior that was discussed in subsection 3.3.4. At any point the potential and the axial and radial velocity components, which are the components in the plane containing the point and the body's axis of symmetry, vary as cos θ. These quantities are characterized by their values for $\theta = 0$, that is, their values at a point in the xy-plane having the same x and R. The circumferential velocity component, which is the component normal to the plane containing the point and

the body's axis of symmetry, varies as $\sin \theta$. This quantity is characterized by its value for $\theta = \pi/2$, that is, its value at the point in the xz-plane having the same x and R. The characteristic values of the potential and the circumferential velocity differ only by a factor equal to the radial coordinate of the point in question; that is,

$$[\varphi]_{\theta=0} = R[V_\theta]_{\theta=\pi/2}. \tag{4.3.4}$$

It is clear that the statements of this paragraph depend only on the fact that the potential varies as $\cos \theta$ and are not related to the fact that the quantities in question are due to a ring source.

In the detailed calculation the circumferential dependence is not directly considered, and the calculated results have no explicit circumferential dependence. The variations of quantities with θ need be kept in mind by a user of the method only when he is considering the flow at a particular value of θ. The essential quantities are the coefficients of $\sin \theta$ and $\cos \theta$ in (4.3.2) and (4.3.3). These are independent of θ and may be evaluated on the assumption that the point to which they are applicable lies in the xy-plane. Thus in calculation R is replaced by y, which becomes in a sense a radial coordinate, and the factors of $\sin \theta$ and $\cos \theta$ are ignored. The computation is reduced to one in the xy-plane, just as in the axisymmetric case.

Subject to the above interpretation, the velocity components at a point with coordinates x and y due to a ring source of radius a in the plane $x = b$ are

$$V_x = 2a \int_0^\pi \frac{(x - b) \cos \psi \, d\psi}{[(x - b)^2 + y^2 + a^2 - 2ay \cos \psi]^{\frac{3}{2}}},$$

$$V_y = 2a \int_0^\pi \frac{(y - a \cos \psi) \cos \psi \, d\psi}{[(x - b)^2 + y^2 + a^2 - 2ay \cos \psi]^{\frac{3}{2}}}, \tag{4.3.5}$$

$$V_\theta = \frac{2a}{y} \int_0^\pi \frac{\cos \psi \, d\psi}{\sqrt{[(x - b)^2 + y^2 + a^2 - 2ay \cos \psi]}}.$$

A corresponding expression for the potential is not required, since that quantity is finally, calculated from the circumferential velocity as described in Section 3.5.

The same substitutions used for the axisymmetric case and some algebraic manipulation enable the formulas (4.3.5) to be expressed in terms of complete elliptic integrals in the form[2]

$$V_x = \frac{-2(x-b)}{y\sqrt{[(y+a)^2+(x-b)^2]}}\left[K(k)-\frac{y^2+a^2+(x-b)^2}{(y-a)^2+(x-b)^2}E(k)\right],$$

$$V_y = \frac{2}{y^2\sqrt{[(y+a)^2+(x-b)^2]}}\left[[(x-b)^2+a^2]K(k)\right.$$

$$\left. - \frac{[(x-b)^2+a^2]^2+y^2\,[(x-b)^2-a^2]}{(y-a)^2+(x-b)^2}E(k)\right],$$

$$V_\theta = -\frac{2}{y^2}\sqrt{[(y+a)^2+(x-b)^2]}\left[\frac{y^2+a^2+(x-b)^2}{(y+a)^2+(x-b)^2}K(k)-E(k)\right].$$

$$(4.3.6)$$

Again, K and E denote complete elliptic integrals of the first and second kinds, respectively, and

$$k^2 = \frac{4ay}{(y+a)^2+(x-b)^2},\qquad (4.3.7)$$

which is identical with (4.2.4). A comparison of the formulas (4.3.6) with the corresponding expressions (4.2.3) for the axisymmetric case reveals their considerable computational similarity. Not only are the elliptic integrals the same in both cases, but many algebraic quantities are common. The two sets of formulas may be calculated together in only a little more time than that required for one set.

To obtain the velocity components induced by an element at a point in space, formulas (4.3.6) must be integrated over a line segment. This is accomplished in exactly the same way as in the axisymmetric case. For points not on the element, that is, for all points except the midpoint of the line segment, the integration is performed numerically in the manner described in Section 4.2.

The effect of the element at its own midpoint is calculated as the sum of three contributions, just as in the axisymmetric case. The singular sub-element is as shown in Fig. 8, and its contributions to the velocity components at the midpoint are obtained by integrating expansions in s/y_0 as described in Section 4.2. The results are

$$V_x' = -\sin 2\beta \left(\frac{d}{y_0}\right)\left\{1-\frac{1}{48}\left(\frac{d}{y_0}\right)^2\left[9-2\sin^2\beta+6\ln\left(\frac{1}{8}\frac{d}{y_0}\right)\right]+\ldots\right\},$$

$$V_y' = -2\left(\frac{d}{y_0}\right)\left\{\left[2+\sin^2\beta+\ln\left(\frac{1}{8}\frac{d}{y_0}\right)\right]+\frac{1}{144}\left(\frac{d}{y_0}\right)^2\right.$$

$$\times\left.\left[9-43\sin^2\beta+6\sin^4\beta+(27-24\sin^2\beta)\ln\left(\frac{1}{8}\frac{d}{y_0}\right)\right]+\ldots\right\},$$

$$V_\theta' = 4\left(\frac{d}{y_0}\right)\left\{\left[1+\ln\left(\frac{1}{8}\frac{d}{y_0}\right)\right]-\frac{1}{144}\left(\frac{d}{y_0}\right)^2\right.$$

$$\times\left.\left[10\sin^2\beta+(6\sin^2\beta-9)\ln\left(\frac{1}{8}\frac{d}{y_0}\right)\right]+\ldots\right\}. \qquad (4.3.8)$$

The series are terminated after the third-order terms shown, and $\dot{d}$ is determined by (4.2.7). The contributions of the "ends" of the element are calculated as if these portions were separate elements. The third contribution, that due to the limiting process of approaching the surface, is again given by (4.2.8) and nothing is added to V_θ.

When the above formulas are used to calculate the velocity components at each other's midpoints, the results give the components X_{ij}, Y_{ij}, and Θ_{ij} directly. It is not necessary to perform a transformation into the reference coordinate system.

Formulas (4.3.6) are singular for $y = 0$, that is, for points on the axis of symmetry. As was pointed out in Section 4.2, a midpoint of an element cannot lie on the axis of symmetry, but this situation can arise for points off the body surface. For such points different equations must be used for the velocity components due to a ring source. Specifically, the velocity components induced at a point on the x-axis by a ring source whose strength varies as $\cos \psi$ are

$$V_x = 0$$

$$V_y = V_\theta = \frac{-\pi a^2}{[(x - b)^2 + a^2]^{\frac{3}{2}}}.$$

$(4.3.9)$

This expression is integrated over an element in the usual way. The potential is zero, since it equals V_θ multiplied by the zero value of the y-coordinate.

4.4 Three-dimensional Bodies

The integration of the basic point-source formulas over one of the quadrilateral elements used to approximate three-dimensional bodies is most conveniently done in a coordinate system for which the element lies in a coordinate plane. Specifically, the quadrilateral is taken to lie in the xy-plane as shown in Fig. 10. The positive z-axis (upward in Fig. 10) of the coordinate system is in the direction of the unit outward normal vector to the element. The four points at the corners of the quadrilateral are denoted by subscripts 1, 2, 3, 4, where the numbering denotes the order in which the corner points are encountered as the perimeter of the quadrilateral is traversed in the clockwise sense as seen from the positive z-axis. The coordinates of the corner points are $\xi_k, \eta_k, 0$, where $k = 1, 2, 3, 4$, and the maximum dimension of the quadrilateral is denoted by t. For the purposes of the multipole expansion, the origin of the coordinate system is taken as the centroid of the area of the quadrilateral, but this is not essential for the exact analytic integration. For definiteness, the x-axis of the coordinate system is taken parallel to the vector from corner point 1 to corner point 3. This last choice is nonessential, and indeed it affects none of the formulas of this section except Eqs. (4.4.27), the formulas for the moments of the area.

E

It is desired to calculate the potential and velocity induced by the quadri-
lateral at a point in space with coordinates x, y, z in the element coordinate
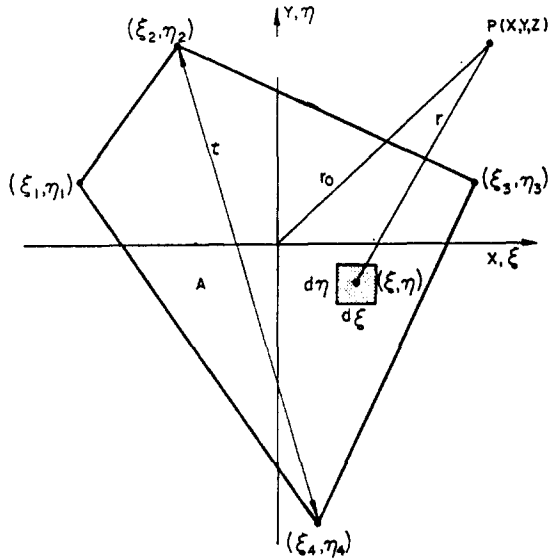
FIG. 10. A plane quadrilateral lying in the xy-plane.

system. The distance between this point and a point on the quadrilateral
with coordinates ξ, η, 0 is

$$r = \sqrt{[(x - \xi)^2 + (y - \eta)^2 + z^2]} \qquad (4.4.1)$$

For a unit value of source density, the potential due to the quadrilateral
at the point (x, y, z) is

$$\varphi = \iint_A \frac{dA}{r} \qquad (4.4.2)$$

where A denotes the area of the quadrilateral. The integral in (4.4.2) can
be obtained exactly by analytical means. The approach adopted here differs
somewhat from that of Ref. 3. First, a cylindrical coordinate system is intro-
duced, whose axis is parallel to the z-axis and whose origin is the point
$(x, y, 0)$ as shown in Fig. 11. The polar angle θ is measured clockwise from
any convenient reference direction, which is shown as the negative x-axis in
Fig. 11. Distance from the axis of the cylindrical coordinate system is denoted
by R. In terms of these variables,

$$r = \sqrt{(R^2 + z^2)} \qquad (4.4.3)$$

and thus

$$\varphi = \oint \int_0^R \frac{R \, dR \, d\theta}{\sqrt{(R^2 + z^2)}} \qquad (4.4.4)$$

The R integration is carried from $R = 0$ to a point on the perimeter, and the θ integration is around the perimeter in the clockwise sense. The contribution of each side of the quadrilateral to the integral in (4.4.4) represents the potential of the plane triangle defined by the endpoints of the side and
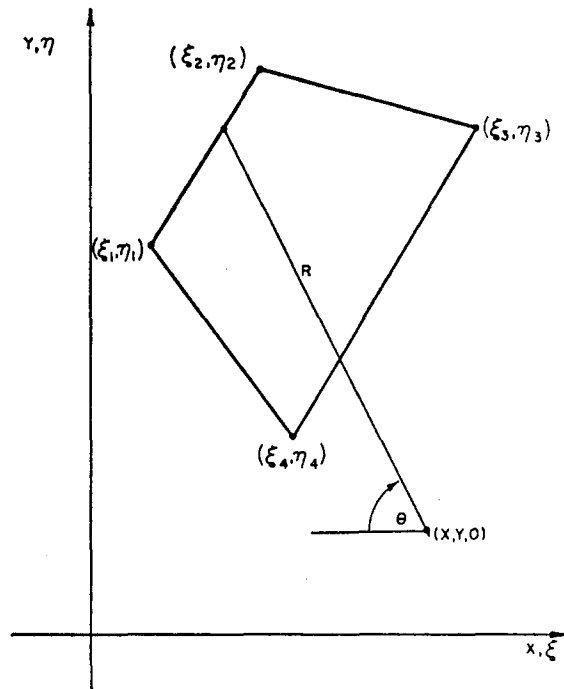
FIG. 11. Introduction of cylindrical coordinates.

the point $(x, y, 0)$. As the perimeter is traversed in the clockwise direction. the incremental angle $d\theta$ is positive if the point $(x, y, 0)$ lies to the right of the side and negative if it lies to the left. Thus when potentials of the triangles corresponding to all four sides of the quadrilateral are summed, the contributions of the portions of the triangles outside the quadrilateral sum to zero, and the result is the potential of the quadrilateral itself. Now from (4.4.3),

$$dr = \frac{R \, dR}{\sqrt{(R^2 + z^2)}} \qquad (4.4.5)$$

and thus (4.4.4) becomes

$$\varphi = \oint [\int_{|z|}^{r} dr]\, d\theta = \oint (r - |z|)\, d\theta \qquad (4.4.6)$$

Since z does not depend on position on the perimeter, this can be written

$$\varphi = \oint r\, d\theta - |z|\, \Delta\theta, \qquad (4.4.7)$$

where $\Delta\theta = 0$ if $x, y, 0$ lies outside the quadrilateral

and $\Delta\theta = 2\pi$ if $x, y, 0$ lies inside the quadrilateral. $\qquad (4.4.8)$

Thus the second term of (4.4.7) is discontinuous as $(x, y, 0)$ crosses a side of the quadrilateral. The first term has an equal and opposite discontinuity, and thus the potential is continuous. (This last is due to the change of sign of $d\theta$ along the side that is crossed.)

The first term of (4.4.7) is evaluated by calculating the contribution of a single side to the integral and summing the results for all four sides. (Obviously the results can be generalized to polygons having any number of sides.) To express the contribution of the side between the points $(\xi_1, \eta_1, 0)$ and $(\xi_2, \eta_2, 0)$ to the integral of (4.4.7), the following geometric quantities, most of which are illustrated in Fig. 12, must be defined. The length of the side is

$$d_{12} = \sqrt{[(\xi_2 - \xi_1)^2 + (\eta_2 - \eta_1)^2]}. \qquad (4.4.9)$$
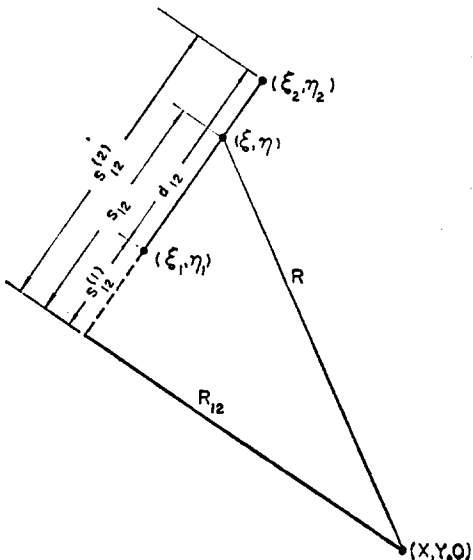
FIG. 12. Integration over a side of a quadrilateral.

The cosine and sine of the slope angle of the side with respect to the x-axis are, respectively,

$$C_{12} = \frac{\xi_2 - \xi_1}{d_{12}} \quad \text{and} \quad S_{12} = \frac{\eta_2 - \eta_1}{d_{12}} \qquad (4.4.10)$$

A perpendicular to the side is drawn from $(x, y, 0)$, and arc length s_{12} is measured along the side from the intersection of the perpendicular with the extension of the side. The positive direction of s_{12} is that from $(\xi_1, \eta_1, 0)$ to $(\xi_2, \eta_2, 0)$. The arc length associated with a general point on the side is

$$s_{12} = (\xi - x) C_{12} + (\eta - y) S_{12} \tag{4.4.11}$$

In particular, the arc lengths associated with the corner points $(\xi_1, \eta_1, 0)$ and $(\xi_2, \eta_2, 0)$ are, respectively,

$$s_{12}^{(1)} = (\xi_1 - x) C_{12} + (\eta_1 - y) S_{12}$$
and
$$s_{12}^{(2)} = (\xi_2 - x) C_{12} + (\eta_2 - y) S_{12} \tag{4.4.12}$$

The signed perpendicular distance of the point $(x, y, 0)$ from the extension of the side is

$$R_{12} = (x - \xi_1) S_{12} - (y - \eta_1) C_{12}. \tag{4.4.13}$$

This distance is positive if $(x, y, 0)$ lies to the right of the side with respect to the direction from $(\xi_1, \eta_1, 0)$ to $(\xi_2, \eta_2, 0)$ and is negative if $(x, y, 0)$ lies to the left. The coordinates ξ_2, η_2 could replace η_1, η_1 in (4.4.13) without changing the value of R_{12}. The distances of the point (x, y, z) to the corner points $(\xi_1, \eta_1, 0)$ and $(\xi_2, \eta_2, 0)$ are, respectively,

$$r_1 = \sqrt{[(x - \xi_1)^2 + (y - \eta_1)^2 + z^2]}$$
and
$$r_2 = \sqrt{[(x - \xi_2)^2 + (y - \eta_2)^2 + z^2]} \tag{4.4.14}$$

The required integral can be expressed in terms of the following two quantities:

$$Q_{12} = \ln\left(\frac{r_2 + s_{12}^{(2)}}{r_1 + s_{12}^{(1)}}\right) = \ln\left(\frac{r_1 + r_2 + d_{12}}{r_1 + r_2 - d_{12}}\right) \tag{4.4.15}$$

and

$$J_{12} = \operatorname{sgn}(R_{12}) \left[\tan^{-1}\left(\left|\frac{z}{R_{12}}\right|\frac{s_{12}^{(2)}}{r_2}\right) - \tan^{-1}\left(\left|\frac{z}{R_{12}}\right|\frac{s_{12}^{(1)}}{r_1}\right)\right]$$

$$= \tan^{-1}\left[\frac{R_{12}\,|z|\,(r_1 s_{12}^{(2)} - r_2 s_{12}^{(1)})}{r_1 r_2 R_{12}^2 + z^2 s_{12}^{(2)} s_{12}^{(1)}}\right] \tag{4.4.16}$$

The second form of the logarithm in (4.4.15) is to be preferred, since the first is indeterminate along the extension of the side. In the first form of (4.4.16), the inverse tangents are evaluated in the principal-value range $-\pi/2$ to $\pi/2$, and in the second form of (4.4.16) the inverse tangent is evaluated in the range $-\pi$ to π by considering the individual signs of the numerator and denominator of its argument.

The contribution of the side between $(\xi_1, \eta_1, 0)$ and $(\xi_2, \eta_2, 0)$ to the integral of (4.4.7) is

$$\varphi_{12} = R_{12}\,Q_{12} + |z|\,J_{12}. \qquad (4.4.17)$$

The contribution φ_{23} of the side between $(\xi_2, \eta_2, 0)$ and $(\xi_3, \eta_3, 0)$ is found by advancing all subscripts and superscripts by unity in Eqs. (4.4.9) through (4.4.17) and similarly for the remaining sides of the quadrilateral.

Thus the potential at the point (x, y, z) induced by the quadrilateral is

$$\varphi = \varphi_{12} + \varphi_{23} + \varphi_{34} + \varphi_{41} - |z|\,\Delta\theta. \qquad (4.4.18)$$

The velocity components may be found by differentiating (4.4.18). If this is done, all algebraic terms resulting from the differentiation of the logarithms and inverse tangents sum to zero and the results are

$$\left.\begin{aligned}
V_x &= -\frac{\partial\varphi}{\partial x} = -\,S_{12}\,Q_{12} - S_{23}\,Q_{23} - S_{34}\,Q_{34} - S_{41}\,Q_{41}, \\[2ex]
V_y &= -\frac{\partial\varphi}{\partial y} = \,C_{12}\,Q_{12} + C_{23}\,Q_{23} + C_{34}\,Q_{34} + C_{41}\,Q_{41}, \\[2ex]
V_z &= -\frac{\partial\varphi}{\partial z} = \operatorname{sgn}\,(z)\,[\Delta\theta - J_{12} - J_{23} - J_{34} - J_{41}].
\end{aligned}\right\} \qquad (4.4.19)$$

These are the required equations.

It may be verified from these equations that no difficulty is encountered in calculating the effects of an element at its own control point. The Q's are singular only on the sides of the quadrilateral. For $z = 0$ all the J's vanish. Thus φ, V_x, and V_y are regular functions, and for $z = 0$

$$V_z = \operatorname{sgn}\,(z)\,\Delta\theta, \qquad (4.4.20)$$

which is $2\pi\operatorname{sgn}(z)$ for a point on the element and zero for a point outside. The control point is defined to have $z = 0+$. Incidentally, $\Delta\theta$ is easy to evaluate; it is 2π if R_{12}, R_{23}, R_{34}, and R_{41} are all positive, and it is zero otherwise.

Evaluation of formulas (4.4.18) and (4.4.19) is quite time-consuming, since at least four logarithms, four inverse tangents, and four square roots are required. The complicated nature of these formulas arises from the fact that they account for the effects of all the details of the shape of the quadrilateral. It is intuitively plausible that if the point (x, y, z) is sufficiently far from the quadrilateral, the details of the shape of the quadrilateral are unimportant, and the potential and velocity at that point depend mainly on certain overall parameters that characterize that shape. This consideration leads naturally to approximation by means of a multipole expansion of the type commonly used in electrostatics.[19]

Again, the situation is that shown in Fig. 10. It is desired to approximate the integral of (4.4.2) that gives the potential induced by the quadrilateral at the point (x, y, z). To accomplish this, the integrand of (4.4.2), which is simply $1/r$, is expanded in a Taylor series in ξ and η about the origin. The coefficients in the series, being independent of ξ and η, may be taken out of the integral. Through terms of second order the result of thus expanding Eq. (4.4.2) is

$$\varphi = I_{00}w - (I_{10}w_x + I_{01}w_y) + \tfrac{1}{2}(I_{20}w_{xx} + 2I_{11}w_{xy} + I_{02}w_{yy}) + \dots,$$
(4.4.21)

where

$$I_{nm} = \iint_A \xi^n \eta^m \, dA$$
(4.4.22)

and where w is the reciprocal of the distance r_0 from the origin of coordinates to the point (x, y, z), that is,

$$w = \frac{1}{r_0} = \frac{1}{\sqrt{(x^2 + y^2 + z^2)}}.$$
(4.4.23)

The subscripts x and y in Eq. (4.4.21) denote partial derivatives with respect to these variables. These derivatives depend only on the location of the point (x, y, z) with respect to the origin of coordinates and are independent of the shape of the quadrilateral. On the other hand, the quantities I_{nm} depend only on the shape of the quadrilateral and are independent of the location of the point (x, y, z). They may be evaluated once and for all for each quadrilateral. The I_{nm} are the moments of various orders of the area of the quadrilateral about the origin. In particular, I_{00} is just the area of the quadrilateral, I_{10} and I_{01} are the first moments, and I_{20}, I_{11}, and I_{02} are the second moments or "moments of inertia". Higher order terms of the expansion consist of products of higher order derivatives of w and higher order moments of the area. Such an expansion may be rigorously shown to converge if the point (x, y, z) is farther from the origin than any point of the quadrilateral.

The designation multipole expansion arises from the fact that the various terms in Eq. (4.4.21) may be interpreted as the potentials of point singularities of various orders located at the origin. Thus the first term is the potential of a point source. The second term consists of the potentials of two point dipoles, whose axes lie along the x-axis and the y-axis, respectively. The third term contains the potentials of the three independent point quadrupoles with axes in the xy-plane. The strengths of the singularities are the various moments of the area of the quadrilateral. The effect of each successive higher order singularity decreases with a successively higher power of the distance r_0. Thus the expansion (4.4.21) may be interpreted as giving the effect of the

quadrilateral in terms of its overall geometric properties "in order of their importance" at some distance from the quadrilateral.

In actual calculation the expansion (4.4.21) is not carried beyond the second-order terms shown. Since the centroid of the area of the quadrilateral is used as the origin of coordinates, the first moments I_{10} and I_{01} are zero. There are no dipole terms in (4.4.21), only a source plus quadrupole. The multipole expansion may thus be written

$$
\left.
\begin{aligned}
\varphi &= I_{00}\, w + \tfrac{1}{2}(I_{20}\, w_{xx} + 2I_{11}\, w_{xy} + I_{02}\, w_{yy}), \\[6pt]
V_x &= -\frac{\partial \varphi}{\partial x} = -\,I_{00}\, w_x - \tfrac{1}{2}(I_{20}\, w_{xxx} + 2I_{11}\, w_{xxy} + I_{02}\, w_{xyy}), \\[6pt]
V_y &= -\frac{\partial \varphi}{\partial y} = -\,I_{00}\, w_y - \tfrac{1}{2}(I_{20}\, w_{xxy} + 2I_{11}\, w_{xyy} + I_{02}\, w_{yyy}), \\[6pt]
V_z &= -\frac{\partial \varphi}{\partial z} = -\,I_{00}\, w_z - \tfrac{1}{2}(I_{20}\, w_{xxz} + 2I_{11}\, w_{xyz} + I_{02}\, w_{yyz}),
\end{aligned}
\right\} \quad (4.4.24)
$$

where w and its derivatives are

$$
\begin{aligned}
w &= r_o^{-1} & w_{xxx} &= 3x(3p + 10x^2)\, r_o^{-7} \\[4pt]
w_x &= -x\, r_o^{-3} & w_{xxy} &= 3y\, p\, r_o^{-7} \\[4pt]
w_y &= -y\, r_o^{-3} & w_{xyy} &= 3x\, q\, r_o^{-7} \\[4pt]
w_z &= -z\, r_o^{-3} & w_{yyy} &= 3y(3q + 10y^2)\, r_o^{-7} \\[4pt]
w_{xx} &= -(p + 2x^2)\, r_o^{-5} & w_{xxz} &= 3z\, p\, r_o^{-7} \\[4pt]
w_{xy} &= 3xy\, r_o^{-5} & w_{xyz} &= -15x\, y\, z\, r_o^{-7} \\[4pt]
w_{yy} &= -(q + 2y^2)\, r_o^{-5} & w_{yyz} &= 3z\, q\, r_o^{-7}
\end{aligned}
$$

$$(4.4.25)$$

The distance r_o is given by (4.4.23) and

$$
p = y^2 + z^2 - 4x^2, \qquad q = x^2 + z^2 - 4y^2. \qquad (4.4.26)
$$

These formulas appear somewhat lengthy. However, their evaluation involves only simple arithmetic plus one square root, r_o. They thus require much less computing time than the exact formulas. For the same reason, the multipole expression is faster than a numerical integration over the element, which employs point sources located at a set of mesh points and thus must evaluate a square root for each mesh point.

The moments I_{nm} may be expressed in terms of the coordinates of the corner points, $(\xi_k, \eta_k, 0)$ where $k = 1, 2, 3, 4$. The x-direction is taken as parallel to the direction from $(\xi_1, \eta_1, 0)$ to $(\xi_3, \eta_3, 0)$. This choice gives $\eta_1 = \eta_3$, and the moments required for use in (4.4.24) are

$$I_{00} = \tfrac{1}{2}(\xi_3 - \xi_1)(\eta_2 - \eta_4),$$

$$I_{20} = \tfrac{1}{12}(\xi_3 - \xi_1)[\eta_1(\xi_4 - \xi_2)(\xi_1 + \xi_2 + \xi_3 + \xi_4)$$

$$+ (\eta_2 - \eta_4)(\xi_1^2 + \xi_1\xi_3 + \xi_3^2) + \xi_2\eta_2(\xi_1 + \xi_2 + \xi_3)$$

$$- \xi_4\eta_4(\xi_1 + \xi_3 + \xi_4)],$$

$$I_{11} = \tfrac{1}{24}(\xi_3 - \xi_1)[2\xi_4(\eta_1^2 - \eta_4^2) - 2\xi_2(\eta_1^2 - \eta_2^2)$$

$$+ (\xi_1 + \xi_3)(\eta_2 - \eta_4)(2\eta_1 + \eta_2 + \eta_4)],$$

$$I_{02} = \tfrac{1}{12}(\xi_3 - \xi_1)(\eta_2 - \eta_4)[(\eta_1 + \eta_2 + \eta_4)^2 - \eta_1(\eta_2 + \eta_4) - \eta_2\eta_4].$$

$$(4.4.27)$$

If the point (x, y, z) is far enough from the element, the quadrupole terms of (4.4.24) are not required. The quadrilateral may be approximated by a point source at its centroid. This is equivalent in accuracy to a source plus dipole. For the point-source calculation there is no need to use a coordinate system based on the element, and the calculation may be performed directly in the reference coordinate system in which the body was input. Let x_0, y_0, z_0 be the reference coordinates of the centroid of the quadrilateral, and let x', y', z' be the reference coordinates of the point where potential and velocity are to be evaluated (the point (x, y, z) in element coordinates). If the element is approximated by a point source, the potential and velocity components are calculated from

$$\varphi = \frac{1}{r_0} I_{00},$$

$$V_x = \frac{x' - x_0}{r_0^3} I_{00},$$

$$V_y = \frac{y' - y_0}{r_0^3} I_{00}, \qquad (4.4.28)$$

$$V_z = \frac{z' - z_0}{r_0^3} I_{00},$$

where

$$r_0 = \sqrt{[(x' - x_0)^2 + (y' - y_0)^2 + (z' - z_0)^2]} \qquad (4.4.29)$$

The distance r_0 is the same as that of Eq. (4.4.23), but here it is calculated in a different coordinate system.

Thus there are three sets of formulas for calculating the potential and velocity induced by an element at a point in space. The choice of which set to use is determined by the value of the ratio r_0/t, where r_0 is the distance

of the point in question from the centroid of the quadrilateral and t is the maximum dimension of the quadrilateral as shown in Fig. 10. If $r_0/t > 4$, the point-source formulas (4.4.28) are used, and the calculation is performed directly in the reference coordinate system. If $r_0/t < 4$, the coordinates of the point in question are transformed into the element coordinate system. Then if $r_0/t > 2.45$, the multipole formulas (4.4.24) are used, but if $r_0/t < 2.45$, the exact formulas (4.4.18) and (4.4.19) are used. In the latter two cases the calculated velocity components must be transformed into the reference coordinate system. These distance criteria were chosen somewhat arbitrarily and appear to be conservative. Any errors arising from the use of the point source or multipole formulas are apparently negligible with respect to those due to the basic approximation of the body surface by plane elements having a constant value of source density. Thus the use of the approximate formulas involves no loss at all in overall accuracy. The savings in computation time are quite significant, however. In a typical case about 90 per cent of the entries of the induced potential and velocity matrices, Φ_{ij} and $\vec{V}_{ij}$, are calculated from the point-source formulas, and the remaining 10 per cent are divided about evenly between the multipole and the exact formulas. Since the criteria for deciding which set of formulas to use is based on the value of r_0/t, the number of entries of the induced potential and velocity matrices that are computed by the exact and the multipole formulas is approximately proportional to the element number N. The total number of entries is proportional to N^2. Thus the greater the element number, the greater the percentage of entries computed by the point-source formulas.

4.5 Hydrofoils

4.5.1 *The fundamental source function.* A hydrofoil is an airfoil moving beneath the free surface of a liquid that is subject to the force of gravity. It is the presence of this free surface that not only distinguishes hydrofoils from airfoils but also greatly complicates the problem of calculation. The study is restricted to the problem of steady motion in infinitely deep water or other liquid, and, as in the preceding sections, viscosity is neglected. Again, the location of the boundary must be known, which essentially restricts the treatment to hydrofoils free of cavitation. If local cavitation occurs and the edge of the bubble is known, the method of course remains applicable and calculation of slightly cavitated flow may be accomplished by some sort of iterative process. Another restriction must be mentioned, one that does not exist in an unbounded atmosphere. The depth below the surface is a parameter that enters into the formulation. Therefore a two-dimensional flow requires the body not only to be two-dimensional but also that all sections be at the same depth, for otherwise the flow would change from section to section laterally.

The flow situation is shown in Fig. 13; note that the hydrofoils are located in the lower halfplane and that the onset flow is V_∞ in the x-direction. Because the fluid is assumed to be inviscid, free of vorticity, and incompressible, Laplace's equation applies as usual. The mean free surface is at $y = 0$, and
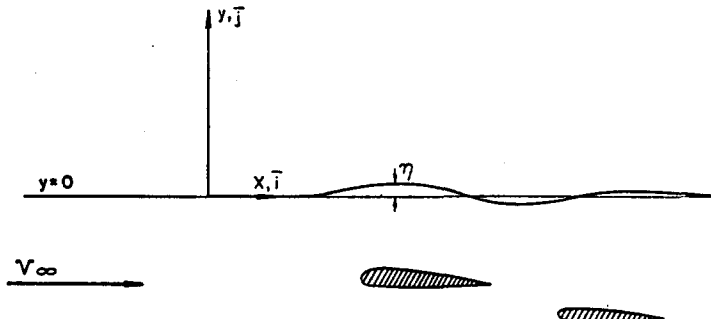
Fig. 13. Diagram for analysis of flow about hydrofoils.

distortions from this mean are indicated by η, as in the sketch. The pressure and velocity can be related by Bernouilli's equation, which is written here in a form slightly different from that of (1.2.10), to exhibit a term for hydrostatic head, as follows:

$$p/\rho + \tfrac{1}{2}|\vec{V}|^2 + g\,y = \text{const.} \qquad (4.5.1)$$

For small disturbances it is easily shown that if p is constant on the free surface, (4.5.1) can be linearized to yield

$$V_\infty \frac{\partial \varphi}{\partial x}(x, 0) = -g\,\eta \qquad (4.5.2)$$

where φ, as usual, means perturbation potential. After the boundary-value problem is solved, this relation can be conveniently used to compute wave height. A second condition, arising from kinematic considerations requires that the free surface $\eta(x)$ be a streamline. In mathematical terms the usual approximate statement of this condition is

$$\frac{\partial \varphi}{\partial y}(x, 0) = V_\infty \frac{\partial \eta}{\partial x} \qquad (4.5.3)$$

Elimination of η between (4.5.2) and (4.5.3) yields

$$\frac{\partial^2 \varphi}{\partial x^2}(x, 0) + \nu \frac{\partial \varphi}{\partial y}(x, 0) = 0, \quad \text{where } \nu = \frac{g}{V_\infty^2}. \qquad (4.5.4)$$

This is the linearized free-surface condition that will be satisfied.

Another characteristic that distinguishes this problem from the usual problem of incompressible aerodynamics is that there are waves in the fluid downstream of the moving body, and any method of solution must exhibit this feature. In the problem of steady motion of a hydrofoil in infinitely deep water, the set of conditions that must be met by an elementary singularity is then as follows:

1. $\nabla^2 \varphi = 0$ for $y < 0$ except at the singularity,

2. $\dfrac{\partial^2 \varphi}{\partial x^2}(x, 0) + \nu \dfrac{\partial \varphi}{\partial y}(x, 0) = 0,$ where $\nu = \dfrac{g}{V_\infty^2}$,

(4.5.5)

3. $\lim\limits_{y \to -\infty} \text{grad } \varphi = 0,$

4. $\lim\limits_{x \to -\infty} \text{grad } \varphi = 0.$

Further details are contained in Refs. 7, 20, 21, and 22. Equations (4.5.5) replace (1.2.7) and (1.2.9), which are appropriate for the case of an unbounded fluid. The distribution of singularity over the body surface is determined from (1.2.8) as usual.

Different types of problems may need different elementary singularities. As in unbounded potential flow, for ordinary three-dimensional bodies the elementary singularity is a point source, which may be integrated into lines or rings to give the elementary singularities appropriate for two-dimensional or axisymmetric bodies, respectively. If the body is near an impervious plane wall, the elementary singularity whose potential inherently satisfies the additional boundary condition imposed by the wall is a source plus its image of the same sign. In the case of a cascade of bodies (see Section 4.6) the elementary singularity is an infinite grid of equally spaced parallel line sources of constant strength. Similarly, the elementary singularity that meets the hydrofoil requirements (4.5.5) has a potential that is the real part of the following expression for the complex potential, $f(z)$:

$$f(z) = K \ln (z - c) + \bar{K} \ln (z - \bar{c}) - 2\pi i \bar{K} \exp \left[-i\nu(z - \bar{c}) \right]$$

$$+ 2\bar{K} \cdot PV \int_0^\infty \frac{\exp \left[-ik(z - \bar{c}) \right]}{k - \nu} \, dk, \qquad (4.5.6)$$

where PV represents the principal value. At this point it becomes convenient to use complex algebra with notation defined as follows:

$K = Q + i\Gamma$, complex source strength, per unit length

$Q = $ line source strength

$\Gamma = $ vortex strength

$z = x + iy$, coordinates of a general point

$c = a + ib$, coordinates of the complex source

k = a parameter of integration

A bar over a symbol denotes complex conjugate.

The geometry of the complex source represented by (4.5.6) is shown in Fig. 14. Equation (4.5.6) is equivalent to Eq. (13.43) of Wehausen,[20] the two equations differing only in that Eq. (4.5.6) has a factor of 2π and two
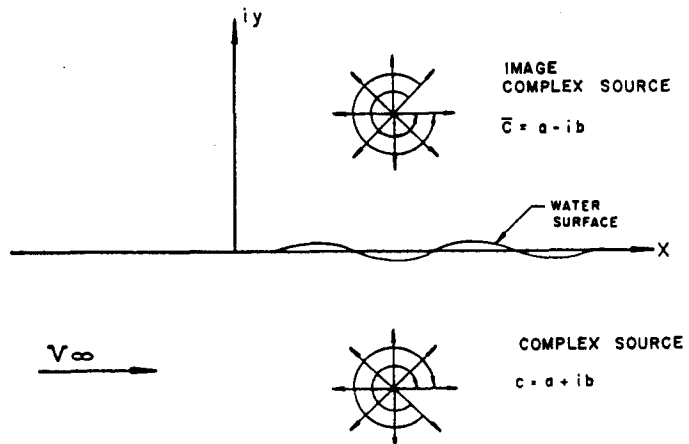
FIG. 14. The complex source and its image.

signs that are opposite to the corresponding signs in Wehausen's equation. These are the sign of $\Gamma(K = Q + i\Gamma)$ and the sign of the third term on the right side of the equation. The difference in signs is due to the opposite sense taken for positive vorticity and to the opposite direction of the onset flow. In Wehausen's formulation of the problem the wake is at the left of the source; in the present formulation it is at the right.

As in the previous section, for purposes of setting up the integral equation, the velocity field is of primary interest. It is easily obtained by determining the complex derivative of (4.5.6) in the usual fashion; that is, (4.5.6), together with the well-known relation $w(z) = df/dz = V_x - iV_y$, yields

$$w(z) = \frac{K}{z - c} + \frac{\bar{K}}{z - \bar{c}} - 2\pi \bar{K}\nu \exp\left[-i\nu(z - \bar{c})\right]$$

$$- 2\bar{K}i\,PV \int_0^\infty \frac{k \exp\left[-ik(z - \bar{c})\right]}{k - \nu}\,dk \qquad (4.5.7)$$

The first term on the right of (4.5.7) contains the basic two-dimensional source, and the second contains the image of the source with respect to the

plane $y = 0$. The last three terms are corrections that make the entire function satisfy the linearized free-surface conditions (4.5.5). Downstream, the quantities given by the last two terms have a reinforcing effect and upstream, the opposite. In this fashion a wake is developed downstream. Now consider the effect of the magnitude of V_∞ on the last two terms of (4.5.7). When V_∞ is small, ν is large. Then, according to condition 2 of (4.5.5), $\varphi_y(x, 0) = 0$. Thus, as in a common ground-plane condition, there is no flow through the plane $y = 0$. Inspection, and a small amount of calculation, will show that (4.5.7) satisfies this condition. Obviously, the last term approaches zero as ν approaches infinity. As long as $z - \bar{c}$ in the third term on the right contains a finite imaginary quantity, it too will approach zero as ν approaches infinity. When V_∞ is very large, ν approaches zero. Then the condition 2 of (4.5.5) reduces to $q_{xx}(x, 0) = 0$. This condition can be met by a source of strength Q whose image with respect to the plane $y = 0$ is one of strength $(-Q)$. Although it cannot be seen simply by inspection, it can be shown that (4.5.7) reduces to such a pair of sources as ν approaches zero.

4.5.2 *Integration over a line-segment element.* If a treatment similar to that for two-dimensional bodies is followed, the problem is to find the velocity components at a point z due to singularities of unit strength distributed over a line-segment element as sketched in Fig. 15. Consider a line source of infinitesimal width such that

$$K = \kappa \, ds = (\sigma + i\gamma) \, ds \; . \tag{4.5.8}$$
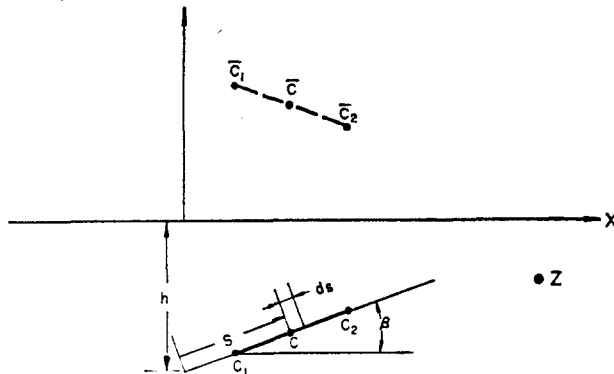
FIG. 15. Integration over a line-segment element.

Now consider the first term on the right of (4.5.7). Integration requires evaluation of the following quantity:

$$\kappa \int_{c_1}^{c_2} \frac{ds}{z - c} \; .$$

To perform the integration, an expression for ds in terms of c is needed. According to Fig. 15, the equation for a point c lying on the element is $c = -ih + s\,e^{i\beta}$. Hence $ds = e^{-i\beta}\,dc$, and the above integral becomes

$$\kappa\,e^{-i\beta} \int_{c_1}^{c_2} \frac{dc}{z - c} = \kappa\,e^{-i\beta} \ln \frac{z - c_1}{z - c_2}. \tag{4.5.9}$$

A similar expression can be written for the image source. Integration of the third term can be performed in a like manner. Finally, consider the definite integral. Upon introducing the relation $ds = e^{i\beta}\,d\bar{c}$, this becomes

$$2\bar{\kappa}e^{i\beta} \left[\int_0^\infty \frac{\exp\,[-ik(z - \bar{c}_2)]}{k - \nu}\,dk - \int_0^\infty \frac{\exp\,[-ik(z - \bar{c}_1)]}{k - \nu}\,dk \right]$$

Then the entire expression for the complex velocity $W(z) = V_x - iV_y$ of the line-segment element can be written

$$W(z) = \kappa\,e^{-i\beta} \ln \frac{z - c_1}{z - c_2} + \bar{\kappa}\,e^{i\beta} \ln \frac{z - \bar{c}_1}{z - \bar{c}_2}$$

$$+ 2\pi\,i\bar{\kappa}\,e^{i\beta} \{\exp\,[-i\nu(z - \bar{c}_2)]$$

$$- \exp\,[-i\nu(z - \bar{c}_1)]\}$$

$$- 2\bar{\kappa}\,e^{i\beta}\,PV \left[\int_0^\infty \frac{\exp\,[-ik(z - \bar{c}_2)]}{k - \nu}\,dk \right.$$

$$\left. - \int_0^\infty \frac{\exp\,[-ik(z - \bar{c}_1)]}{k - \nu}\,dk \right] \tag{4.5.10}$$

From this expression the flow due to either a source or a vortex may be obtained by setting $\kappa = \sigma$ or $\kappa = i\gamma$, respectively. The flow due to an interior vortex is used as an onset flow to obtain a circulatory flow that is needed to satisfy the Kutta condition as stated in Section 3.5. No expression similar to (4.5.10) has been derived for the potential, because no need has arisen.

4.5.3 *Evaluation of the Definite Integral.* Practical computation of the coefficients in the large $\vec{V}_{ij}$ matrices demands rapid evaluation of the velocities induced by a line-segment element of unit strength. Evaluation of (4.5.10) constitutes no particular problem for a large computer except for the last terms, the two integrals of the type

$$I = PV \int_0^\infty \frac{\exp\,[-ik(z - \bar{c})]}{k - \nu}\,dk. \tag{4.5.11}$$

As will be shown, such integrals can be reduced to an expression containing the complex exponential integral, but that accomplishment is of no great advantage, because there are no simple formulas, applicable over a wide range of constants, for evaluating complex exponential integrals. Therefore a special method for evaluating them was developed, which involves the following three essential steps:

1. Transform (4.5.11) in such a way that the exponential becomes real.
2. Develop a rational-fraction approximation of this exponential that is valid over the entire range of 0, ∞.
3. Integrate the resulting expression by the partial-fraction process.

To obtain a real exponential, consider contour integration according to Fig. 16. Let $k = r + im$. Then a pole exists on the real axis at $r = \nu$, and according to the sketch (Fig. 16)

$$PV \int_0^{\infty} \frac{\exp\left[-ir(z - \bar{c})\right]}{r - \nu}\, dr + \int_2 + \int_4 + \int_5 \frac{\exp\left[-ik(z - \bar{c})\right]}{k - \nu}\, dk = 0 \quad (4.5.12)$$
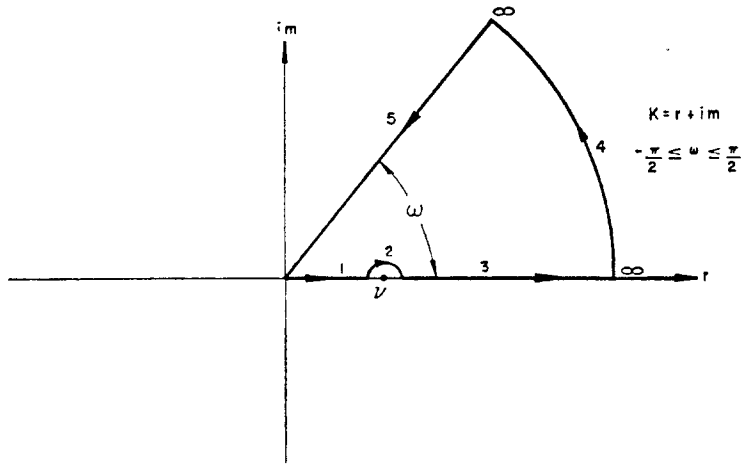
FIG. 16. Contour integration for obtaining a purely real exponential. Line 1, 3, is the original path. Line 5 is the one for which the exponential is purely real.

For integrating along line 5 the angle ω must be so selected that the exponential is purely real. This amounts to the requirement that Im $[-ik(z - \bar{c})] = 0$ or that, upon introducing the expressions for k, z, and $\bar{c}$,

$$m(y + b) - r(x - a) = 0, \quad (4.5.13)$$

which gives

$$\omega = \tan^{-1}\frac{m}{r} = \tan^{-1}\frac{x-a}{y+b}. \tag{4.5.14}$$

The sign of ω is opposite to the sign of $x - a$, since $y + b$ is always negative.

It can be shown that for these conditions the integral along 4 is zero. The detour 2 around the point ν in Fig. 16 will be above or below according to the sign of ω. Therefore the integral along 2 is

$$\int_2 = -(\text{sgn }\omega)\,\pi i \exp\left[-i\nu(z-\bar{c})\right]. \tag{4.5.15}$$

Then if a substitution based on this special path of integration is made, that is, if k is set equal to $R(1 + i \tan \omega)$, where R is radial distance, and, finally, if a scaling transformation is made to remove the constant in the exponential, the relation below is obtained.

$$PV \int_0^\infty \frac{\exp\left[-ik(z-\bar{c})\right]}{k-\nu}\,dk = (\text{sgn }\omega)\,i\pi\,\exp\left[-i\nu(z-\bar{c})\right] + \int_0^\infty \frac{e^{-t}\,dt}{t - i\nu(z-\bar{c})} \tag{4.5.16}$$

Substitution of the expression on the right-hand side of (4.5.16) with $\gamma = 0$ into (4.5.10) yields the formula

$$
\begin{aligned}
W_Q(z) = \sigma\Bigg\{ &e^{-i\beta} \ln\frac{z-c_1}{z-c_2} + e^{i\beta}\ln\frac{z-\bar{c}_1}{z-\bar{c}_2} \\
&+ 4\pi i\, e^{i\beta}\left[\delta_2 \exp\left[-i\nu(z-\bar{c}_2)\right] - \delta_1 \exp\left[-i\nu(z-\bar{c}_1)\right]\right] \\
&- 2\,e^{i\beta}\left[\int_0^\infty \frac{e^{-t}\,dt}{t-i\nu(z-\bar{c}_2)} - \int_0^\infty \frac{e^{-t}\,dt}{t-i\nu(z-\bar{c}_1)}\right]\Bigg\},
\end{aligned} \tag{4.5.17}
$$

where

$$
\begin{array}{llll}
\delta_1 = 0 & \omega_1 > 0 & z \text{ upstream of} & c_1 \\
\delta_1 = 1 & \omega_1 < 0 & z \text{ downstream of} & c_1 \\
\delta_2 = 0 & \omega_2 > 0 & z \text{ upstream of} & c_2 \\
\delta_2 = 1 & \omega_2 < 0 & z \text{ downstream of} & c_2
\end{array}
$$

The expression (4.5.17) supplies values of u and v at any point z for use in forming the $\overline{V_{ij}}$ matrix. In practice it is evaluated by means of complex arithmetic. Step one is now accomplished, and what remains is the evaluation c tegrals of the type

$$\int_0^\infty \frac{\cdot\ e^{-t}\,dt}{t - i\nu(z-\bar{c})}$$

F

where t is real. This is recognizable as an exponential integral form whose value is written as $\exp[-i\nu(z - \bar{c})] E_1[-i\nu(z - \bar{c})]$. Tables, for example Ref. 23, and formulas are available for evaluation of this quantity. Tables are inconvenient for machine calculation, and the known formulas are not valid over the entire range of interest. Accordingly, a suitable formula valid for any value of the argument was developed. If e^{-t} is approximated by a rational fraction, the indicated integration can be performed analytically by breaking the integrand down into partial fractions. Representation of e^{-t} by the quotient of a fourth-degree polynomial and a sixth-degree polynomial has been found to provide the desired accuracy with the minimum amount of computation. The following is an approximation of e^{-t} having equalized extremal errors valid from $0 < t < \infty$. Because all extremal errors are made equal, it can be considered the best approximation in the sense of Chebyshev.

$$e^{-t} = \frac{1 + p_1 t + p_2 t^2 + p_3 t^3 + p_4 t^4}{1 + q_1 t + q_2 t^2 + q_3 t^3 + q_4 t^4 + q_5 t^5 + q_6 t^6} + \epsilon(t) \qquad (4.5.18)$$

where

$$p_1 = -0.23721365 \qquad q_1 = 0.76273617$$
$$p_2 = 0.02065430 \qquad q_2 = 0.28388363$$
$$p_3 = -0.00076330 \qquad q_3 = 0.06678603$$
$$p_4 = 0.00000977 \qquad q_4 = 0.01298272$$
$$q_5 = 0.00087009$$
$$q_6 = 0.00029892$$

$$|\epsilon(t)| \leqslant 1.6 \times 10^{-6} \quad \text{for} \quad 0 < t < \infty.$$

The rational-fraction approximation of Step 2 is now available. When it is used, and the integration is performed by the partial-fraction method, the following formula results, where ζ represents the complex quantities $-i\nu(z - \bar{c})$ in (4.5.17).

$$\int_0^\infty \frac{e^{-t}\,dt}{t + \zeta} = \frac{M + N}{D} + \epsilon(\zeta) \qquad (4.5.19)$$

where

$$M = -(1 + m_1\zeta + m_2\zeta^2 + m_3\zeta^3 + m_4\zeta^4)\ln\zeta$$
$$N = -\gamma(0.99999207 + n_1\zeta + n_2\zeta^2 + n_3\zeta^3 + n_4\zeta^4 + n_5\zeta^5)$$
$$D = 1 + d_1\zeta + d_2\zeta^2 + d_3\zeta^3 + d_4\zeta^4 + d_5\zeta^5 + d_6\zeta^6$$

and where

$$m_1 = 0.23721365 \qquad n_1 = -1.49545886 \qquad d_1 = -0.76273617$$

$$m_2 = 0.020654300 \qquad n_2 = 0.041806426 \qquad d_2 = 0.28388363$$

$$m_3 = 0.00076329700 \qquad n_3 = -0.03000591 \qquad d_3 = -0.066786033$$

$$m_4 = 0.0000097687007 \quad n_4 = 0.0019387339 \qquad d_4 = 0.012982719$$

$$n_5 = -0.00051801555 \quad d_5 = -0.00087008610$$

$$d_6 = 0.00029892040$$

$$|\epsilon| \leqslant 7 \times 10^{-6}$$

$$0 < |\zeta| < \infty \qquad \gamma = \text{Euler's number} = 0.5772156649$$

No explicit bound for the error could be developed. Therefore more than 50 combinations of values of $\zeta = \xi + i\eta$ were tried over the range $0.1 < -x$, $y < 20$, and the results were compared with the values given in Ref. 23. The greatest error was less than that noted above, and most were less than one-fifth as much. When ζ becomes small it is known that $E_1(\zeta)$ approaches $(-\ln \zeta - \gamma)$. Equation (4.5.19) approaches this limit very closely.

4.6 Cascades

A cascade is considered to be an infinite number of identical two-dimensional bodies, all having the same orientation and spaced at equal distances along a straight line. The cascade may be lifting or nonlifting, and it is possible with certain restrictions to have an ensemble of cascades, each having a different body shape. The treatment and development of the elementary singularity is generally similar to that of the previous section, in that complex notation is used. The full exposition of the cascade solution is given in Ref. 4.

The general flow under consideration is illustrated in Fig. 17. The onset flow field is unbounded and the flow is steady. Because of the infinite extent of the cascade and because the onset flow is uniform, the values of source density at corresponding points on the individual bodies must be equal. Let one of this set be called the reference source and assume it to be located at a point $c = a + ib$. Its complex potential is

$$f(z) = K \ln (z - c). \tag{4.6.1}$$

The notation is the same as that listed after (4.5.6). Now for convenience, assume the cascade of sources to be vertical, and let the spacing be called S. Then the complex potential at some point z for the entire set of sources is

$$f(z) = K[\ln (z - c) + \ln (z - c + iS) + \ln (z - c - iS) + \ln (z - c + 2iS)$$
$$+ \ln (z - c - 2iS) + \ldots], \tag{4.6.2}$$
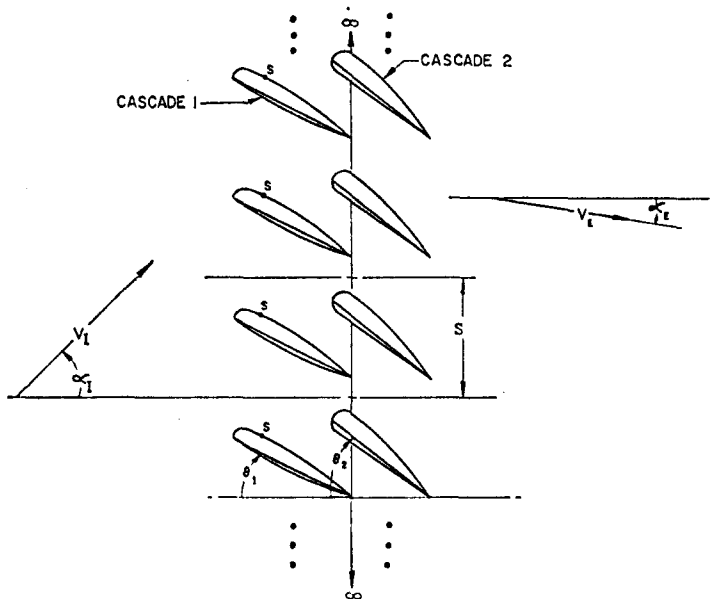
FIG. 17. Vector diagram showing inlet and exit velocities, angles, and some parameters.

which can be reduced to the following equation by combining pairs symmetrical about the reference source:

$$f(z) = K\{\ln (z - c) + \ln [(z - c)^2 + S^2] + \ln [(z - c)^2 + (2S)^2] + \ldots\}$$

(4.6.3)

The real part of this expression is the potential of the elementary singularity for the cascade, just as (4.1.3) is the similar expression for simple two-dimensional flows. A closed form equivalent to this infinite series will be presented later. Velocity components are obtained by differentiating (4.6.3), which gives the following result:

$$\frac{df}{dz} = w(z) = V_x - iV_y = K\left[\frac{1}{z - c} + \frac{2(z - c)}{(z - c)^2 + S^2}\right.$$
$$\left. + \frac{2(z - c)}{(z - c)^2 + (2S)^2} + \ldots\right],$$

(4.6.4)

This can be rearranged to yield

$$\frac{df}{dz} = \frac{K\pi}{S}\left\{\frac{1}{\pi(z - c)} + \frac{2\pi(z - c)}{S}\left[\frac{1}{\pi^2 + \pi^2(z - c)^2/S^2}\right.\right.$$
$$\left.\left. + \frac{1}{4\pi^2 + \pi^2(z - c)^2/S^2} + \ldots\right]\right\}.$$

(4.6.5)

A well-known series, valid for complex numbers, is

$$\coth z = \frac{1}{z} + 2z \left[\frac{1}{\pi^2 + z^2} + \frac{1}{4\pi^2 + z^2} + \ldots \right]. \tag{4.6.6}$$

Hence, (4.6.5) can be written as

$$\frac{df}{dz} = w = \frac{K\pi}{S} \coth \frac{\pi(z - c)}{S}. \tag{4.6.7}$$

This expression is easily integrated to yield the following expression for the complex potential, which is the closed-form equivalent of (4.6.3).

$$f = K \ln \sinh \frac{\pi(z - c)}{S}. \tag{4.6.8}$$

The method of integrating over a line-segment element is like that used in Section 4.5.2. Again let $K = \kappa\, ds = (\sigma + i\gamma)\, ds$, and substitute in (4.6.7) to get

$$W(z) = \frac{\kappa\pi}{S} \int_{c_1}^{c_2} \coth \frac{\pi(z - c)}{S}\, ds. \tag{4.6.9}$$

But, as was seen in Section 4.5.2, $ds = e^{-i\beta}\, dc$. Therefore

$$W(z) = \frac{\pi\kappa}{S} e^{-i\beta} \int_{c_1}^{c_2} \coth \frac{\pi(z - c)}{S}\, dc = -\kappa\, e^{-i\beta} \ln \frac{\sinh\,[\pi(z - c_2)/S]}{\sinh\,[\pi(z - c_1)/S]}. \tag{4.6.10}$$

This formula supplies values of both V_x and V_y at any point z needed in forming the $\vec{V}_{ij}$ matrix. For such calculations let $\kappa = 1$. Vortex flows of unit strength are obtained by letting $\kappa = i$. In the machine program (4.6.10) is evaluated by complex arithmetic. It does not appear possible to obtain by analytic integration a companion expression for the potential over a cascade of line-segment elements.

5. SOLUTION OF THE LINEAR ALGEBRAIC EQUATIONS FOR THE VALUES OF THE SURFACE SOURCE DENSITY

5.1 General Remarks

The coefficient matrix A_{ij} of the linear equations (3.4.2) for the values of surface source density is nonsymmetric and in general has no zero entries. Therefore, many results of matrix theory cannot be applied, and many methods for solving linear equations either fail or are inefficient. Accordingly, investigations of matrix solution methods were conducted largely by trial and numerical experimentation. The comparatively simple methods that

were tried gave satisfactory computing times in most cases, but efforts to discover faster methods continue to be made.

Both direct methods and iterative methods are used to solve the linear equations. The choice depends on the number N of elements used to approximate the body surface. This approach was adopted because the number of arithmetic operations required for a direct solution of N linear equations is nearly proportional to N^3 (for N sufficiently large to give acceptable accuracy in most applications), and the number of operations for one iteration of an iterative solution is proportional to N^2. Thus if the number of iterations required for convergence to a satisfactory solution is independent of N, or at least increases more slowly than N itself, a "cross-over point" can be expected to exist. That is, for N below a certain value a direct method is more efficient, and for larger values of N an iterative solution is preferable. Experience verified that this is the case for exterior flows. The "cross-over point" is really a range of values of N, since the number of iterations required to obtain a solution by any iterative method depends on the body shape and the onset flow. Because the required number of iterations is quite different for different body shapes, this range of values of N is rather wide. The situation is complicated by the fact that the computing time is determined more by the amount of information that must be transferred from the computer's large low-speed storage to its comparatively small high-speed storage than by the amount of arithmetical calculation that is performed. This has made direct solution attractive for higher order matrices than it had been expected to be.

There is a range of values of N that is seldom used. It lies between the largest element number that is used for multiple two-dimensional and axisymmetric bodies (approximately 300) and the smallest element number that is used for most three-dimensional configurations of practical interest (approximately 500). This seemed to be a natural division, and at present virtually all two-dimensional and axisymmetric cases use a direct method of solution, while all three-dimensional cases use an iterative solution. Recent evidence indicates that perhaps direct solution should be used even for some three-dimensional cases, but the matter needs further investigation.

5.2 Some Properties of the Coefficient Matrix

Certain properties of the coefficient matrix A_{ij} determine the effectiveness of iterative methods of solution and to a lesser extent affect the choice of a direct method of solution. The general nature of this matrix is discussed in this section and is applied to the analysis of solution methods in subsequent sections, particularly in Section 5.4, where iterative solutions are discussed.

Few general statements concerning the matrix A_{ij} can be made. For two-dimensional and three-dimensional cases where symmetry of the body surface is not employed, a few observations can be stated that are based

on numerical results and study of the integral equation (2.5), whose properties are approximated by corresponding properties of the coefficient matrix A_{ij}. In these cases the diagonal entries A_{ii} are simply 2π, the local contribution to the normal velocity. (When symmetry is utilized, particularly the symmetry associated with an axisymmetric body, contributions of other portions of the surface appear in the diagonal entries, and any analysis is complicated. All that can be said is that experience shows that the results for these cases are roughly similar to those for the nonsymmetric cases.) As was discussed in Section 2, the nature of the kernel of the integral equation (2.5) is such that in the approximating matrix A_{ij} the sum of all diagonal entries is approximately equal to the sum of all off-diagonal entries. For a single closed convex body surface the off-diagonal terms all have the same sign, and the previous statement holds for the sums of absolute magnitudes of the entries. However, for concave-convex bodies or for several disjoint bodies the off-diagonal terms vary in sign, and the sum of their absolute magnitudes is greater than the sum of the magnitudes of the diagonal entries.

For the cases of the previous paragraph, where symmetry of the body surface is not utilized, some information on the eigenvalues of A_{ij} has been obtained by numerical experimentation. It is known[15] that all eigenvalues of the integral equation (2.5) are real and lie in a certain range. Experiments indicate that this is also true for the matrix A_{ij} whose eigenvalues are apparently exactly real and lie in the interval from 0 to 4π. As stated in the discussion of Section 2, for a single closed body the integral equation is indeterminate for a case of interior flow in that there is a non-trivial solution of the homogeneous equation. The integral equation would be indeterminative for exterior flow if the sign of the $2\pi\sigma$ term outside the integral were reversed. If this behavior were carried over to the approximating matrix, there should be a zero eigenvalue for the case of interior flow and an eigenvalue equal to 4π for the case of exterior flow. It turns out that this is only approximately true. For interior flow the matrix A_{ij} has a small positive eigenvalue whose magnitude decreases as the order N of A_{ij} increases; that is, as the calculation is made more accurate. For exterior flow, A_{ij} has an eigenvalue that is less than 4π by a small amount that decreases with N. For the same body and the same order N the matrices A_{ij} for exterior and interior flow differ only in the signs of the off-diagonal entries, and the amount that the exterior-flow eigenvalue is less than 4π exactly equals the small interior-flow eigenvalue. The other $(N - 1)$ eigenvalues of the matrix A_{ij} do not necessarily correspond to any property of the integral equation, but may depend only on properties of the matrix. For example, for a circular cylinder the integral equation has one eigenvalue, although the matrix of course has N. For thick, smooth bodies the remaining $(N - 1)$ eigenvalues are apparently clustered near 2π. As the body is made thinner, they move toward the ends of the interval from 0 to 4π. It seems that half of them move each way. In the

limit of a body of zero thickness, corresponding elements of the upper surface and lower surface are coincident (assuming they are distributed symmetrically). Clearly, source densities on a pair of coincident surface elements cannot be determined individually. The most that can be found is their sum. Thus for a body of zero thickness, the matrix A_{ij} is singular to such a degree that zero is an eigenvalue of multiplicity $N/2$. These properties of the eigenvalues of A_{ij} are used in Section 5.4 to explain the behavior of iterative methods of solution.

5.3 *Direct Method of Solution*

At an early stage in the development of the present method, it was rather arbitrarily decided that in any direct method of solution of the linear equations the coefficient matrix A_{ij} would be transferred only once from the low-speed storage. Although this has the advantage of minimizing computing time for a case of the size that can actually be handled, it restricts use of the direct solutions to sets of equations whose order N is less than some maximum determined solely by the high-speed storage capacity of the computer. By chance this maximum happened to coincide with the natural division for N mentioned in Section 5.1. It now seems that it may be desirable to utilize procedures involving repetitive transfers of portions of the coefficient matrix in order to apply direct methods of solution to higher order systems. The present method has been programmed for IBM computing machines having 32,000 words of high-speed storage, of which approximately 20,000 are available for the storage of numerical information.

. The most obvious way to effect a direct solution is to triangularize the coefficient matrix A_{ij} by means of the standard Gauss reduction. Originally, this method was used. During the process the right sides of the equations (3.4.2) for as many as ten onset flows are carried along and operated on, which has the result that the total computing time is scarcely greater than the time for a single right side. The large diagonal entries of A_{ij} make it possible to use the equations in order and not to have to search at the nth stage for the equation having the largest coefficient of σ_n. This method requires the entire matrix A_{ij} to be in high-speed storage at one time. Accordingly, the order N of A_{ij} is restricted to values less than 140.

To increase the order of the matrix to which the direct method of solution can be applied, a procedure of successive orthogonalization[24] is used. Let the right sides of equations (3.4.2) be abbreviated c_i, and consider the set of N vectors in $(N + 1)$-dimensional space

$$(A_{i1}, A_{i2}, \ldots, A_{iN}, - c_i) \qquad i = 1, 2, \ldots, N \qquad (5.3.1)$$

The solution σ_j of Eqs. (3.4.2) is such that the vector

$$(\sigma_1, \sigma_2, \ldots, \sigma_N, 1) \qquad (5.3.2)$$

is orthogonal to all the vectors of (5.3.1). Thus the solution of Eq. (3.4.2)

is equivalent to determining an $(N + 1)$-dimensional vector orthogonal to the N vectors of (5.3.1) and having unity as its $(N + 1)$-th component.

First, N linearly independent vectors are determined that are orthogonal to (5.3.1) for $i = 1$. By linear combinations of the vectors of this set, $(N - 1)$ linearly independent vectors are obtained that are also orthogonal to (5.3.1) for $i = 2$. This process is continued until finally one vector is obtained that is orthogonal to (5.3.1) for $i = N$ and by construction is also orthogonal to (5.3.1) for $i < N$. This is the desired vector (5.3.2). After the nth stage of this process has been completed, there are $(N + 1 - n)$ linearly independent vectors. For each of these vectors the first n components are nontrivial and generally nonzero. All other components are zero except one, which is unity. The first of the $(N + 1 - n)$ vectors has a unit $(n + 1)$-th component (immediately after the nontrivial components). The second has a unit $(n + 2)$-th component, etc. Finally, the last vector, the $(N + 1 - n)$-th has a unit $(N + 1)$-th component. These vectors are clearly linearly independent. To continue the process, that is, to find $(N - n)$ vectors orthogonal to (5.3.1) for $i = n + 1$, the first vector of the set is linearly combined with each of the other $(N - n)$ vectors successively. The combination constant that multiplies each of the $(N - n)$ vectors is taken as unity, and the constant that multiplies the first vector is adjusted to make the combined vector orthogonal to (5.3.1) for $i = n + 1$.

Each row of the coefficient matrix A_{ij} is used at only one stage of the process and is not needed before or after that stage. Thus A_{ij} is transferred from low- to high-speed storage a row at a time, with each row destroying the previous one, and no significant amount of storage is required for this purpose. However, the components of all orthogonal vectors must always be in high-speed storage, since they are used repetitively. After the nth stage there are $(N + 1 - n)$ vectors, each having n nontrivial components. The maximum total number of components occurs when the process is about half finished; that is, when n is approximately $N/2$, at which point the total number of components is approximately $N^2/4$. Thus the order of the matrix to which this method can be applied is about twice that for the triangularization process. At present it is used for matrices having N as large as 275.

The orthogonalization process makes important use of the fact that A_{ij} has large diagonal entries. At any stage the vector with a unit $(n + 1)$-th component is used as the base vector for forming the set orthogonal to (5.3.1) for $i = n + 1$. This eliminates nontrivial numerical problems that can arise for general matrices. If the vectors could not be used in order, but a suitable base vector had to be selected at each stage, either the required storage would greatly increase or the computational logic would become considerably more complicated, with a corresponding increase in computing time.

At any stage of the orthogonalization process, only the last vector of

the set has a nonzero $(N + 1)$-th component. Because of the way the sets of vectors are formed, this means that only the last vector depends on the right side c_i of the linear equations. If solutions for several right sides are desired, several "last" vectors are carried along in the process.

In fluid-dynamics problems only a few onset flows are normally of interest. Thus, although there may be more than one right side for the linear equations, there is never a really large number of them. Accordingly, it is not generally worth while to calculate the inverse of the coefficient matrix A_{ij}, since this requires considerably more computing time than either of the above processes. The only exception to this occurs in certain unsteady flows where solutions are required at many different times.

5.4 *Iterative Method of Solution*

If the order of the coefficient matrix A_{ij} becomes sufficiently large, it seems reasonable to abandon direct methods of solution and to use an iterative method. In the usual application the number N^2 of entries in A_{ij} greatly exceeds the high-speed storage capacity of the computer. The matrix is contained in low-speed storage, and during each iteration it is brought into high-speed storage a little at a time and used to improve the approximation of the solution that was obtained in the previous iteration.

Much work on iterative solution of linear equations has been done in recent years. Varga[25] presents a treatise on this subject, and Forsythe and Wasow[26] give a lengthy discussion. The principal effort has been devoted to the sparse matrices that arise from finite-difference approximations. The majority of the methods thus developed are either inapplicable to a full matrix such as A_{ij} or inefficient for such an application. A few of the advanced methods discussed by Varga are applicable, and it is hoped that their application to the present problem can be studied in the future. However, because of the special nature of A_{ij}, straightforward iterative methods converge rather rapidly, and significant improvements in this area may be difficult to obtain.

The method employed for iterative solution of the linear equations (3.4.2) is based on "solving" these equations for the unknowns on the diagonal in the form

$$\sigma_i = \frac{1}{A_{ii}} \left[c_i - \sum_{\substack{j=1 \\ j \neq i}}^{N} A_{ij} \sigma_j \right], \qquad i = 1, 2, \ldots, N \qquad (5.4.1)$$

where again the right side of (3.4.2) has been abbreviated by c_i. Let the mth approximation of the solution σ_i be denoted $\sigma_i^{(m)}$. An obvious way to use (5.4.1) is to substitute the values $\sigma_i^{(m)}$ on the right side to obtain the

$(m + 1)$-th approximation $\sigma_i^{(m+1)}$, namely,

$$\sigma_i^{(m+1)} = \frac{1}{A_{ii}} \left[c_i - \sum_{\substack{j=1 \\ j \neq i}}^{N} A_{ij}\, \sigma_j^{(m)} \right]. \qquad i = 1, 2, \ldots, N \quad (5.4.2)$$

The iterative method described by (5.4.2), which is called the point Jacobi method,[25] obtains the new approximation entirely from the values of the old approximation. Now the values of $\sigma_i^{(m+1)}$ are calculated in the order $i = 1, 2, \ldots, N$. It seems natural, therefore, to use these improved values in the iteration scheme as soon as they are computed, rather than to continue to use values from the previous iteration. If this is done, the iterative procedure is

$$\sigma_i^{(m+1)} = \frac{1}{A_{ii}} \left[c_i - \sum_{j=1}^{i-1} A_{ij}\, \sigma_j^{(m-1)} - \sum_{j=i+1}^{N} A_{ij}\, \sigma_j^{(m)} \right]. \qquad (5.4.3)$$

The iterative method described by (5.4.3) is commonly known as the Gauss–Seidel method. It always converges faster than the method of (5.4.2), and, since it is also easier to use, it is employed in all applications. The point Jacobi method of (5.4.2) is considerably easier to analyze theoretically, and it is useful for investigating properties of the matrix A_{ij}. In the present application the initial approximation $\sigma_j^{(0)}$ is taken as zero for both iterative methods.

A few general results that hold for any iteration method will now be quoted. The error vector for the mth iteration has the components

$$E_i^{(m)} = \sigma_i^{(m)} - \sigma_i, \qquad i = 1, 2, \ldots, N \qquad (5.4.4)$$

where σ_i is the true solution. The error of the mth iteration may be defined as the length of this vector, namely,

$$E^{(m)} = [\sum_{i=1}^{N} (\sigma_i^{(m)} - \sigma_i)^2]^{\frac{1}{2}}. \qquad (5.4.5)$$

It is known[25, 26] that in the limit of large numbers of iterations the ratio of successive errors approaches a constant; that is,

$$\frac{E^{(m+1)}}{E^{(m)}} \to \lambda \quad \text{as} \quad m \to \infty. \qquad (5.4.6)$$

For a convergent process $\lambda < 1$, and (5.4.6) expresses the fact that eventually the error is reduced by a factor of λ per iteration. The quantity λ is accordingly designated the asymptotic convergence factor of the iteration process. The asymptotic number of iterations required to reduce the error by a factor of ten, that is, to improve the accuracy by one decimal place, is given by

$$\text{Iterations per decimal place} = -\frac{1}{\log_{10} \lambda}. \qquad (5.4.7)$$

Any iteration process may be written

$$\sigma_i^{(m+1)} = \sum_{j=1}^{N} Q_{ij}\, \sigma_j^{(m)} + D_i. \qquad (5.4.8)$$

The matrix Q_{ij} may be called the iteration matrix of the process.[25, 26] It is defined as the matrix which, when multiplied by the mth approximation $\sigma_j^{(m)}$, gives the $(m + 1)$-th approximation $\sigma_i^{(m+1)}$ (with the addition of the term D_i, which is independent of m). The asymptotic convergence factor is known[25] to be equal to the maximum absolute magnitude of the eigenvalues of Q_{ij}. If the eigenvalue of maximum absolute magnitude is unique, say λ_M, successive error vectors (not just their lengths as in (5.4.6)) eventually satisfy

$$\frac{E_i^{(m+1)}}{E_i^{(m)}} \to \lambda_M \quad \text{as} \quad m \to \infty. \qquad (5.4.9)$$

For this case the error vectors are asymptotically parallel, and each component is reduced by a factor of λ_M per iteration. The factor λ_M may be either positive or negative, but not complex, or there would be two eigenvalues having the maximum magnitude. There is one exceptional case. When the initial vector $E_i^{(0)}$ is orthogonal to the characteristic vector associated with the eigenvalue of maximum magnitude, this eigenvalue does not affect the iteration process. In this case (5.4.9) holds, with λ_M now denoting the eigenvalue of second largest magnitude, if this is unique. In general, of course, errors cannot be estimated, but for the special case of (5.4.9) the asymptotic convergence factor can be estimated from the relation

$$\frac{\sigma_i^{(m+1)} - \sigma_i^{(m)}}{\sigma_i^{(m)} - \sigma_i^{(m-1)}} \to \lambda_M \quad \text{as} \quad m \to \infty, \qquad (5.4.10)$$

as can be easily shown. That is, the ratio of the changes in σ_i for two successive iterations approaches the unique eigenvalue of maximum magnitude. Any value of i could be used in (5.4.10), that is, any component of σ_i. Practically, it is most accurate to select the component whose change per iteration is the largest.

For the present method the theory of the previous paragraph has been used as a guide for numerical experimentation and as a means of interpreting the results. For the point Jacobi iterative solution, (5.4.2), the iteration matrix is simply related to the coefficient matrix A_{ij}, but for the Gauss–Seidel process, (5.4.3), this is not so. Apparently, both iteration matrices have all eigenvalues real in the range -1 to $+1$, and thus both are always convergent. Some discussion of the two processes is given below.

The iteration matrix Q_{ij} for the point Jacobi iterative procedure is obtained from the coefficient matrix A_{ij} by (1) dividing the entries of each row by the diagonal entry, (2) setting the diagonal entries equal to zero, and (3) reversing the signs of all terms. For two-dimensional and three-dimensional bodies

without symmetry, all diagonal entries of A_{ij} equal 2π, and the eigenvalues β of Q_{ij} are related to the eigenvalues μ of A_{ij} by

$$\beta = 1 - \frac{\mu}{2\pi} \tag{5.4.11}$$

From the discussion of the eigenvalues of A_{ij} contained in Section 5.2, it is clear that for interior flows for which A_{ij} is nearly singular there is a β near $+1$ and that for exterior flows when A_{ij} can be made nearly singular by reversing the sign of the diagonal entries there is a β near -1. For all bodies of practical interest, the β arising from this condition is the largest in magnitude and is called the critical value of β. Also from Section 5.2, it follows that this value of β is a function of N that approaches $+1$ or -1 as N increases. For sufficiently simple bodies the largest β is sufficiently larger than any of the others for the asymptotic convergence factor to be approached after a fairly small number of iterations and can be estimated from (5.4.10). Thus, normally, the iteration process converges slowly and converges more slowly as the element number N is increased. Since the critical value of β depends only on N, the rate of convergence is independent of the body shape and is also independent of the onset flow, which does not affect the matrix A_{ij}. Moreover, there is evidently no difference in the magnitude of the asymptotic convergence factors for an exterior flow and for an interior flow about the same body. (In the former the error alternates in sign, and in the latter it does not.) In the limit of zero-thickness bodies, approximately half the eigenvalues of the iterative matrix approach $+1$ (see Section 5.2), but these do not become larger in absolute value than the critical value of β for the thicknesses occurring in applications. The exceptional case described above occurs when there is a uniform onset flow to a body (and element distribution) having fore and aft symmetry in the free-stream direction. In this case the characteristic vector corresponding to the eigenvalue $\beta = 1$ also has fore and aft symmetry; that is, the components corresponding to symmetrically placed elements are equal. The solution is antisymmetric, in that there are sources on the front of the body and sinks on the back. For this iterative procedure the initial error vector $E_i^{(0)}$ is just the negative of the solution, and it is also antisymmetric. The second largest eigenvalue thus becomes dominant. This eigenvalue is much smaller if the body is not very thin; and it usually does not vary significantly with N, but does depend on the body shape. Thus the convergence of the iterative procedure does not change with element number, but varies from body to body for this exceptional case. Clearly, any onset flow that has the proper symmetry is also exceptional.

The considerations of the previous paragraph may be illustrated by examples. Consider the two two-dimensional bodies shown in Fig. 18. The

first is a 20 per cent-thick ellipse, and the other is a 20 per cent-thick semi-ellipse joined to a semicircle. For each body two flows were computed. The first is that due to a uniform onset flow parallel to the x-axis, and the second is that due to a unit outflow velocity over the boundary. The symmetries of
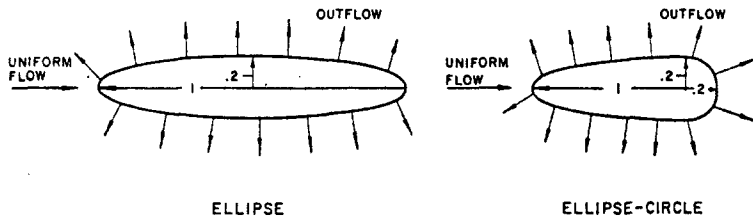
FIG. 18. Profile curves of two two-dimensional bodies.

the bodies were not utilized. Two-dimensional examples were selected even though in applications such cases are solved by a direct method, because of the large amount of computing time required to calculate a systematic series of three-dimensional cases. Asymptotic convergence factors and numbers of iterations required to obtain one decimal place improvement in accuracy are shown, in Table 1, as functions of the element number N. The number of

TABLE 1

ASYMPTOTIC CONVERGENCE FACTORS AND NUMBERS OF ITERATIONS PER DECIMAL PLACE OF
ACCURACY FOR THE POINT JACOBI ITERATIVE METHOD

	Ellipse			
	Uniform onset flow		Unit outflow	
N	Convergence factor	Iterations per decimal place	Convergence factor	Iterations per decimal place
28	−0.60	4	−0.959	55
56	−0.63	5	−0.978	104
112	−0.65	5	−0.988	191
224	−0.65	5	−0.994	383

	Ellipse-Circle			
N	Convergence factor	Iterations per decimal place	Convergence factor	Iterations per decimal place
28	−0.956	51	−0.956	51
56	−0.977	99	−0.977	99
112	−0.988	191	−0.988	191
224	−0.994	383	−0.994	383

elements was simply doubled each time, so that the element distribution remained similar.

The asymptotic convergence factor for the ellipse-circle is essentially the same for both flows, and it increases with N. In this case the convergence factor differs from -1 by an amount proportional to $1/N$; therefore the number of iterations per decimal place of accuracy is proportional to N. For the ellipse with unit outflow the convergence factor is identical to that for the ellipse-circle at equal values of N. The exceptional nature of the ellipse in a uniform onset flow is evident. The asymptotic convergence factor is much smaller, and it varies slowly with N. For the same element number, convergence rates for three-dimensional bodies are much more favorable than those shown above, essentially because the eigenvalue of the integral equation is not approximated as well.

A comparison of (5.4.3) and (5.4.8) shows that the iteration matrix for the Gauss–Seidel procedure is not simply related to the coefficient matrix A_{ij}. The behavior of this iterative procedure cannot be related to the properties of A_{ij} to the same extent that it could be for the point Jacobi method. Information on this method has come principally from numerical experimentation. The most important fact is that the Gauss–Seidel method is faster than the point Jacobi, much faster for exterior flows and at least a little faster for interior flows. The point Jacobi method responds unfavorably to the fact that the coefficient matrix can be made nearly singular by reversing the signs of the diagonal entries, but the Gauss–Seidel method is not affected by this condition. However, it is affected by a condition of near singularity of the matrix. For exterior flows the asymptotic convergence factor depends on the shape of the body and in particular on its thickness, becoming larger as the body becomes thinner (and thus the matrix becomes more nearly singular), but convergence is virtually independent of element number N for a given body. For interior flows the convergence factor increases with element number, because the coefficient matrix becomes more nearly singular. The dominant eigenvalue of the iteration matrix is always positive, and approach to the asymptotic condition (5.4.10) is very rapid for simple bodies. Apparently, there is no exceptional case that arises in applications.

The above observations will be illustrated by showing results for the same two bodies and flows that were discussed above for the point Jacobi method. Also shown are the results for an interior flow in the 20 per cent-thick ellipse. The normal-derivative boundary conditions for this latter case were those corresponding to a uniform onset flow in the x-direction. The asymptotic convergence factors and numbers of iterations required to obtain one decimal-place improvement in accuracy are shown in Table 2.

The four exterior flows show that the asymptotic convergence factor is independent of the element number and the flow, but does depend on the body shape, being larger for the 20 per cent-thick ellipse than for the 33

TABLE 2

ASYMPTOTIC CONVERGENCE FACTORS AND NUMBERS OF ITERATIONS PER DECIMAL PLACE OF
ACCURACY FOR THE GAUSS–SEIDEL ITERATIVE METHOD

Ellipse

N	Uniform onset flow		Unit outflow	
	Convergence factor	Iterations per decimal place	Convergence factor	Iterations per decimal place
28	0.45	3	0.45	3
56	0.45	3	0.44	3
112	0.43	3	0.43	3
224	0.43	3	0.42	3

Interior Flow

N	Convergence factor	Iterations per decimal place
28	0.915	23
56	0.956	51
112	0.977	99
224	0.988	191

Ellipse-Circle

N	Uniform onset flow		Unit outflow	
	Convergence factor	Iterations per decimal place	Convergence factor	Iterations per decimal place
28	0.27	2	0.28	2
56	0.27	2	0.26	2
112	0.29	2	0.25	2
224	0.29	2	0.25	2

per cent-thick ellipse-circle. The interior-flow case exhibits large convergence
factors that increase with N. (It is interesting to note that for the interior
flow the Gauss–Seidel convergence factors are the squares of those for the
point Jacobi method with the same element number. As derived by Varga,[25]
this is a general property of a certain class of matrices, but a class to which
the iteration matrices of the present method apparently do not belong.
Whether or not this condition occurs for all body shapes has not been deter-

mined.) For cases of two-dimensional exterior flows that would arise in applications (if this method were used instead of the direct method), convergence is somewhat slower than in the cases listed below. A 6 per cent-thick double-wedge body, which is an unusually unfavorable shape, had an asymptotic convergence factor of 0.81, which means 11 iterations for each decimal place of accuracy. Convergence can be much slower for flow about several two-dimensional bodies in close proximity than it is for flow about a single two-dimensional body. In three-dimensional cases, for which this procedure is actually used, convergence is more rapid than it is in two-dimensional cases. Asymptotic convergence factors for exterior flows rarely exceed 0.6 (4 iterations per decimal place of accuracy); a typical value for an interior flow is 0.8 (11 iterations per decimal place of accuracy).

In the present application the asymptotic convergence factor is by far the most important parameter in determining the number of iterations required for satisfactory accuracy. Tables 1 and 2 thus provide a very useful measure of the efficiency of the iteration methods. Other considerations, however, do have some effect. One is the rapidity with which the asymptotic convergence factor is approached. For simple bodies the rate of approach is quite rapid. Perhaps a half dozen iterations suffice to establish the asymptotic convergence factor with an error of a few per cent. For certain cases of multiple bodies the approach may be much slower, and whether the initial reduction in error is larger or smaller than the asymptotic reduction may be significant. A more important consideration is the magnitude of the error after the first iteration. For smooth bodies this error is often quite small and the number of iterations required for convergence is correspondingly smaller than might be expected. Near a corner, on the other hand, the values of source density are often large, and the iterative procedure requires a considerable number of iterations to attain the proper value.

On the whole, Gauss–Seidel is a fairly satisfactory method for three-dimensional exterior flows. Efforts to find faster methods continue, and certain methods[25] remain to be studied. One attempt to accelerate convergence was based on the above-mentioned fact that the asymptotic convergence factor is often approached very closely after a comparatively small number of iterations. After this point the change in the values of source density for any iteration is nearly a constant multiple of the change for the previous iteration [see (5.4.10)]. It seemed possible to obtain a large increase in accuracy by analytically summing the indicated geometric series. This works very well for smooth bodies. Unfortunately, the common three-dimensional case in applications consists of several bodies, usually intersecting, such as wing-pylon-nacelle combinations. For such configurations each component body has what amounts to an individual convergence factor, and quite a considerable number of iterations are required before a common convergence factor is attained.

G

6. OTHER EXACT NUMERICAL METHODS OF SOLUTION

Exact numerical methods for the solution of the direct problem of potential flow are characterized by the fact that, at least in principle, any degree of accuracy may be obtained by sufficiently refining the calculational procedure without changing the analytical formulation. For example, the present method will yield an increasingly accurate solution as the number of elements used to approximate the body surface is increased. This reduction in error does not require changing the procedures of the method and, in particular, does not require new programming. In contrast, a perturbation technique normally uses an expansion that is terminated at a particular order, which may be calculated accurately. But to increase the order of the approximation requires additional analysis and programming. (Also, many expansion techniques in fluid dynamics are asymptotic and cannot reduce errors below a certain level.) Furthermore, to be exact in a useful sense, a method must be applicable to a general class of boundary surfaces. An axial source distribution can give exact results for a prolate spheroid in axisymmetric flow, but is approximate for general bodies and is thus not exact in this sense. Exact numerical methods capable of attaining high accuracy must invariably make use of high-speed computing machines.

Many of the classical theoretical approaches to the solution of Laplace's equation are unsuitable for use in the fluid-dynamics problem. For example, determining Green's function for a boundary shape is more time consuming than simply calculating a solution. This approach would be useful for problems in which solutions for a large number of boundary conditions on a particular body surface were of interest, but such problems are rare in fluid dynamics. (The present method can essentially find Green's function numerically by calculating the inverse of the coefficient matrix A_{ij}.)

There appear to be two classes of exact numerical solutions that have been applied to the general fluid-dynamics problem: network methods based on finite-difference approximations of the derivatives of the potential and methods based on solution of an integral equation over the boundary surface. The latter class of methods usually involves determination of a singularity distribution over the boundary surface. For two-dimensional flows there are also methods based on conformal transformation.

6.1 Network Methods

Network methods are perhaps the most straightforward way of attacking a partial differential equation. Of the several essentially equivalent ways of deriving the governing equations, the most straightforward is to approximate the differential operator, in this case the Laplacian, by differences of the values of the potential at various control points. This approximation becomes

more nearly exact as the spacing between the control points is decreased. However the derivation is accomplished, the result is a set of linear algebraic equations relating the values of the potential at the control points, which are distributed throughout the field of flow, usually on a rectangular grid. Each equation relates the value of the potential at a control point to the values at neighboring control points, and the form of all the equations is identical, except at points near the boundary. The finite-difference approach has several general advantages, one of which is the fact that it is applicable to any partial differential equation. However, if attention is restricted to Laplace's equation, it has only two advantages: the coefficient matrix of the linear equations that must be solved, although of very high order, is sparse, and extensive calculations are not required to obtain this matrix. For some applications of Laplace's equation network methods are feasible, but certain special features of the fluid-dynamics problem make the present method clearly superior for that application.

It is characteristic of the fluid-dynamics problem that in most cases the solution is of interest only, on the boundary. The natural advantage of the present method is that it reduces the dimensionality of the problem by one, and its control points are distributed only over the boundary. The control points of a network method must be distributed throughout the flow field; that is, the solution must be obtained for the whole field even if it is required only on the boundary. Moreover, the most common application is that of the exterior flow about a closed body, where the flow field is infinite in extent but the boundary is finite. The situation is illustrated in Fig. 19,
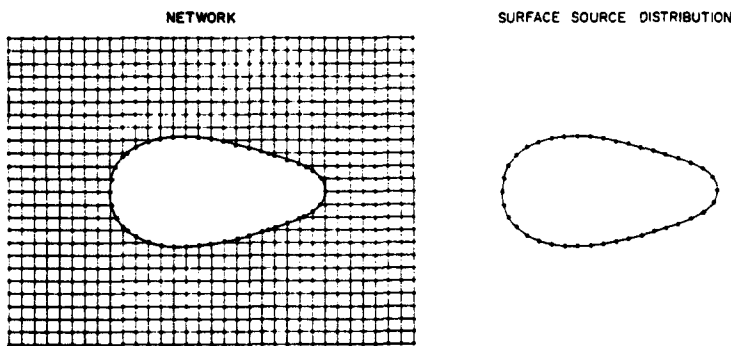
FIG. 19. Control points for network and surface source distribution methods.

which shows control points of comparable spacing for the two methods. For example, suppose that 30 control points are used along the length of the body and that the network is carried a few body lengths in each direction, to where the disturbance field of the body may be taken as zero. If increased spacing

is used at some distance from the body, perhaps roughly 100 control points in each coordinate direction are required. (Actually, this would be insufficient in the direction parallel to the long dimension of the body, since it would allow only 35 control points in each direction from the ends of the body.) The total number of control points for the network method is thus 10^4 for a two-dimensional case and 10^6 for a three-dimensional case. For comparable spacing, the present method requires 60 control points for a two-dimensional case, 30 on the top and 30 on the bottom, and 900 for a three-dimensional case, 30 around the cross section at each of 30 stations along the length. (It is assumed that symmetry, if any, is not utilized by either method.) Thus the number of unknowns in the network method is greater than the square of the number of unknowns in the present method and thus greater than the total number of entries in the coefficient matrix of the present method. If the accuracies of the two calculations are increased by decreasing the spacing, the ratio of the number of unknowns in the network method to the number in the present method is increased.

In the fluid-dynamics problem, the accuracy required in applications is considerably greater than that required in other physical problems. As any experienced fluid dynamicist knows, two bodies of quite similar shape may have very different surface pressure distributions, so that one may be a good aerodynamic shape and the other may not (see examples of Section 9). This accuracy requirement increases the efficiency of the present method relative to a network method. The computational labor of a network method increases more rapidly with the degree of accuracy attained than the computational labor of the present method does. This is due both to the more rapid increase of the number of control points and to the difficulty of solving the resulting matrix equation. For the large matrices that must be solved, iterative solution methods must be used. As was stated in Section 5.4, if the Gauss–Seidel iterative method is used with the coefficient matrix of the present method, the number of iterations required for convergence is essentially independent of the number of control points. However, for network methods the number of iterations required for convergence apparently always increases with the number of control points. Varga[25] and Forsythe and Wasow[26] discuss solution by network methods of the interior Dirichlet problem for the square (potential specified on the boundary). For both the point Jacobi and Gauss–Seidel methods, the asymptotic number of iterations required to obtain a one-decimal-place improvement in accuracy is proportional to the total number of control points in the field. For the more sophisticated successive-over-relaxation technique, the corresponding number of iterations is proportional to the number of boundary points. Other advanced methods are faster for the square, but it appears from the discussion presented by Varga that for general boundaries these latter methods are not faster except for very small point spacings.

The example outlined above may be used to provide a comparison of computing times. Using a very approximate analysis, Forsythe and Wasow estimate the computing times required for solutions by network methods as one hour for the two-dimensional case and one week for the three-dimensional case. These estimates are based on a computer able to perform a typical arithmetic operation in 50 μsec. If it is assumed that computers currently in use are five times faster overall, these times become 12 min for the two-dimensional case and 34 hr for the three-dimensional case. The present method solves the example with computing times that are less than these by a factor of approximately twenty.

The accuracy obtainable with network methods is reduced by the fact that these methods calculate the potential, rather than the gradient of the potential, the velocity, which is the quantity of physical significance in the fluid-dynamics problem. Since a rectangular grid of control points is highly desirable, the application of a condition on the normal derivative of the potential along a curved boundary is troublesome. Forsythe and Wasow[26] state: "Boundary conditions of Dirichlet type offer comparatively little difficulty in making the transition to difference equations, even when the boundary c is a curved one. The situation is much more complicated for boundary conditions involving the normal derivative, and it is far from clear how best to deal with curved boundaries." Varga's[25] developments apparently alleviate this problem. However, the quantity of final interest is the tangential derivative of the potential along the boundary. It seems that in network methods this derivative must essentially be evaluated numerically, with a consequent loss of accuracy. The present method, on the other hand, calculates velocity directly.

6.2 Integral-Equation Methods

Exact integral-equation representations of the direct problem of potential flow may be formulated in a variety of ways, all leading to a Fredholm integral equation of either the first or the second kind. Most of the methods that have been formulated are equivalent to determining a distribution of singularity over the body surface. Both source and vortex distributions have been used. Methods have been formulated for two-dimensional bodies and for axisymmetric bodies. The present method is apparently the only one that has been formulated for three-dimensional bodies.

The idea of using a surface source distribution, which is determined as the solution of a Fredholm integral equation of the second kind for the exterior normal velocity on the body surface, was first stated by Lotz[18] for the case of an axisymmetric body in cross flow. This method was developed and extended by Vandrey,[27, 28] who formulates[28] a complete set of integral equations for axisymmetric bodies, including the case of cross flow and that

of rotation. Vandrey's formulation is precisely that of the present method, and the resulting integral equations are identical. The integral equations are solved by an iteration method that uses the trapezoidal rule to evaluate the integrals (after certain transformations). Boundary conditions are applied and velocities are calculated at a set of control points distributed along the profile curve of the body. Vandrey's intention was to develop a method of hand calculation, and considerable analysis is devoted to putting the procedure in a form suitable for human computers using desk calculators. The labor involved in calculating a single flow is clearly quite large, even for a fairly small number of control points. Accordingly, the number of control points is limited to about two dozen. Apparently the method has not been programmed for an electronic computer.*

For two-dimensional flows, a general computer method based on a surface vorticity distribution has been developed. The problem was originally formulated by Praeger.[29] The method was developed, extended, and adapted for computer by Martensen[30] and Jacob.[31] It works with the stream function, rather than the velocity potential, and expresses the perturbation stream function due to the body as an integral over the profile curve of the body. The integrand is the product of the stream function due to a unit line vortex located at a point on the profile curve and the local value of vorticity. The stream function at the point x, y due to a line vortex at ξ, η may be written

$$\psi = \frac{1}{4\pi} \ln \left[\frac{1}{(x - \xi)^2 + (y - \eta)^2} \right]. \tag{6.2.1}$$

If the vortex strength along the profile curve is denoted by v, the perturbation stream function is

$$\psi(x, y) = \frac{1}{4\pi} \oint v \ln \left[\frac{1}{(x - \xi)^2 + (y - \eta)^2} \right] ds, \tag{6.2.2}$$

where the integration is performed over the entire profile. Expression (6.2.2) could be set equal to the negative of the stream function of the onset flow along the body profile. This would lead to an integral equation of the first kind for the vorticity strength v. Instead, a different condition is applied. As was pointed out in the references, the surface vorticity distribution that makes a closed body a streamline for the exterior flow also makes the interior of the closed body a region of zero velocity. The condition applied is that the total tangential velocity—perturbation plus onset flow—be zero on the inside of the profile curve of the body. The perturbation tangential

velocity is obtained as the normal derivative of (6.2.2). Evaluating this derivative on the body surface involves exactly the limiting process described in Section 2 and has the same result, namely, a term outside the integral as well as the integral itself. Thus an integral equation of the second kind is obtained for the vorticity strength v. It can be shown that v is exactly the surface velocity for the exterior flow, that is, this important quantity is obtained directly.

It is interesting to note that the integral equation obtained by the above procedure is virtually identical to that of the present method. A comparison of (6.2.1) with (4.1.3) shows that the stream function due to a line vortex is identical to the potential due to a line source. (With the definitions used here, they differ by a nonessential factor of 4π.) Thus a vortex may be thought of as a "source" of the stream function in two dimensions. Similarly the perturbation stream function (6.2.2) is identical to the two-dimensional form of (2.3) for the perturbation potential. As was described above, the integral equation for v is obtained by evaluating the normal derivative of (6.2.2) on the body surface. The integral equation in the present method is obtained in exactly this way from (2.3). The only difference is in the direction of the normal derivative—exterior in the present method, interior in the Martensen–Jacob method. Thus the left side of the integral equation obtained by the Martensen–Jacob method for the exterior flow about a closed body is identical to that of the two-dimensional form of the equation (2.5) obtained by the present method for interior flow within the same body. The right sides of the integral equations differ in that one is the normal component of the onset flow and one the tangential component.

The Martensen–Jacob procedure approximates the integral equation by a set of linear algebraic equations. After certain transformations the integral is evaluated by the trapezoidal rule, which uses values of the integrand at the control points where the integral equation is required to hold. This is calculationally equivalent to approximating the portion of the body profile in the neighborhood of a control point by a line vortex at the control point and calculating influence matrices $\vec{V}_{ij}$ and A_{ij} from the line-vortex formulas, which can be done considerably faster than evaluating the more complicated formulas of Section 4.1 for a line-segment element. But it is less accurate and therefore requires special care near the trailing edge of an airfoil*. The integral equation is indeterminative, and its solution is therefore non-unique (see discussion of Section 2). When solving the approximating set of linear algebraic equations an auxiliary condition is employed that fixes the total vorticity on the body profile. Solution of the linear equations gives values

---

* Addition in proof: An extension of this method leading to an improved treatment of the trailing-edge region has recently been described by P. Pal, Untersuchungen über den Interfereuzeinfluss bei Strömungen durch Tandem-Schaufelgitter. *Ing. Arch.* 34, 173 (1965).

of surface velocity directly, and the calculations of Section 3.5 are avoided. (For the present method this part of the calculation requires about 10 per cent of the total computation time.) As the method is presently formulated, flow at points off the body surface cannot be calculated, but this capability could certainly be incorporated. In summary, the method of Martensen and Jacob appears to be roughly equivalent to the present method for the calculation of exterior flow about closed two-dimensional bodies.

Another approach was adopted by Landweber.[32, 33] His method is applicable to two-dimensional bodies symmetric about a line and to axisymmetric bodies for axisymmetric flow, cross flow, or rotation. Annular bodies, such as tori or inlets are beyond the scope of this method, as are interior flows. This method uses Green's theorem to relate the perturbation potential of the body to another auxiliary potential function by means of the integral relation

$$\oiint_S \varphi \, \frac{\partial \varphi'}{\partial n} \, \mathrm{d}S = \oiint_S \varphi' \, \frac{\partial \varphi}{\partial n} \, \mathrm{d}S \qquad (6.2.3)$$

where φ is the perturbation potential, φ' is the auxiliary potential, $\partial/\partial n$ denotes the normal derivative, and the integrals are taken over the body surface. For the various kinds of flows, the auxiliary potential φ' is identified with the potentials of various doublet distributions along the axis of symmetry or line of symmetry in two dimensions. Certain manipulations of (6.2.3) then lead in each case to an integral equation of the first kind for the tangential velocity along the surface (except for rotational motion, where the unknown function in the integral equation is the perturbation potential). The kernels of the integral equations are very simple functions. The integral is evaluated by Gaussian quadrature, and the integral equation is approximated by a set of linear algebraic equations. Since the integral equation is of the first kind, the approximating coefficient matrix does not in general have a dominant main diagonal, although the diagonal is relatively large if the interval between control points is of the order of the half-thickness of the body. Since this method was intended for a small computer, the number of control points was usually less than twenty, and this relation between control-point interval and thickness existed for bodies of practical interest. If a large computer were used, this condition would not be important, because the equations could be solved directly rather than iteratively, as was done by Landweber. The nature of the method can be illustrated by examining the axisymmetric case. Let ξ and η denote the coordinates of a point on the profile curve of the body (η is essentially a radial coordinate), and let s denote arc length along the profile curve. The integral equation for the tangential velocity v along the surface is

$$\frac{1}{2} \int_0^L v \, \frac{\eta^2}{[(x - \xi)^2 + \eta^2]^{\frac{3}{2}}} \, \mathrm{d}s = - V_\infty \qquad (6.2.4)$$

where V_∞ is the velocity of the uniform onset flow, and the integration is performed over the entire arc length L of the profile curve. Equation (6.2.4) must hold for all values of x inside the body, where x is the axial coordinate of a general point on the axis of symmetry. It is easy to verify the fact that the kernel of Eq. (6.2.4) is the axial velocity at a point x, 0 on the axis of symmetry due to a ring vortex of unit strength lying in the body surface and passing through the point ξ, η. Solution of Eq. (6.2.4) is equivalent to determining the distribution v of ring vorticity on the body surface that exactly cancels the onset flow on the axis and thus gives zero total velocity. The similarity to the previously mentioned method is evident. A surface vorticity distribution, which is identically equal to the tangential velocity, is determined in such a way as to give zero velocity inside the body. In the previous method the boundary condition is applied on the surface; in this method a condition is applied some distance away from the surface on the axis of symmetry. This approach gives good results for smooth bodies. But it is evident that, even if a large number of control points are used, the surface vorticity can respond only with difficulty to details of the shape of the profile curve whose characteristic dimensions are small compared with their distance from the axis of symmetry. Landweber[33] concludes: "Experience with a large number of bodies of revolution indicates that, for well-rounded bodies sufficiently accurate solutions can be obtained without difficulty by [Landweber's method]. For bodies with sudden changes in slope and curvature, or with local bumps, the method of [the present article] has been remarkably successful."

A method that uses a distribution of ring vorticity on the surface of an axisymmetric body and that determines this distribution by applying a boundary condition on the surface of the body is presented by Chaplin.[34] The formulation is restricted to axisymmetric flows. The boundary condition requires that the value of the Stokes's stream function be constant on the body surface. This leads to an integral equation of the first kind for the surface vorticity. As in the present method, the body profile is approximated by a polygon. The surface vorticity is assumed to vary linearly over each line-segment element in such a way that it is continuous from element to element. The effects of the elements on each other's midpoints are calculated by integrating over the elements, and the integral equation is approximated by a set of linear algebraic equations. In the original formulation,[34] Chaplin's method was intended for use with open axisymmetric bodies such as ducts, and certain details of the procedure made it awkward to apply to general bodies, for example an ordinary closed body. However, this deficiency was subsequently remedied. A few applications to general closed bodies are presented by Chaplin,[34] and the calculated results are quite accurate. Since only a few such examples are presented, it is difficult to compare this method with the present method in detail. Both appear equally general for

axisymmetric flows. The use of a singularity distribution that varies linearly over the elements might enable the method to obtain greater accuracy than the present method with the same number of elements. But computing times cannot be compared, because Chaplin's method is programmed for a special computer. The use of surface vorticity may have certain advantages for inlets or propeller shrouds.

6.3 *Conformal-Transformation Methods*

In two dimensions the direct problem of potential flow is equivalent to the problem of finding a conformal transformation that transforms the profile curve of the body to a curve for which the solution is known. The numerical determination of the proper conformal transformation is thus an alternative approach to the solution of potential-flow problems. A very well-known method of this type was formulated by Theodorsen.[35] Descriptions of the method are contained in many standard works.[12] As originally formulated Theodorsen's method directly calculates the transformation of the given curve into a circle. In current usage the profile curve is first altered by analytical transformations to remove corners, for example, airfoil trailing edges, and produce a smooth shape, preferably one of approximately circular shape. (This is sometimes done in the present method, as was mentioned in Section 3.2.) The transformation of this smooth shape to a circle is then determined numerically. This method gives excellent results for the flow about any single two-dimensional body. It is not known how the computing time compares with that of the present method. The Theodorsen method cannot be applied to the flow about several bodies, for example, multiple airfoils, but it can be applied to a single cascade of identical airfoils.

7. COMPARISON OF CALCULATED VELOCITY DISTRIBUTIONS WITH EXACT ANALYTIC SOLUTIONS

In order to determine the accuracy of the present method, surface velocity distributions for a variety of body shapes were calculated and compared with exact analytic solutions. In most such solutions the onset flow is a uniform stream. The accuracies of the examples presented here are typical of those of all the calculations that have been made by the present method. In all the comparisons, the calculated value is plotted for each control point, and thus the number of elements used to approximate the body surface can be determined from the figure.

On any portion of a body surface where the curvature is nonzero, the control points used by the present method do not lie exactly on the surface. There is thus some uncertainty as to how the calculated and analytic solutions should be compared. It was decided to relate the two solutions by means of the unit normal vector. A given control point is taken to correspond to the point on the true body surface where the unit normal vector to the surface is identical

to the unit normal vector of the element on which the control point is located. On three-dimensional bodies velocity distributions are often compared along curves lying in a plane of symmetry of the body. Since there are no control points in a symmetry plane, the calculated results are extrapolated into the plane.

7.1 Two-Dimensional Flows

Figures 20 and 21 compare analytic and calculated velocity distributions on two elliptic cylinders in uniform onset flows parallel to the x-axis. Figure 20 presents a comparison for an elliptic cylinder of thickness ratio $1/8$,
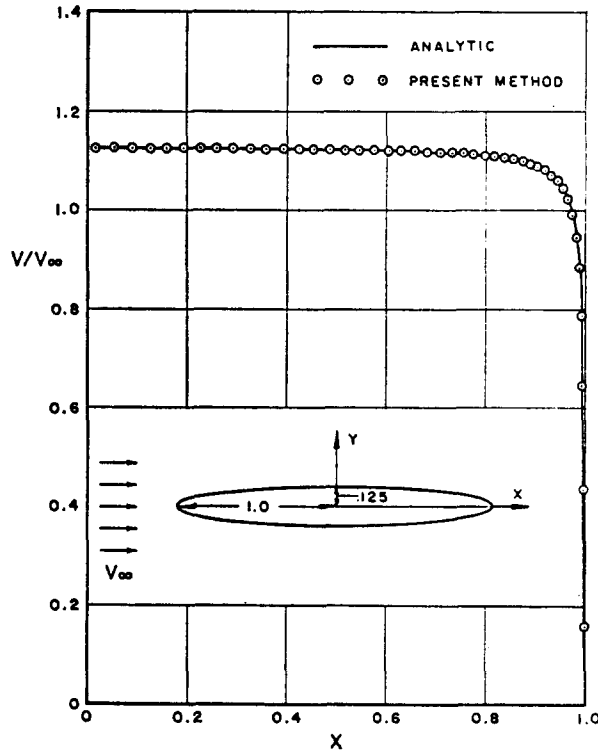
FIG. 20. Comparison of analytic and calculated velocity distributions on an elliptic cylinder of thickness ratio $1/8$.

and Fig. 21 shows results for an elliptic cylinder of thickness ratio 8. The first body has a thickness representative of those usually encountered in applications, and the second is a thick body that gives rise to an extreme flow with a maximum velocity equal to nine times free-stream velocity. Accurate calculation of the latter type of flow is required for obtaining flow at angle of attack. In both cases the agreement of the calculated and analytic

solutions is good. Each body was represented by 90 elements on the top half; the bottom half was accounted for by symmetry. For the elliptic cylinder of thickness ratio 1/8 the velocity distribution could be calculated to plotting accuracy with fewer surface elements. For the elliptic cylinder of thickness ratio 8 this number of elements is apparently adequate, but the distribution should be altered from that shown in Fig. 21. A more dense distribution of
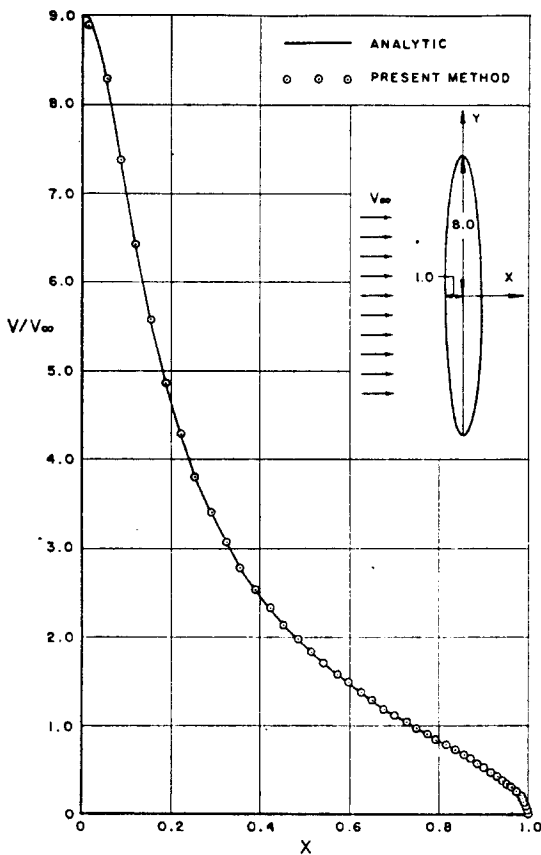
FIG. 21. Comparison of analytic and calculated velocity distributions on an elliptic cylinder of thickness ratio 8.

elements near the location of maximum velocity would be desirable to reduce errors in this region, and it is clear that fewer elements would suffice in the neighborhood of the stagnation point. However, the accuracy shown in Fig. 21 is sufficient for most purposes.

As is stated in Section 2, the present method cannot be guaranteed a priori to be successful for bodies with corners. It is successful, however,

for bodies with convex corners, as is illustrated in Fig. 22, which shows the analytic and calculated surface velocity distributions on a semi-infinite, two-dimensional body of rectangular cross-section. The agreement is seen
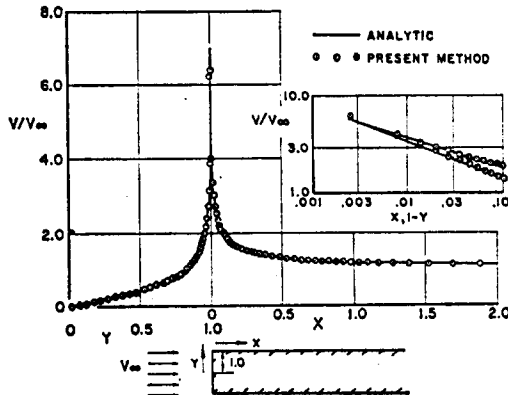
FIG. 22. Comparison of analytic and calculated velocity distributions on a semi-infinite two-dimensional body of rectangular cross-section. Insert shows log–log plot of velocities near corner.

to be quite satisfactory even very near the corner. Since the control points are midpoints of the elements, the velocity is not evaluated at the corner itself but at a distance of half an element width away from it.

The present method is also successful when the normal velocity on the surface of a body is specified as a discontinuous function of position (another exceptional case mentioned in Section 2). The example selected is that of a circular cylinder having a uniform inward normal velocity over half its circumference and zero normal velocity over the other half. This is thus a case of distributed suction. For this flow the integral equation (2.5) can be solved analytically and the solution thus obtained is identical with that obtained by separation of variables. The calculations of the present method are compared with the analytic solution in Fig. 23, which shows tangential velocities on the surface of the cylinder. Agreement is good. The control point nearest the discontinuity of normal velocity is half an element away. As can be seen from the insert of Fig. 23, near the discontinuity of normal velocity the velocity approaches infinity as the logarithm of the distance from the discontinuity. This is in contrast to the flow near a convex corner where the velocity approaches infinity as a negative power of distance from the corner. In addition to the expected symmetry of the flow about the line $\theta = \pm 90°$, the tangential velocity on the cylinder is also symmetric about the line $\theta = 0°$ or $180°$, although the complete velocity field is not.

Airfoils occur much more frequently in applications than any other kind

of two-dimensional shape. Lift is accounted for by the use of a circulatory onset flow (see Section 3.5). Figure 24 compares analytic and calculated pressure coefficients on a Kármán–Trefftz airfoil, whose profile curve is
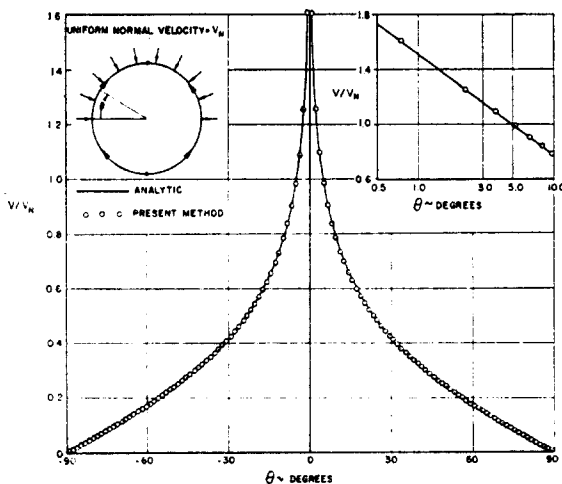
FIG. 23. Comparison of analytic and calculated tangential velocity distributions on a circular cylinder having a discontinuous normal velocity distribution. Insert is a semi-log plot of velocities near the discontinuity of normal velocity.

shown in the figure, at a lift coefficient of 0.5. (This figure compares pressure coefficients rather than velocities so that the magnitude of the lift can be seen directly.) The two pressure distributions are identical except for a small region near the negative pressure peak.

A simple example of a multiple-body problem is that of the flow about two identical circular cylinders. In the case considered, the distance between the centers is one and one-half times the length of a diameter, and the free-stream direction is perpendicular to the line joining the centers. Calculated and analytic velocity distributions on one of the circular cylinders are shown in Fig. 25. The two are in good agreement. It is interesting to compare this flow to that about a single circular cylinder. When two cylinders are present, the magnitude of the maximum surface velocity is 30 per cent larger than that for a single circular cylinder, and the location of the stagnation point is shifted about 4° towards the other cylinder.

One interesting two-dimensional flow that is not irrotational can be calculated by the present method. This is the case of a uniform shear onset flow, which may be defined without loss of generality as a flow parallel to the x-axis having a velocity that varies linearly with y. The vorticity of this flow is constant. Since vorticity is constant along streamlines, the flow
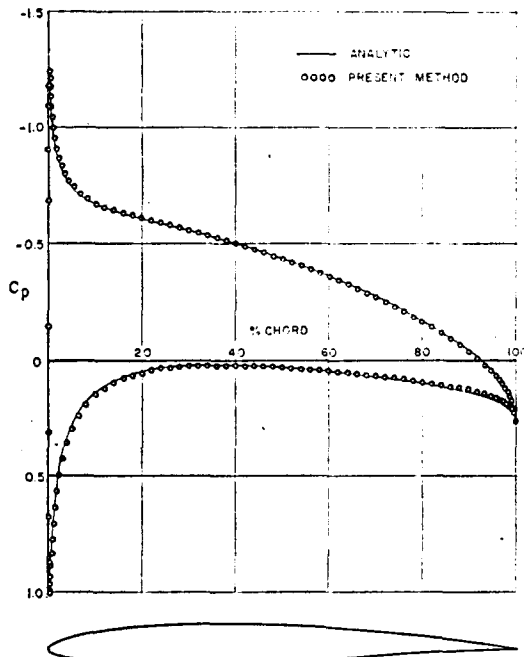
FIG. 24. Comparison of analytic and calculated pressure distributions on a Kármán–Trefftz airfoil at a lift coefficient of 0.5.
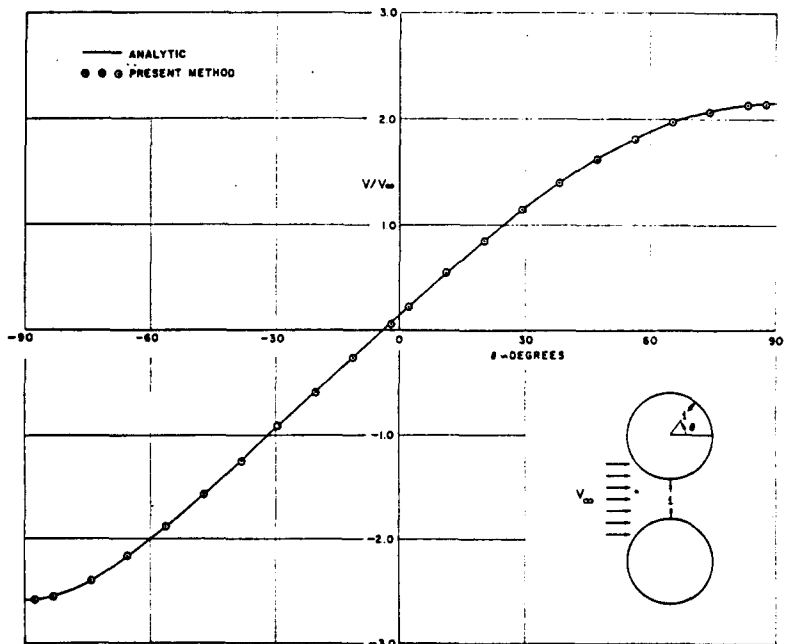
FIG. 25. Comparison of analytic and calculated velocity distributions on one of two identical circular cylinders whose centers are one and one-half diameters apart.

about any body immersed in this onset flow has the same constant value of vorticity as the onset flow. Therefore the perturbation flow due to the body is irrotational and may be calculated by the present method. As an example the flow about a circular cylinder was computed. The cylinder has a unit radius and its center lies on the x-axis. The onset flow is

$$V_{\infty x} = 1 + \tfrac{4}{3} y, \qquad V_{\infty y} = 0. \tag{7.1.1}$$

This flow was chosen because it gives rise to three stagnation points on the body. If the onset flow velocity on the x-axis is unity, a coefficient of y in (7.1.1) less than 4/3 leads to two stagnation points on the body, and a coefficient greater than 4/3 leads to four stagnation points. A sketch of the streamline pattern is given in Fig. 26. It can be seen that the "dividing"
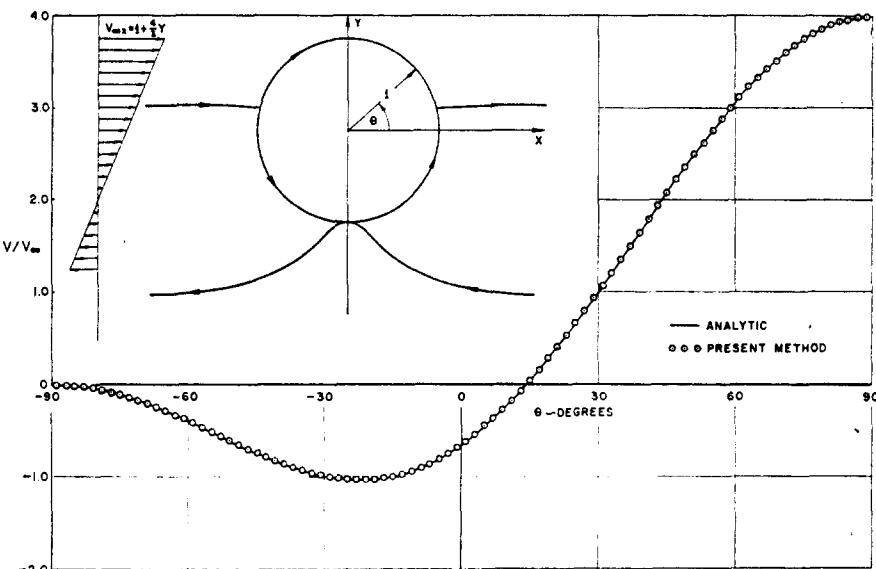
Fig. 26. Comparison of analytic and calculated velocity distributions on a circular cylinder in a uniform shear onset flow.

streamlines that meet the cylinder at the stagnation points do not intersect the surface perpendicularly. In fact the streamline through the lower stagnation point is a tangent to the cylinder. This figure also shows how well the calculated and analytic velocity distributions on the cylinder agree for this somewhat unusual flow.

7.2 *Axisymmetric Flows*

Figures 27 and 28 compare analytic and calculated velocity distributions on two ellipsoids of revolution in uniform onset flows parallel to their
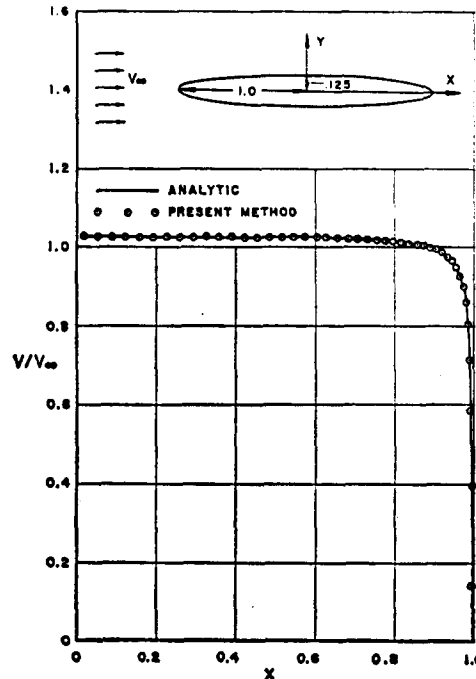
FIG. 27. Comparison of analytic and calculated velocity distributions on a prolate spheroid of thickness ratio 1/8 in axisymmetric flow.
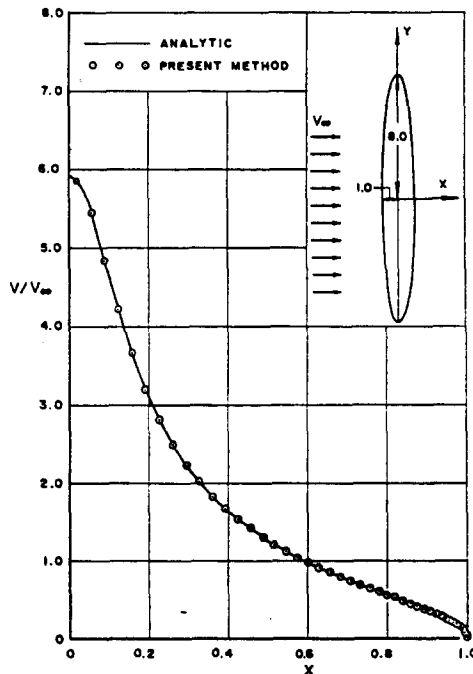

FIG. 28. Comparison of analytic and calculated velocity distributions on an oblate spheroid of thickness ratio 8 in axisymmetric flow.

H

symmetry axes. Figure 27 shows results for a prolate spheroid of thickness ratio 1/8, and Fig. 28 is a comparison for an oblate spheroid of thickness ratio 8. The latter is an extreme flow with a maximum surface velocity equal to 5.91 times free-stream velocity (compare the two-dimensional case of Section 7.1). For both bodies 90 surface elements were used. This is more than the number required to obtain plotting accuracy for the prolate spheroid. For the oblate spheroid some improvement in accuracy could be obtained by concentrating additional elements near the location of maximum velocity and by using a more sparse distribution near the stagnation point. With the element distribution used in Fig. 28, the calculated and analytic solutions are identical to plotting accuracy.

Indirect methods may be used to obtain exact analytic solutions of flows about bodies of revolution that can be generated by known source distributions along the axis of symmetry (see Section 1.3). Such methods can generate solutions for comparison with the calculations of the present method. Such a comparison is shown in Fig. 29. The body has a blunt nose and a pointed
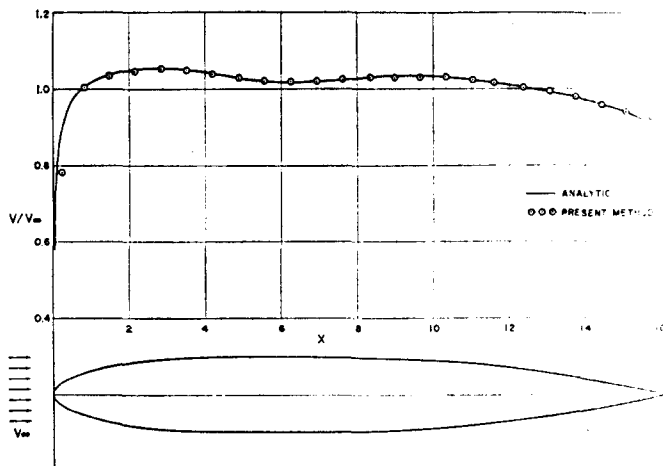
FIG. 29. Comparison of analytic and calculated velocity distributions on a source–sink body.

tail. The calculated surface velocity distribution agrees fairly well with the analytic solution, despite the fact that only 24 elements were used to approximate the surface. This shows that useful results can be obtained with small numbers of elements if the body is simple enough.

An analytic solution for an interior flow was generated by superposing the flow due to a ring vortex and that due to a uniform stream parallel to the axis of the ring. One of the stream surfaces of the resulting flow was considered to be an axisymmetric duct, and the flow in this duct was calculated

by the present method. The analytic and calculated velocity distributions on the surface of the duct are compared in Fig. 30. The calculated solution is quite accurate, despite the fact that it used only 80 surface elements—a small number for an interior flow with this rather severe contraction ratio.
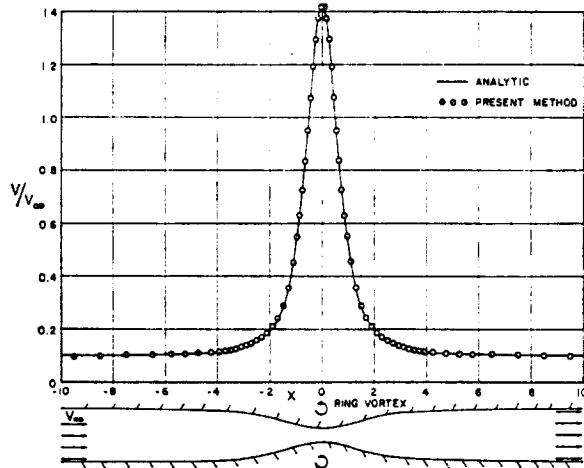
FIG. 30. Comparison of analytic and calculated velocity distributions on the wall of an axisymmetric duct generated by superposition of a ring vortex and a uniform stream.

7.3 Cross Flow about Axisymmetric Bodies

The term cross flow applied to an axisymmtric body is defined in subsection 3.3.4 and in Section 4.3. The two important cases of cross flow are the flow due to a uniform onset flow perpendicular to the axis of symmetry of the body and the flow due to a body rotating about an axis normal to and intersecting its axis of symmetry. Exact analytic solutions for cases of cross flow are not abundant. The examples of this section are ellipsoids of revolution. The quantities that are compared are T_2 and T_3, which are defined in Section 3.5 and illustrated in Fig. 4. They represent the velocity tangent to the profile curve of the body and the circumferential velocity around the circular cross-section, respectively. These quantities depend only on axial position along the body.

Figures 31 and 32 compare analytic and calculated velocity distributions on two ellipsoids of revolution in uniform onset flows perpendicular to their axes of symmetry. The comparison of Fig. 31 is for a prolate spheroid of thickness ratio 1/8, and that of Fig. 32 is·for an oblate spheroid of thickness ratio 8. The quantity T_3 is a constant for each body, which is a special property of ellipsoids. For any body, T_2 and T_3 must be equal at the ends
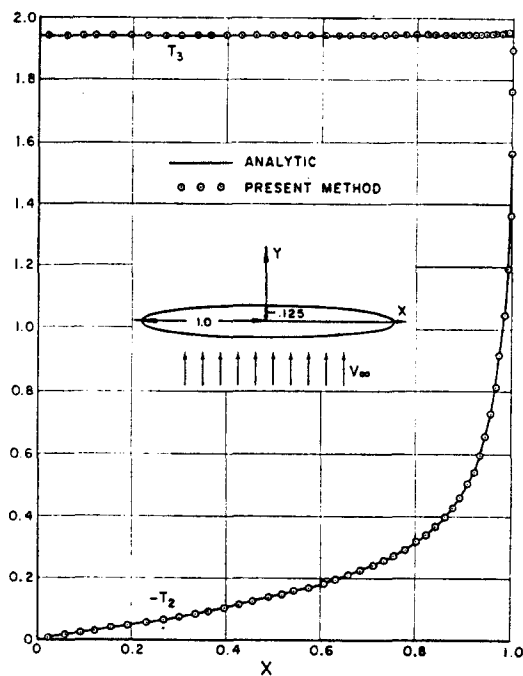
FIG. 31. Comparison of analytic and calculated velocity distributions on a prolate
spheroid of thickness ratio 1/8 in uniform cross flow.
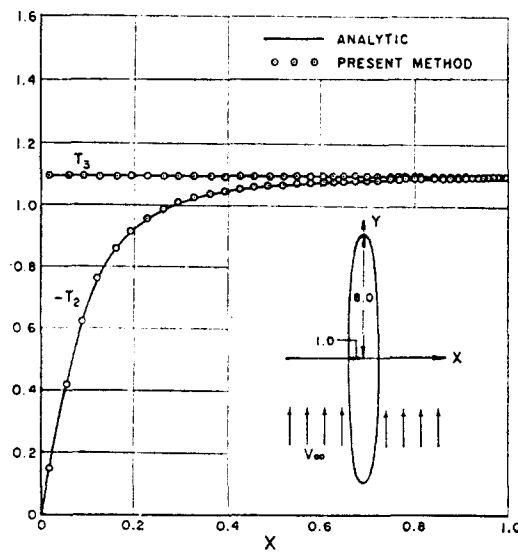
FIG. 32. Comparison of analytic and calculated velocity distributions on an oblate
spheroid of thickness ratio 8 in uniform cross flow.

of the body on the axis of symmetry. The accuracy of the calculated solutions is seen to be good.

To provide an example of the flow due to a rotating body, calculations were performed for a rotating prolate spheroid of thickness ratio 1/2. Its center is at the origin, and it is rotating about the z-axis at a rate of one radian per unit time. In a coordinate system fixed in the body, the onset flow to the body is a rigid-body rotation of the surrounding fluid, and this onset flow is not irrotational. The perturbation velocity field due to the body, which is the entire velocity field in a coordinate system fixed with respect to the fluid at infinity, is irrotational. The quantities whose calculated and analytic values are compared are the perturbation velocity components. Figure 33 compares calculated and analytic values of T_2 and T_3 on the body
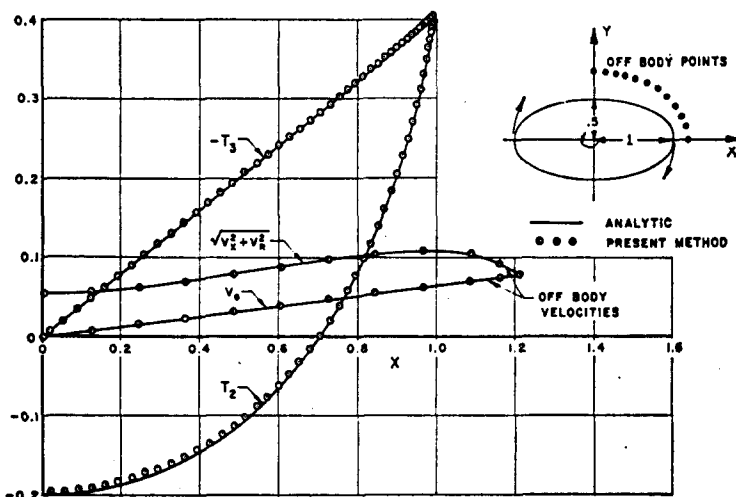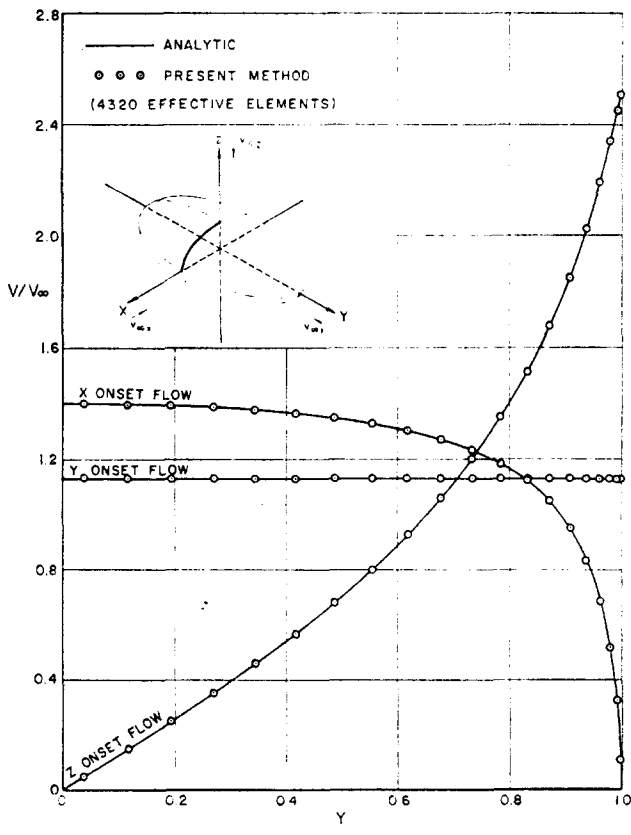
FIG. 33. Comparison of analytic and calculated velocity distributions on a prolate spheroid of thickness ratio 1/2 that is rotating about its center.

surface and also compares velocity components at points along a curve off the body surface in the flow field. The velocity components at off-body points are the total velocity V_T in the xy-plane, which is the vector sum of V_x and V_R of Fig. 4, and the circumferential velocity V_θ, whose significance is also illustrated in Fig. 4. The calculated and analytic values of T_2 are slightly different near the middle of the body, and the calculated values of T_3 deviate slightly from the analytic curve near the ends of the body. The calculated solution shown in Fig. 33 used 90 surface elements, which is sufficient to obtain plotting accuracy for this body in a uniform onset flow. It is not known whether rotational flows in general require more elements for equal accuracy or whether this case is special in some sense. The accuracy of the calculations at points off the body is quite satisfactory.

7.4 *Three-dimensional Flows*
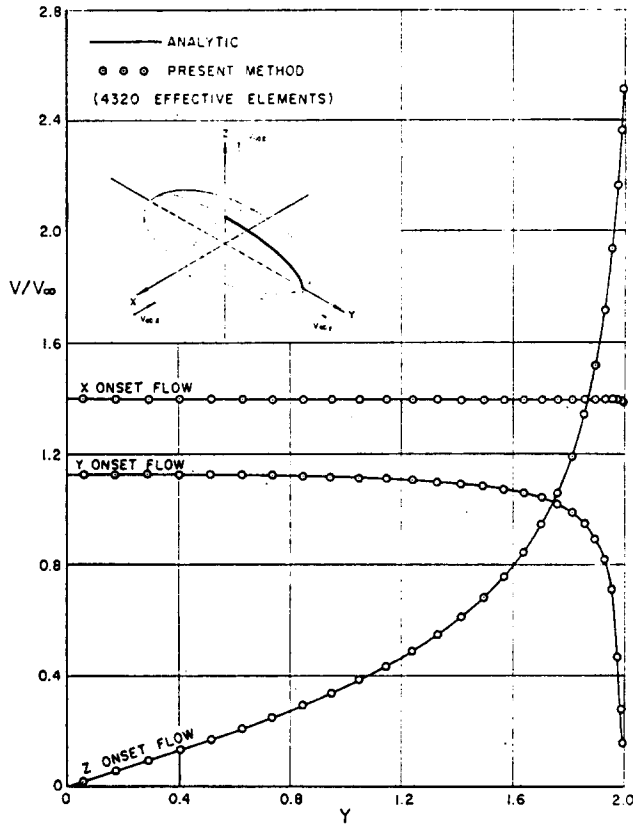
As was pointed out in Section 1.3, virtually the only truly three-dimensional flow for which an exact analytic solution is available is the flow about an ellipsoid with three unequal axes. The ellipsoid selected as an example has semi-axes in the x, y, and z directions equal to 1, 2, and $\frac{1}{2}$, respectively. The calculation utilized three symmetry planes with 540 elements on the nonredundant portion of the body (4320 total elements). Comparisons of analytic and calculated velocity distributions on this body are presented

(a)

FIG. 34. Comparison of analytic and calculated velocity distributions on an ellipsoid with semi axes 1, 2, $\frac{1}{2}$ in the x, y, z directions, respectively. (a) Flow in the xz-plane. (b) Flow in the yz-plane. (c) Flow in the xy-plane.

in Fig. 34. Each of the three parts of Fig. 34 shows velocity distributions along a curve on the body surface that lies in one of the symmetry planes. On each such curve velocity distributions are given for three uniform onset flows, one along each of the coordinate axes. In all cases the velocity in a

(b)

FIG. 34 (contd).

plane perpendicular to the onset flow is a constant equal to the maximum velocity of the flow. This is a characteristic of ellipsoids. For all the flows, the calculated and analytic velocity distributions agree well everywhere except near the end of the longest axis of the ellipsoid, the y-axis, for an onset flow parallel to the shortest axis of the ellipsoid, the z-axis, (Fig. 34c). The two solutions disagree slightly in this region, which is one of relatively high curvature, but even there the accuracy is probably sufficient for many purposes.

8. COMPARISON OF CALCULATED AND EXPERIMENTAL PRESSURE DISTRIBUTIONS ON VARIOUS CONFIGURATIONS

8.1 Preliminary Remarks

In order to justify the use of the present method as a design tool, calculated pressure distributions have been compared with experimental data for a large number of body shapes and flow conditions. In view of the good

(c)
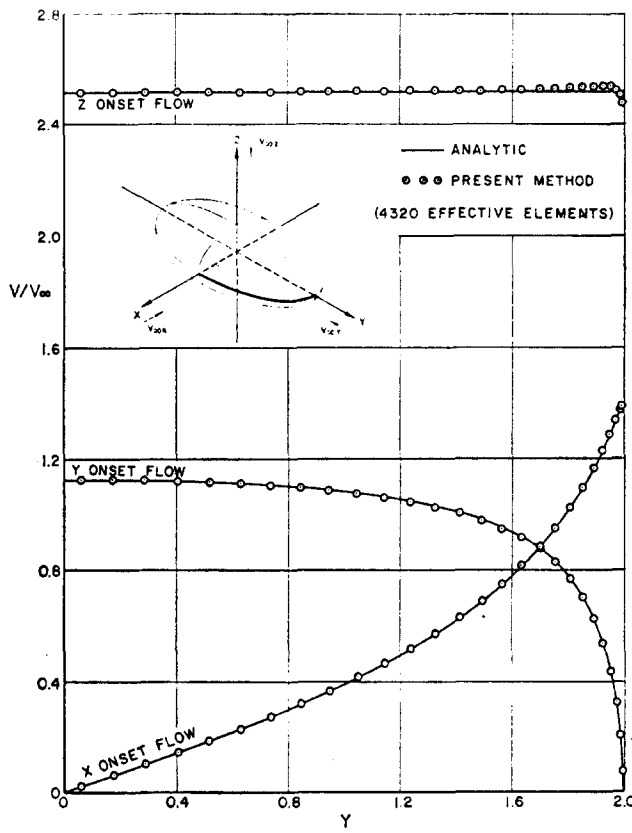
FIG. 34 (contd).

agreement between calculated and analytic solutions that is shown in Section 7, such comparisons essentially show how well potential flow agrees with real flow, that is, to what extent the neglect of viscosity and compressibility is justified. The results are most gratifying. The range of flow conditions over which potential flow is a useful approximation is quite surprisingly large.

As a result of comparing the calculations with experiment, it is concluded that for ordinary aircraft and marine applications viscosity has an unimportant effect on the surface pressure distribution, except in or near regions of catastrophic separation. Local regions of separation and reattachment do not significantly affect the pressure distribution. This is illustrated by several examples in this section for which calculated and experimental pressure distributions agree despite the obvious presence of local separation, which is indicated by the values of the pressure gradient. Even on bodies where catastrophic separation does occur, examples of which are the axisymmetric bodies at angles of attack up to 20° shown in Section 8.4, the

pressure distribution on the portion of the body ahead of the separation point is not affected very much. The method can be refined by using the calculated pressure distribution to obtain the boundary-layer displacement thickness, which is then added to the body shape (including an assumed wake if desired) and the calculation repeated. In nonlifting cases, this procedure is straight-forward, but it is rarely necessary, and it has not been done for any of the examples of this section. In lifting cases, the procedure, which is described in Section 8.2, is somewhat more complicated. A single example of the use of this refinement is given in that section.

The compressibility of the fluid does not significantly affect the pressure distribution if the value of the local Mach number is everywhere smaller than approximately one-half. This means that, for the types of bodies occur-ring in aircraft applications, compressibility effects may be safely ignored for free-stream Mach numbers below about 0.3 or 0.4. For higher Mach numbers, the calculations still agree with experiment if a suitable com-pressibility correction is used. In axisymmetric and three-dimensional cases the well-known Goethert transformation[17] is used to account for compres-sibility. For axisymmetric bodies at angle of attack, Mach number effects on the cross-flow terms are ignored, and the axial component of the flow is handled in the same manner as an axisymmetric flow. For two-dimensional lifting flows compressibility effects are usually accounted for by use of the Kármán–Tsien Mach number correction.[17] If these corrections are used, the calculated and experimental pressure distributions agree for all entirely subsonic flows. That is, the method gives good results except near stagnation points for all free-stream Mach numbers that do not give rise to local regions of supersonic flow. This is illustrated by several examples in this section. The use of these compressibility corrections restricts the type of body for which pressure distributions can be calculated at high subsonic numbers (in contrast to the incompressible case, for which the present method is valid for any body shape). For example, very blunt bodies cannot be handled. However, good results are obtained for most bodies designed to operate in this Mach number range, including some rather complicated shapes that are beyond the capability of approximate methods.

The remainder of this section presents comparisons of calculated and experimental pressure distributions. Over the years, a large number of comparisons have been collected. Some of these were obtained by the authors to evaluate the various parts of the method immediately after they were developed. Others were obtained by users of the method during the course of design studies. In 1964 all these comparisons, approximately 60 of them, were presented in a report.[6] The figures of this section show selected examples from Ref. 6 and also some more recent comparisons. Examples have been selected to illustrate various types of cases, and preference has been given to extreme or unusual flow situations.

Calculated and experimental pressures are compared in terms of the pressure coefficient C_p. In all cases for which the free-stream Mach number is large enough to necessitate the use of a compressibility correction, the Mach number is given on the figure. When no Mach number is listed, compressibility is ignored, because the flow Mach number is small enough to make compressibility unimportant. References for all published data are given both on the figure and in the text. When no reference is given, it is to be understood that the data were collected by personnel of the Douglas Aircraft Company during the course of design studies. In many examples of this section the body is considered to be semi-infinite. For calculational purposes such a body is assumed to have a segment of constant cross-section about five times as long as the segment over which the cross-section is varying (an afterbody length equal to about five times the nose length). No attempt has been made to account for the wind-tunnel walls in the calculations, although in some cases it would have been possible to do so. Usually, the wind-tunnel sting is also ignored.

8.2 *Two-dimensional Bodies*

Figure 35 shows calculated and experimental pressure distributions on a single airfoil, a Douglas design known as DSMA 387. The experimental data,
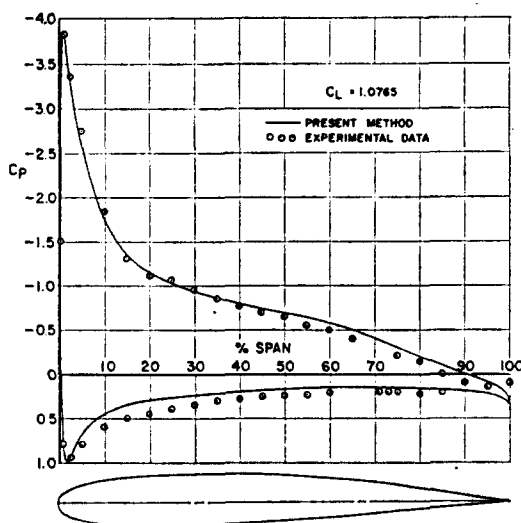
FIG. 35. Comparison of calculated and experimental pressure distributions on a Douglas DSMA 387 airfoil at a lift coefficient of 1.0765.

which were obtained by Douglas personnel in the Ames 12-ft low-speed wind tunnel, were taken from a three-dimensional wing model along a section

located 40 per cent of the semispan from the wing's plane of symmetry. Both calculated and experimental pressure distributions correspond to a lift coefficient of 1.0765; but they correspond to different angles of attack, because of the effect of viscosity on the relation between lift and angle of attack. The experimental and the calculated pressure distributions agree in the neighborhood of the pressure peaks but differ somewhat on the lower surface of the airfoil, on the rear portion of the upper surface, and at the trailing edge. The difference near the trailing edge is due to a viscous effect whose correction is discussed below.

An example of a triple airfoil is the wing section with slot and slotted flap illustrated in the sketch of Fig. 36. The calculated pressure distribution
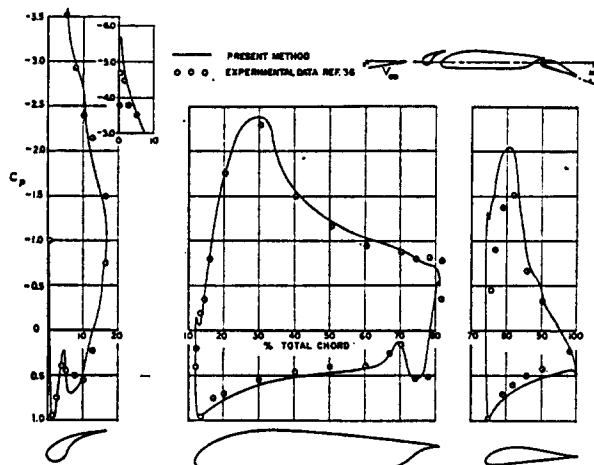
Fig. 36. Comparison of calculated and experimental pressure distributions on an NACA 23012 airfoil with fixed slot and with flap deflected 20° at 8° angle of attack.

is compared to low-speed wind tunnel data[36] for an angle of attack of 8°. Pressure distributions on the three airfoils are shown with the airfoil shapes below them, so that the pressure at a particular location can be determined immediately. The actual relative positions of the airfoils are shown only in the sketch. It can be seen that the calculated pressure distributions agree very well with experiment for this extreme flow, except on the flap, whose lift is overestimated by the calculations.

A method of compensating for possible viscous effects has been formulated.[8] It gives satisfactory results, but because it is rather time consuming, it is rarely used. First the pressure distribution on the airfoil is calculated in the usual way and used to calculate the boundary layer. The displacement thickness of the boundary layer is added to the actual body shape to produce a modified body shape. The flow about the modified shape is then calculated.

Velocities and pressures are evaluated, not on the modified shape, but at points in the flow field along the edge of the boundary layer of the original body. In particular, the Kutta condition is satisfied at the edge of the boundary layer at the trailing edge of the airfoil. An example of the results of using this refinement of the method is shown in Fig. 37, which compares calculated and experimental[37] pressure distributions on an 11.8 per cent-thick Joukowski
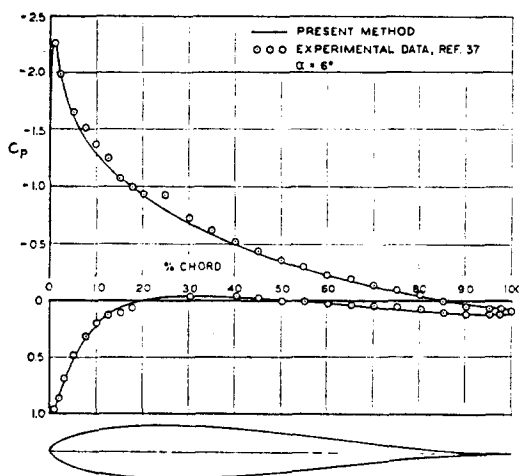
FIG. 37. Comparison of a calculated pressure distribution corrected for boundary layer effects with experimental data for an 11.8 per cent thick Joukowski airfoil at 6° angle of attack.

airfoil. Both pressure distributions correspond to an angle of attack of 6°. The good agreement of the calculation with experiment shows that the effect of the boundary-layer thickness on the pressure distribution and the effect of viscosity on the relation between lift and angle of attack have been accounted for correctly.

Figure 38 shows a comparison of calculated and experimental pressure distributions for a case where the free-stream Mach number is large enough to make compressibility effects significant. The body is an airfoil having an S-shaped camber line and operating at a lift coefficient of 0.25. The free-stream Mach number is 0.68, and the calculated incompressible pressure distribution has been adjusted by means of the Kármán–Tsien procedure. At the location of minimum pressure on the upper surface of the airfoil, the flow is almost sonic, and the calculated pressure distribution differs somewhat from the experimental in this region and also in the vicinity of the trailing edge, where boundary-layer effects alter the flow. Over the remainder of the airfoil, the agreement of the calculated and the experimental pressure

distributions is good. The data of Fig. 38 were obtained by Douglas personnel.

Section 4.5 describes a generalization of the present method that permits free-surface effects to be accounted for to first order. This generalization was applied to a 12 per cent-thick Joukowski hydrofoil moving at 5° angle of
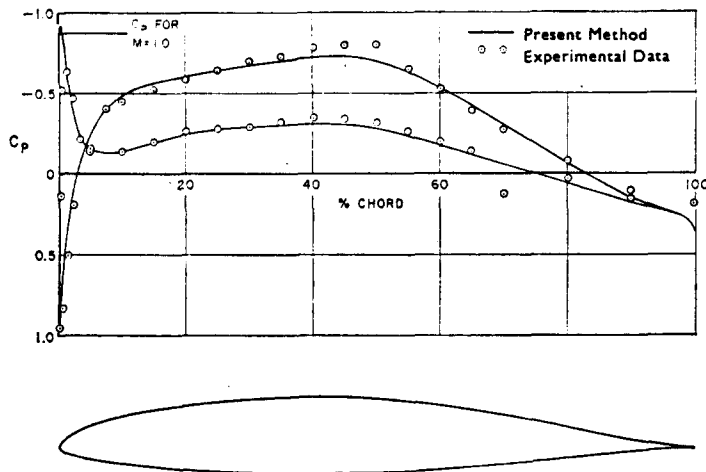
FIG. 38. Comparison of calculated and experimental pressure distributions on an airfoil at a lift coefficient of 0.25 for a free-stream Mach number of 0.68.

attack at a depth beneath the undisturbed free surface equal to 0.35 chord. Calculated and experimental[38] pressure distributions on the upper surface of the foil are shown in Fig. 39. Experimental pressures on the lower surface were not available. To exhibit the magnitude of the free-surface effect, the calculated pressure distribution at 5° angle of attack for the case when no free surface is present is also shown. Most of the free-surface effect is predicted by the calculations.

A modification of the present method (Section 4.6) can calculate flow about an infinite cascade of airfoils. Figure 40 compares calculated and experimental[39] pressure distributions on an airfoil in a cascade. The airfoil is an NACA 65-010 cascade blade, the stagger angle of the cascade is −15°, and the flow has an inclination of 30° at an infinite distance upstream of the cascade. The agreement of calculated and experimental pressure is good.

8.3 *Axisymmetric Bodies in Axisymmetric Flow*

Figure 41 shows pressure distributions on a prolate spheroid with an annular bump. The low-speed experimental pressure distribution[40] is compared with two calculated pressure distributions, one calculated by the
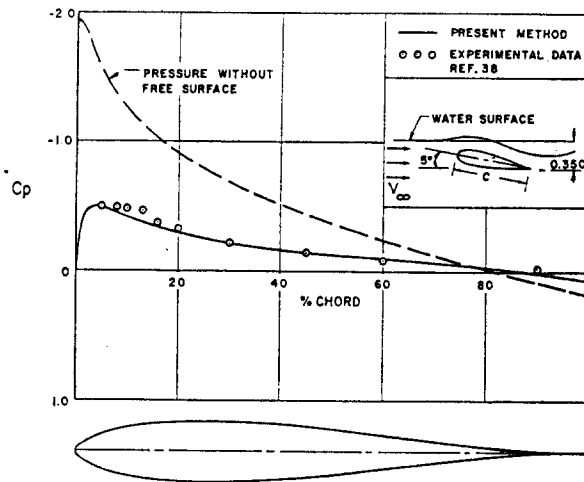
FIG. 39. Comparison of calculated and experimental pressure distributions on the upper surface of a 12 per cent thick symmetric Joukowski hydrofoil at 5° angle of attack, Froude number of 0.95, and a trailing-edge depth of 35 per cent chord. Also shown is the calculated pressure distribution without free-surface effect.
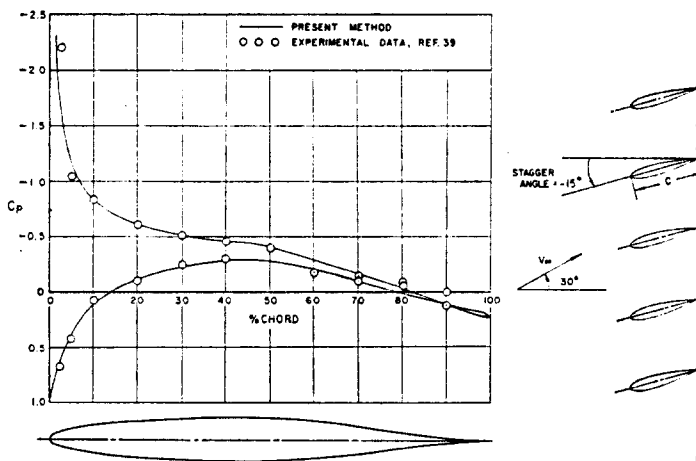
FIG. 40. Comparison of calculated and experimental pressure distributions on a symmetric NACA 65-010 airfoil in cascade at an inlet angle of 30° and a stagger angle of −15°.

present method and one calculated by a conventional approximate method.[41] The calculations of the present method agree closely with experiment, but the conventional method completely fails to respond to the presence of the bump. This case is admittedly an unfavorable one for the conventional method, but it shows how such a method may break down unexpectedly.
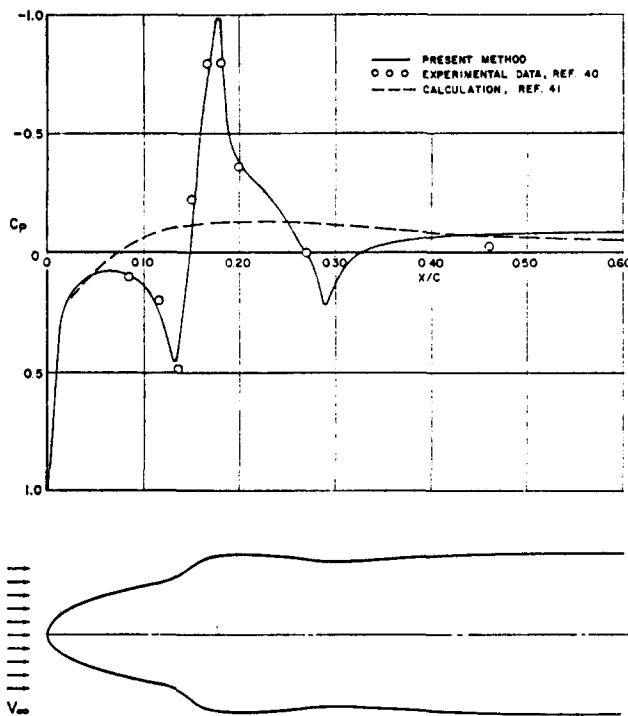
FIG. 41. Comparison of calculated and experimental pressure distributions on a
prolate spheroid with an annular bump.
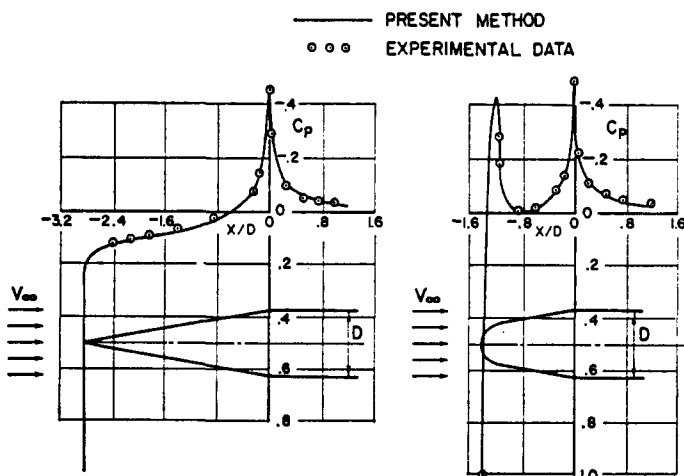
FIG. 42. Comparison of calculated and experimental pressure distributions on a
pointed cone-cylinder and a blunted cone-cylinder.

Figure 42 compares calculated and experimental pressure distributions on two bodies with corners, a pointed cone-cylinder and a blunted cone-cylinder. The data were obtained by Douglas personnel in the Douglas low-speed wind tunnel. The present method accurately predicts the experimental pressures even in the vicinity of the corners. This example shows that a pressure distribution calculated by the present method may actually be superior to an experimental one. Since the calculations for the blunted cone-cylinder agree with the data everywhere there are data points, it seems reasonable to conclude that the magnitude of the calculated forward pressure peak is also correct. This peak was missed in the tests simply because there was no pressure orifice at the proper location.

Inlets and propeller shrouds are special cases, because it is necessary to specify the flow through them, that is, the mass-flow ratio. To accomplish this, the present method calculates the flow about an altered configuration consisting of the desired inlet or shroud-lip shape followed by a semi-infinite afterbody (having constant inner and outer final diameters). Despite the necessary alteration of the body shape, the calculated results are quite satisfactory. In fact, inlets represent the type of body that occurs most frequently in design applications of the present method. Figure 43 compares
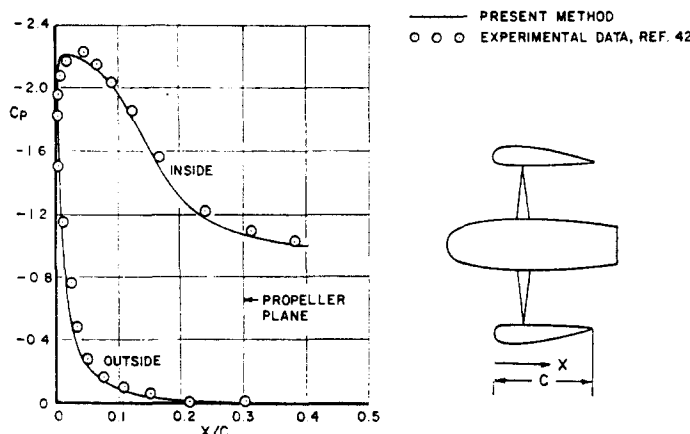
FIG. 43. Comparison of calculated and experimental pressure distributions on a propeller shroud with center-body in static operation.

calculated and experimental[42] pressure distributions on the forward portion of a propeller shroud in static operation (infinite mass-flow ratio). The center-body of the shroud was accounted for in the calculations, but the propeller itself was, of course ignored. The actual shroud has a small chord-to-diameter ratio, but it was treated as a semi-infinite body in the calculation. The agreement of calculated and experimental pressures on the inside and on the

outside of the shroud is good. A different calculation scheme is required to obtain pressures on the aft portion of the shroud.

For axisymmetric flows, compressibility effects are accounted for by means of a Goethert transformation. Figure 44 compares calculated and experimental[43] pressure distributions of a slender body for free-stream Mach
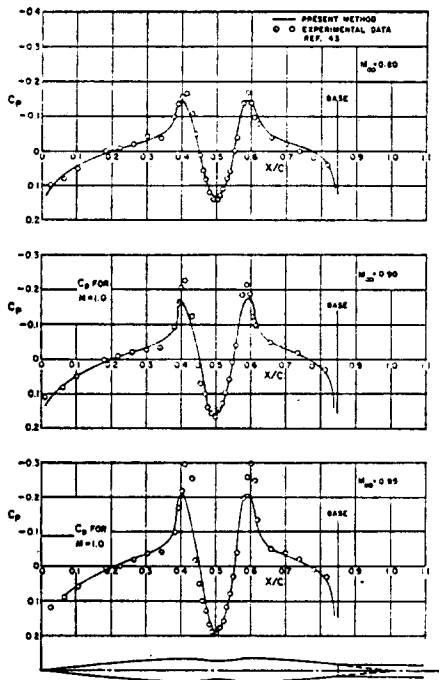
FIG. 44. Comparison of calculated and experimental pressure distributions on an indented body at three high subsonic free-stream Mach numbers.

numbers of 0.8, 0.9, and 0.95. The body profile is a symmetric parabolic arc that has been modified by an indentation in the region of maximum thickness. The rear of the body has been modified to accommodate the wind-tunnel sting, which has been accounted for in the calculation. It can be seen from Fig. 44 that only for the Mach number of 0.8 is the flow subsonic everywhere. For this Mach number, the agreement between the calculated and the experimental pressure distributions is quite good. At the higher Mach numbers, the agreement is also good, except in the regions where the flow is supersonic. No doubt this agreement is partly fortuitous, but it also reflects the fact that local effects are of chief importance in determining surface pressures.

Blunt bodies provide a more severe test of the validity of using the Goethert transformation with the present method than pointed bodies do, because

I

the region of sizable perturbation velocity near the nose is much larger. Calculated pressures near the stagnation point are meaningless, but they are usually quite good over the remainder of the body, where the perturbation velocity is not too large. A usable result is obtained by fairing the calculated pressures to the known pressure at the stagnation point. Figure 45
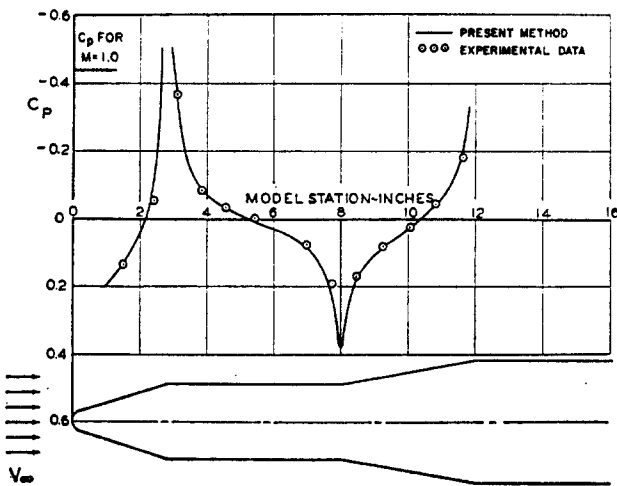
Fig. 45. Comparison of calculated and experimental pressure distributions on a Skybolt missile at a free-stream Mach number of 0.8.

shows calculated and experimental pressure distributions on a Skybolt missile for a free-stream Mach number of 0.8. The agreement is good even near the corners, which were not rounded in the calculation. The experimental data of Fig. 45 were obtained in the Douglas Aircraft Company Aerophysics Laboratory.

8.4 *Axisymmetric Bodies at Angle of Attack*

The flow about axisymmetric bodies at angle of attack generally separates somewhere on the body, and accordingly it might be expected that the present method of flow calculation would not give useful results for such cases. However, it has been found that calculated and experimental pressure distributions agree quite satisfactorily forward of the separation point. Moreover, it is remarkable how large the angle-of-attack effect on the pressure may be in some cases.

The present method calculates a pure cross flow (90° angle of attack) about the body in question and combines this with the axisymmetric flow (zero angle of attack) to obtain the flow at any angle of attack. The calculated cross flow may be combined with either the calculated or the experimental

axisymmetric flow. In some of the following comparisons, experimental zero-angle-of attack pressure distributions were used with the calculated cross flow, and in others calculated zero-angle-of-attack pressure distributions were used. In view of the agreement of calculation and experiment shown in Section 8.3, it does not appear to matter which is used. For some bodies, data were available for several angles of attack. In such cases, the data at the largest angle of attack were selected for comparison with the calculation.

In his Master's thesis, Johnson[44] compared pressure distributions computed by the present method with experimental data for a series of sharp and blunted cone-cylinders at zero angle of attack and at $\pm 20°$ angle of attack. This rather high angle of attack is an extreme test of the present method. Figure 46 shows an example of these comparisons. The body is a cone-cylinder having a semivertex angle of $15°$ that has been blunted by means of a
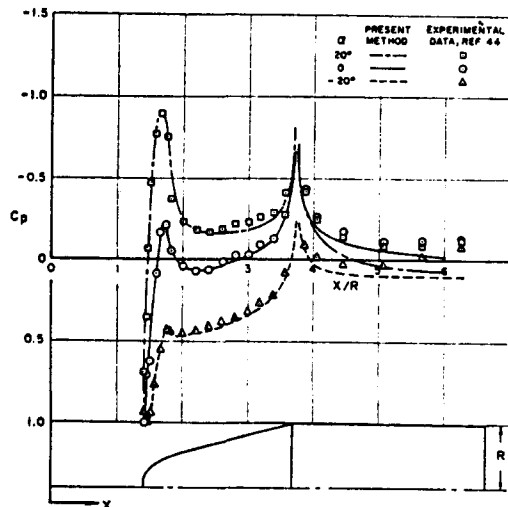
Fig. 46. Comparison of calculated and experimental pressure distributions on a blunted $15°$ cone-cylinder at $0°$ and $\pm 20°$ angle of attack.

spherical segment whose radius is equal to one-half the radius of the cylindrical afterbody. The cylindrical afterbody of the wind-tunnel model had a length equal to 1.45 times its diameter. In the calculations, however, the body is assumed to be semi-infinite. The difference between the body tested and the body calculated leads to discrepancies between calculated and experimental pressure on the aft portion of the afterbody, but its effect should be negligible over the nose region. In the comparison the calculated zero-angle-of-attack pressures are used with the calculated cross flow. In Fig. 46 pressures along

the top of the body are compared at 0°, 20°, and −20° angles of attack. Thus comparisons are made for both the leeward and windward sides of the body. Agreement is good over the nose section of the body, but less satisfactory over the afterbody. On the forward portion of the afterbody, the effect of flow separation around the sharp corner is important; on the aft portion of the afterbody, the effect of the finite length of the body is important. On the basis of the results of his comparisons, Johnson concludes: "As a result of the correlation, it is seen that the theoretical method studied [the method of the present article] produces such excellent agreement with experiment that it seems to be unnecessary to perform wind tunnel tests on bodies of revolution when very low speed pressure distributions are desired. This could result in considerable savings in time and money."

Tests were conducted in the Douglas Aircraft Company, Santa Monica Division Low-Speed Wind Tunnel on an inlet consisting of an NACA 1-70-100 cowling rounded to a constant inner diameter. In Fig. 47 calculated
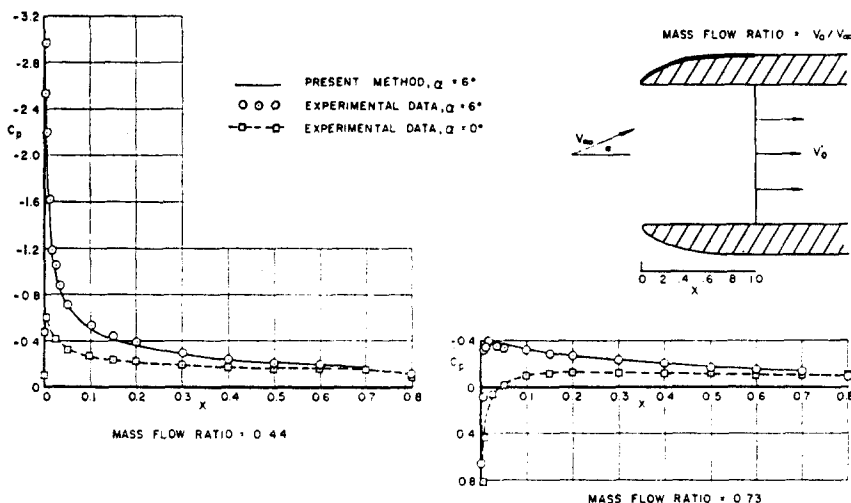
FIG. 47. Comparison of calculated and experimental pressure distributions on the exterior of an inlet lip at 6° angle of attack for two mass flow ratios.

and experimental pressure distributions are compared on the upper (leeward) side of the exterior surface of the inlet lip at 6° angle of attack. Comparisons are shown for two different values of mass-flow ratio. The experimental zero-angle-of-attack pressure distributions, which are used with the calculated cross flow, are also shown to exhibit the magnitude of the angle-of-attack effects. Agreement is good. The calculations correctly predict the presence of a large negative pressure peak at the smaller mass-flow ratio and the absence of such a peak at the higher mass-flow ratio.

An example of a multiple body is the cowling with spinner shown in Fig. 48. This figure compares calculated and experimental[45] pressure distributions on the upper (leeward) side of the spinner at 6° angle of attack. Also
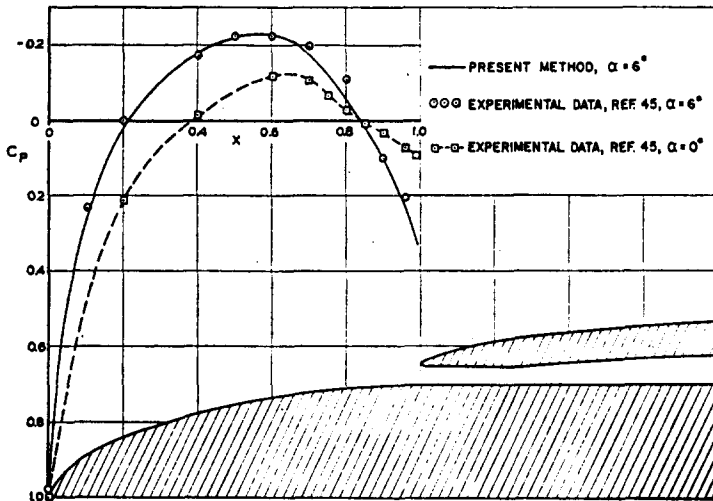
FIG. 48. Comparison of calculated and experimental pressure distributions on an
NACA 1-60-060 spinner in an NACA 1-70-100 cowling.

shown is the zero-angle-of-attack pressure distribution, which is used with the calculated cross flow. The calculated and experimental pressures are in good agreement. Over the forward portion of the spinner, the pressures at 6° angle of attack are more negative than those at 0° angle of attack, as is to be expected on the upper side of a body. On the downstream portion of the spinner, however, the effect of the cowling reverses the situation, and the change of pressure due to angle of attack is positive near the cowling. This somewhat unexpected behavior is accurately predicted by the present method.

To calculate pressure distributions on bodies of revolution at angle of attack for Mach numbers at which compressibility effects are significant, the calculated incompressible cross flow is used with the zero-angle-of-attack pressure distribution—calculated or experimental—at the proper Mach number. Figure 49 compares calculated and experimental[46] circumferential pressure distributions on a body of fineness ratio 12. The figure shows results for two Mach numbers at an axial location 10 per cent of the length of the body from the nose. The zero-angle-of-attack pressure, which is simply a constant for each Mach number, is used with the calculated cross flow. The good agreement of the calculated and the experimental pressure distributions justifies the use of an incompressible cross flow.

Nelson[47] has developed a procedure for using the results of the present method to calculate hydrodynamic coefficients for a blunt-based axisymmetric body, that is, to calculate hydrodynamic forces and moments on a maneuvering body due to translation, rotation, and acceleration. (The best-known hydrodynamic coefficient is the apparent mass.) He has compared calculated results
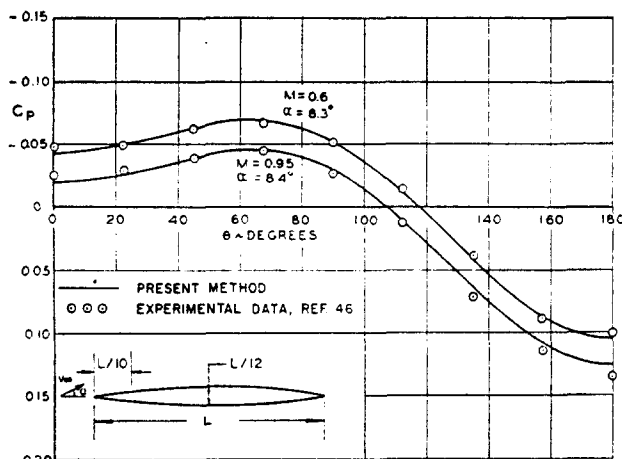

FIG. 49. Comparison of calculated and experimental circumferential pressure distributions at an axial location 0.1 of body length on a body at angle of attack for two high-subsonic free-stream Mach numbers.

with experimental data for eight hydrodynamic coefficients of a Polaris missile. Table 3 lists the average of the absolute values of the percentage errors obtained for the eight coefficients by calculations using the present method and the same average percentage error resulting from the use of a conventional calculation. Also shown are the maximum percentage errors in an individual coefficient for the two methods. The superiority of the calculation using the present method is evident.

TABLE 3

COMPARISON OF ERRORS IN CALCULATED HYDRODYNAMIC COEFFICIENTS
OF A POLARIS MISSILE

	Average absolute value of percentage error for eight coefficients	Maximum percentage error in an individual coefficient
Calculation using present method	4.9	7.3
Conventional calculation	11.7	23.5

8.5 *Three-dimensional Bodies*

For three-dimensional bodies an entire surface must be approximated by elements instead of just a single curve. Even if many more elements are used, the present method is less accurate for three-dimensional bodies than for two-dimensional and axisymmetric bodies. The calculations are quite satisfactory for single bodies of fairly simple shape. For complicated bodies, and in particular for multiple-body interference problems, the calculations give useful information in the sense that a fair approximation of experiment is obtained, but the high degree of accuracy that is apparent in the comparisons of the preceeding sections is not normally realized.

Recently, Douglas personnel drastically redesigned the nose region of a C-135 aircraft, in order to accommodate a 70-in. steerable antenna for communication with the Apollo spacecraft. Essentially, the airplane was fitted with a very large radome. The present method was used in evaluating some of the designs considered, and in some cases comparisons with experiment were obtained. Figure 50 shows the surface elements used to approximate one
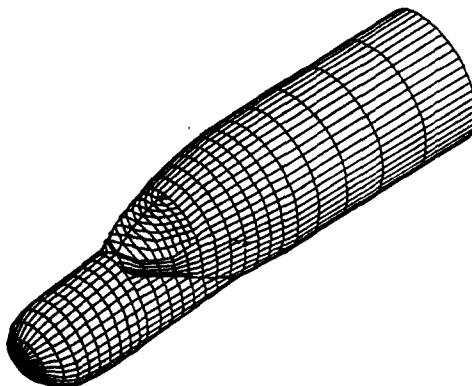
FIG. 50. Elements used to approximate a C-135 fuselage with a large radome. (Unretouched output from an automatic plotter.)

shape that was considered. (Such graphical displays of the elements are obtained automatically and are often useful in detecting input errors.) Calculated and experimental pressure distributions along three curves on the surface are compared in Fig. 51. Pressures along the top and bottom of the body in the symmetry plane are shown, as are pressures along the curve of maximum breadth on the side of the body. The data of Fig. 51 are from a test at a free-stream Mach number of 0.4, but the calculated pressure distributions are for incompressible flow. The good agreement of calculation and experiment justifies the neglect of compressibility in the former. Figure 52 shows the isobars calculated by the present method. Experimental isobars could not be obtained, because pressures were not recorded at enough locations to define them accurately.

120   J. L. HESS AND A. M. O. SMITH
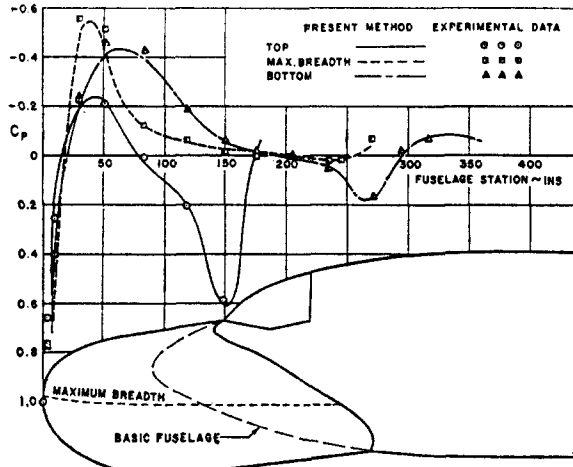
FIG. 51. Comparison of calculated and experimental pressure distributions on a
C-135 fuselage with a large radome at zero angle of attack.
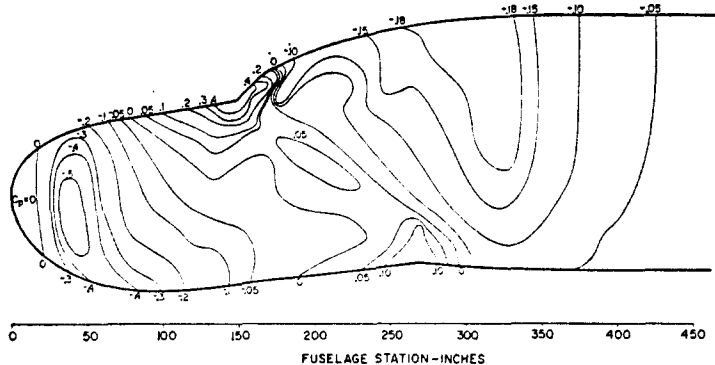
FIG. 52. Calculated isobars on a C-135 fuselage with a large radome at zero angle
of attack.

Figure 53 shows a delta wing of aspect ratio unity whose section shape is
a 12 per cent thick parabolic arc. The calculated and experimental[48] isobars
for the condition of zero lift are also presented. The two patterns are seen to
be essentially identical. More precise comparisons are shown in Fig. 54, which
compares calculated and experimental spanwise pressure distributions for
three chordwise locations in the midplane, that is, pressures are plotted
versus distance perpendicular to the midplane at three stations along the
midplane chord. Experimental data are shown for both the upper surface
and the lower surface. By symmetry, the pressure at any locations hould be
identical on the upper and lower surfaces, so that the differences between
these pressures give a measure of the experimental error. The calculated
and experimental pressures agree to within experimental error.

SECTION SHAPE- CONSTANT ACROSS SPAN   ASPECT RATIO- 1

THICKNESS RATIO- CONSTANT ACROSS SPAN   THICKNESS- 12%
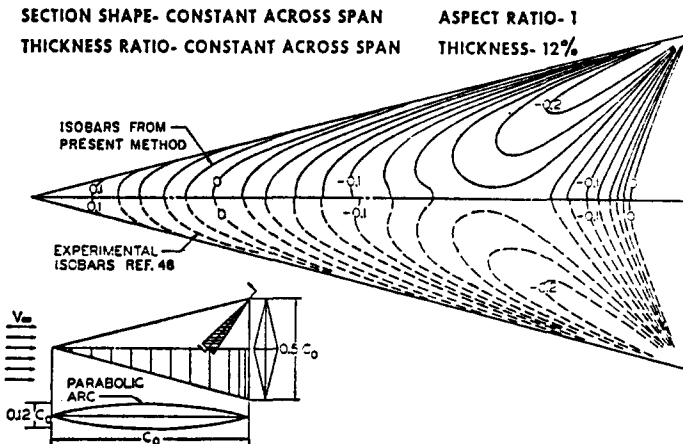
FIG. 53. Comparison of calculated and experimental isobars on a symmetric delta wing at zero lift.
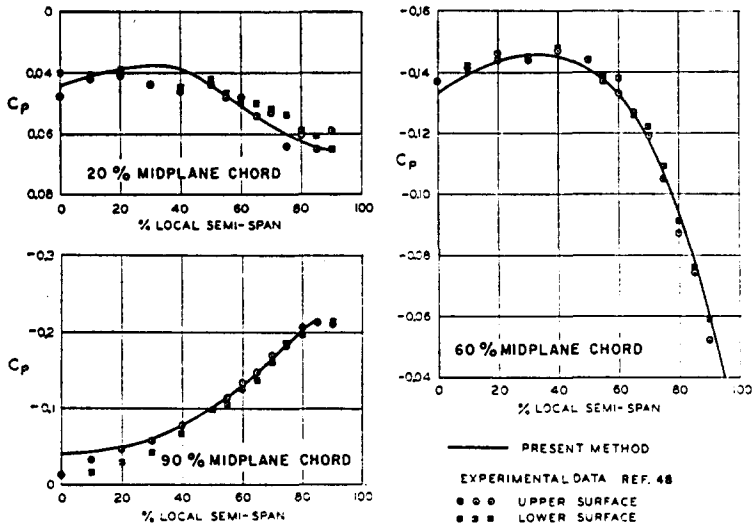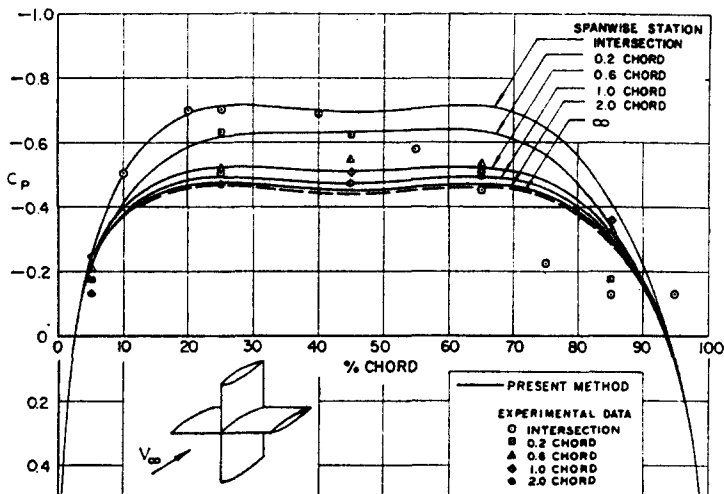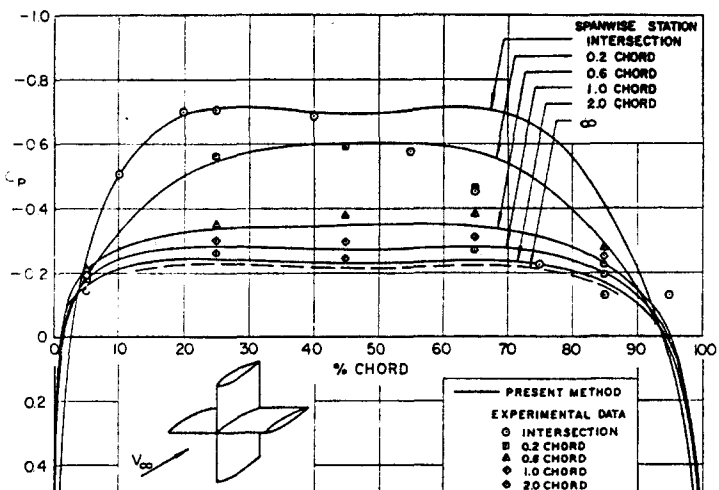
FIG. 54. Comparison of calculated and experimental spanwise pressure distributions on a symmetric delta wing at zero lift.

W. L. Moore of the David Taylor Model Basin, Carderock, Maryland used the present method to calculate the pressure distribution on a pair of intersecting wings, as shown in Fig. 55. The wings were straight and untapered, and had constant, symmetric airfoil sections that differed only in thickness ratio, one being 20 per cent thick and the other 10 per cent thick. The wings, which were considered to be infinite in both spanwise directions, intersected at a right angle, and thus the complete configuration had two

(a)

(b)

FIG. 55. Comparison of calculated and experimental pressure distributions on a pair of straight non-lifting wings of constant symmetric airfoil section that intersect at a right angle. (a) Pressures on the 20 per cent thick wing. (b) Pressures on the 10 per cent thick wing.

perpendicular planes of symmetry. The direction of the onset flow was parallel to both symmetry planes, and thus both wings were nonlifting. Tests of this configuration were conducted in the David Taylor Model Basin Low Speed Wind Tunnel. Comparisons of the calculated and experimental pressure distributions were made and furnished the authors by Mr. Moore in

a private communication.* The comparisons are shown in Fig. 55. The effect on the pressures of the thickening of the boundary layer in the intersection is quite evident from the data on the aft portion of the wings in the intersection and at the spanwise station nearest to the intersection (0.2 chord). At these locations, calculated and experimental pressures agree only over the forward half of the wings. At the spanwise stations farther from the intersection, the agreement is fairly good over the entire chord, with calculated pressures generally less negative than experimental ones. The pressure distributions on the wings, identical in the intersection, become almost two-dimensional far out along the span. The variations of pressure with distance along the span are quite different for the two wings, since their thicknesses, which determine their two-dimensional pressure distributions, differ by a factor of two. The spanwise variation of pressure distribution is predicted fairly well by the calculations.

Probably the most extreme case to which the present method has been applied is the calculation of the mutual interference between the wing, pylon, and nacelle of the DC-8. The configuration about which the flow was calculated is sketched in Fig. 56. It consists of a short portion of the DC-8 wing to which is attached the inboard nacelle and pylon, and the mirror image of
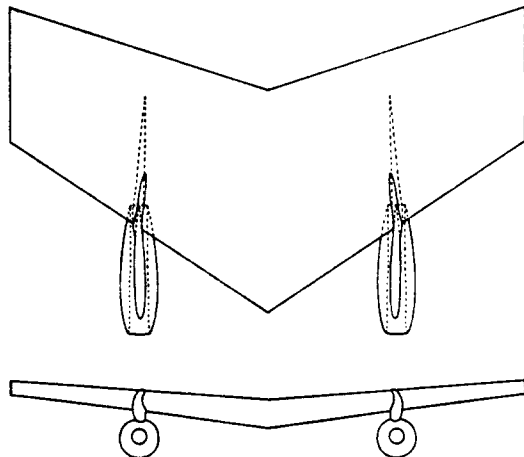

FIG. 56. Adjusted DC-8 wing-pylon-nacelle combination.

this wing-pylon-nacelle combination. Thus the two pylon-nacelles are much closer together in the calculated configuration than they are on the airplane. It was hoped that the resulting increase in mutual interference between the pylon-nacelles would partially compensate for the omission of the fuselage.

*Addition in Proof: Mr. Moore subsequently collected his findings into David Taylor Model Basin Report No. 2131, Some Theoretical and Experimental Results on Pressure Interaction of Hydrofoil Boat Components (November 1965).

In any event, such an effect should be small. The pressure distribution is chiefly determined by the local wing-pylon-nacelle geometry. The calculations were performed for the nonlifting condition. This rather complicated geometry includes both the upper and lower wing surfaces and both interior and exterior nacelle surfaces. The wind-tunnel data with which the calculations were compared were obtained, by Douglas personnel, at the Mach number of 0.825, which was high enough to cause local regions of supersonic flow. The model tested was a complete DC-8 and thus differed from the calculated configuration by the presence of the fuselage, outboard wing, and outboard nacelles. Figure 57 compares calculated and experimental pressure distributions on the pylon. The Goethert transformation was used to account for compressibility. As is indicated in the figure, the calculated and the experimental pressures were obtained at slightly different locations. The Regions
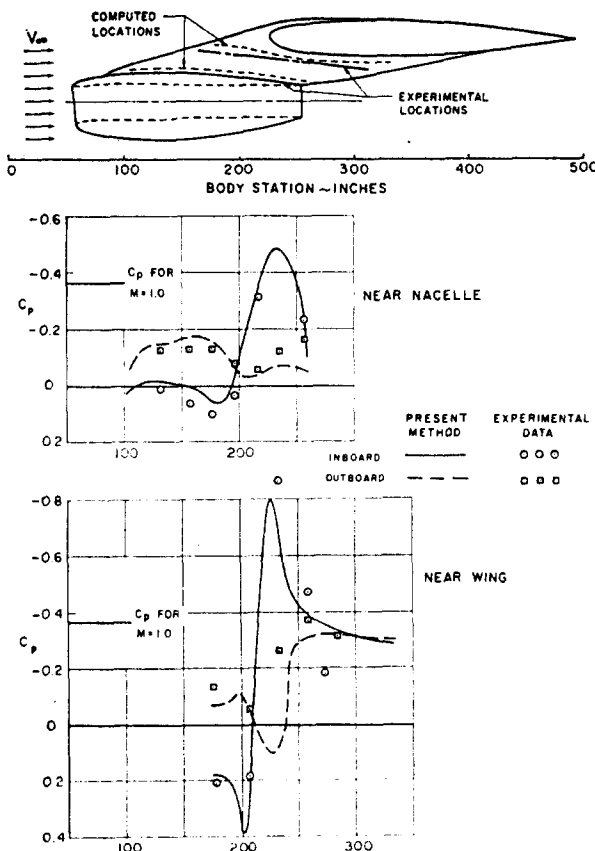
FIG. 57. Comparison of calculated and experimental pressure distributions on a DC-8 pylon in the presence of the nacelle and wing at a free-stream Mach number of 0.825 for the zero-lift condition.

of supersonic flow are evident. The agreement of calculated and experimental pressures is considered to be good, under the circumstances. In particular, the calculations predict, correctly, that the pressure peaks on the inboard side of the pylon are considerably more negative than those on the outboard side, which is the result of chief design interest.

9. CALCULATED FLOWS ABOUT CERTAIN BODIES

9.1 Some Families of Bodies that are Useful in Design Studies

In design applications the present method is usually used to calculate the flow about a specific body of interest, but it has also proved useful in other ways. On several occasions the method has been used to calculate velocity distributions on certain one-parameter families of bodies, when there was no immediate need for this information. The results have been used repeatedly to quickly obtain approximate information about the nature of velocity distributions on a body with the same general geometric properties as a body belonging to one of the families. The bodies for which calculations have been performed are semi-infinite. Each consists of a certain nose shape of finite length followed by a semi-infinite afterbody of constant thickness. (As is stated in Section 8.1, in the calculation the afterbody length is taken to about five times the nose length.) This type of body seems to arise more often in applications than any other. Some examples of calculated velocity distributions on bodies of these families are presented below.
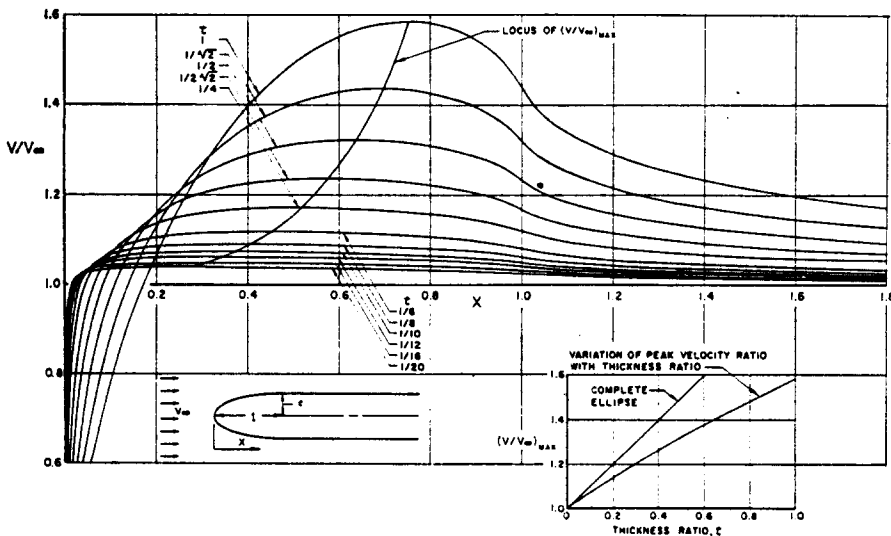

FIG. 58. Calculated velocity distributions on semi-infinite two-dimensional bodies with elliptical noses.

A family that is useful for studying thickness effects for blunt semi-infinite bodies is composed of bodies with elliptical noses. The bodies may be either two-dimensional or axisymmetric. (An axisymmetric body of this shape is commonly called an ellipsoid-cylinder, but apparently there is no name for the two-dimensional analogue.) Figures 58 and 59 show calculated
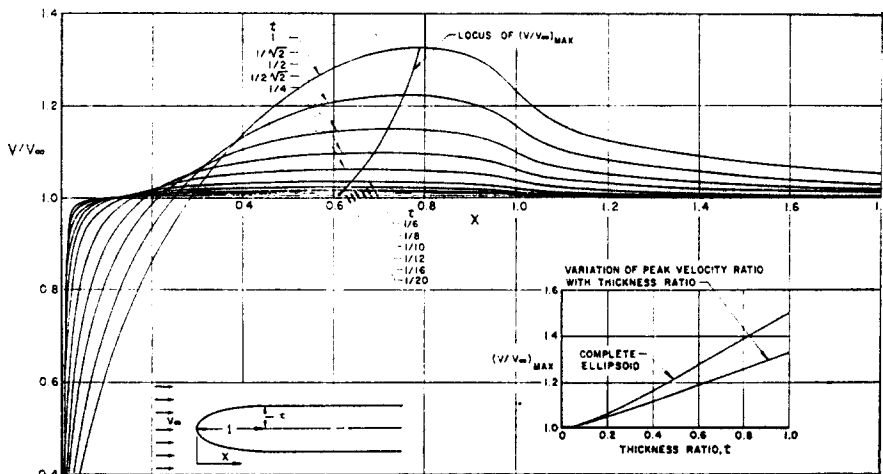

FIG. 59. Calculated velocity distributions on semi-infinite axisymmetric bodies with elliptical noses.

surface velocity distributions on bodies of this family having various nose thickness ratios, two-dimensional bodies in Fig. 58 and axisymmetric bodies in Fig. 59. In every case the onset flow is a uniform stream parallel to the semi-infinite afterbody. A comparison of the two figures shows similarly shaped velocity distributions for corresponding bodies but higher velocities for the two-dimensional bodies. The reduction of surface velocity in the axisymmetric case compared to the two-dimensional case is sometimes called "three-dimensional relief". The variation of maximum surface velocity with nose thickness ratio is shown in each case and compared with the result for the family of bodies whose profile curves are complete ellipses (elliptic cylinder and ellipsoid) to exhibit the reduction of the maximum surface velocity due to the presence of the semi-infinite afterbody.

To illustrate thickness effects for pointed semi-infinite bodies, a family was selected whose members have ogival noses. That is, the profile curve of the nose is a circular arc that joins the afterbody with continuous slope. Calculated surface velocity distributions for various nose thickness ratios are shown in Figs. 60 and 61 for the two-dimensional and axisymmetric
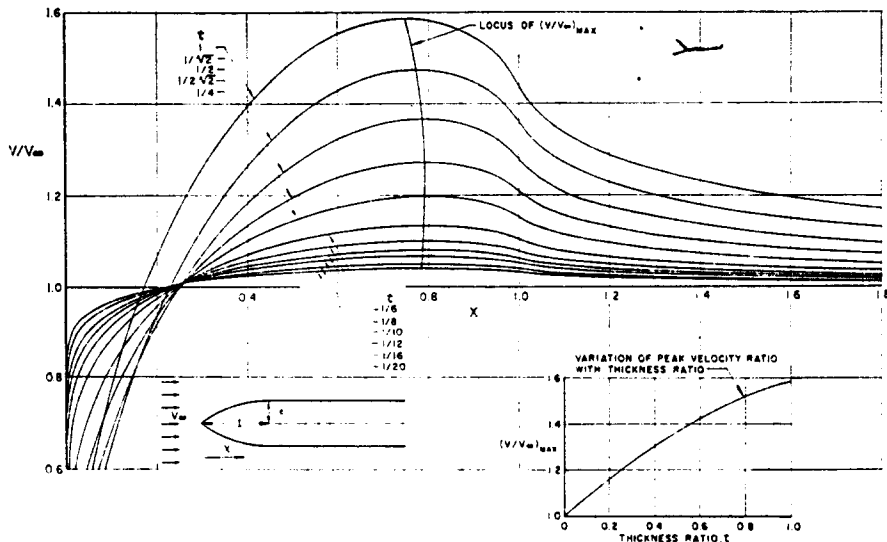
FIG. 60. Calculated velocity distributions on semi-infinite two-dimensional bodies
with circular-arc noses.
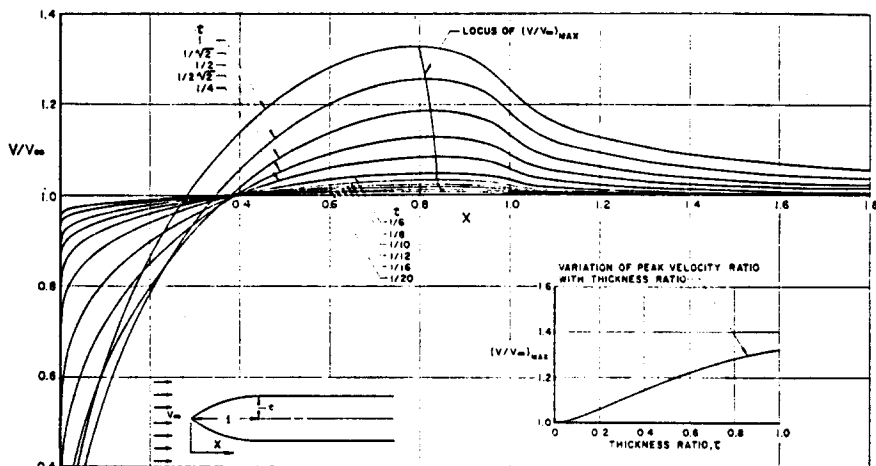
FIG. 61. Calculated velocity distributions on semi-infinite axisymmetric bodies
with circular-arc noses.

cases, respectively. The onset flows are uniform streams parallel to the semi-infinite afterbodies. The variation of maximum surface velocity with nose thickness ratio is also shown in each figure.

Another frequently occurring application is that in which the nose thickness ratio is fixed and it is desired to investigate the effects on the surface velocity distribution of other geometric parameters of the nose shape, for example,

nose bluntness. Figures 62 and 63 show calculated velocity distributions on a family of blunt shapes whose nose lengths are 2.5 times the thicknesses of their afterbodies. The equations of the nose shapes, which are shown
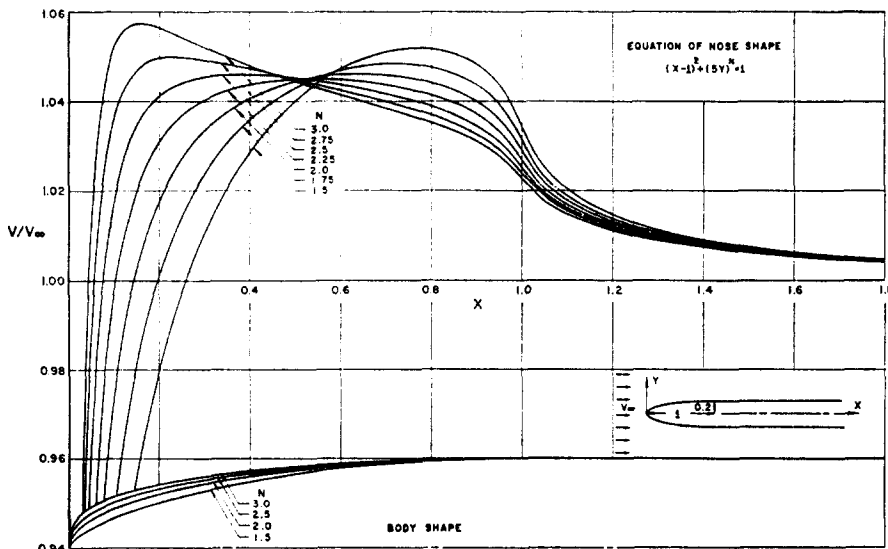

FIG. 62. Calculated velocity distributions on semi-infinite two-dimensional bodies with modified elliptical noses of 20 per cent semi-thickness.
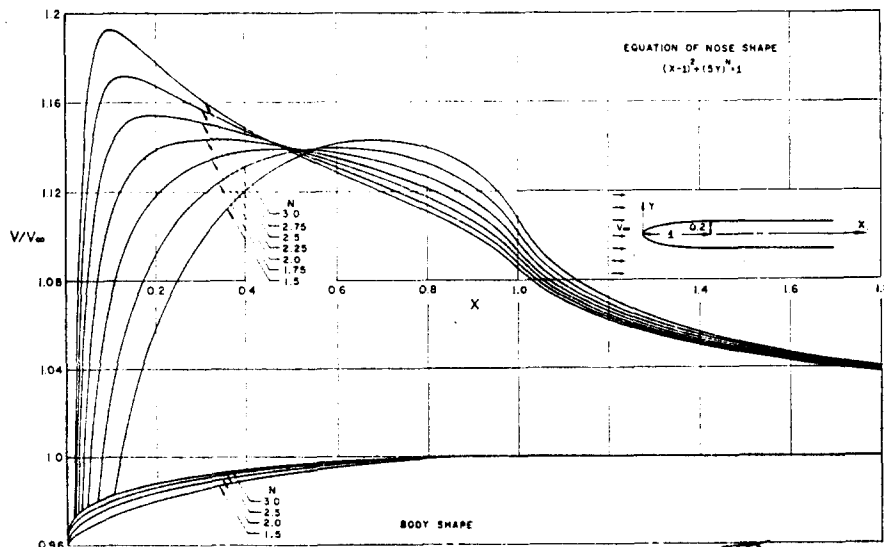

FIG. 63. Calculated velocity distributions on semi-infinite axisymmetric bodies with modified elliptical noses of 20 per cent semi-thickness.

in the figures, are obtained by varying the exponent of y in the standard equation of an ellipse. Both the two-dimensional shapes of Fig. 62 and the axisymmetric shapes of Fig. 63 are in uniform onset flows parallel to their afterbodies. For members of this family, the velocity distribution is rather sensitive to the value of the exponent, although at approximately 50 per cent of the nose length the velocity is nearly the same for all bodies. For the two-dimensional case, the body with the elliptical nose has very nearly the smallest maximum velocity of any member of the family, but this is not true for the axisymmetric case.

9.2 *Some Unusual Bodies*

On several occasions flow calculations have been performed for certain bodies that are rather different from those that occur in ordinary applications. Often the motivation is simply curiosity. Some of these calculations illustrate flow phenomena that do not occur in any of the well-known examples of potential flow. Others show applications that may sometime be of practical use. Some examples of these calculated flows are presented in this section.

Figure 64 shows a symmetric, 20 per cent-thick two-dimensional body that
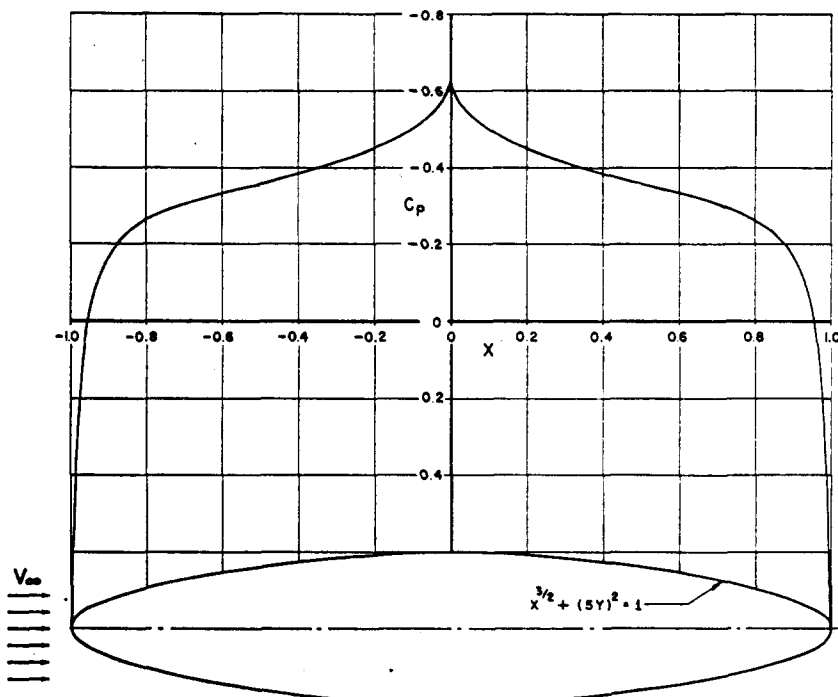

FIG. 64. Calculated pressure distribution on a two-dimensional body having zero curvature radius at the location of maximum thickness.

appears qualitatively similar to an ellipse. The equation of the profile curve
of the body is given in the figure. Although the radius of curvature of the
profile appears to be rather large at the point of maximum thickness, $x = 0$,
it is easily verified from the equation that the radius of curvature is zero
there. On each side of the point $x = 0$ there is a small region in which the
radius of curvature falls rapidly to zero. The slope of the profile curve is
continuous. The calculated surface pressure distribution due to a uniform free
stream parallel to the x-axis is shown in the figure. A very dense concentra-
tion of elements near $x = 0$ was used. It can be seen that the unusual curva-
ture variation of the profile is reflected in the pressure distribution, which
has a sharp peak at $x = 0$. The pressure distribution on an elliptic cylinder
of the same thickness ratio is, on the contrary, very flat, with a significantly
lower value of peak pressure (the minimum value of C_p on a 20 per cent-thick
elliptic cylinder is -0.44). The ability to account for small details of a
body surface that may have significant effects on the flow is an important
advantage of the present method.

A "yo-yo"-type body is an axisymmetric shape that has a small circular
neck joining two circular flanges. The profile curve of such a body is shown
in Fig. 65, with the symmetry axis vertical. The cross flow about this body
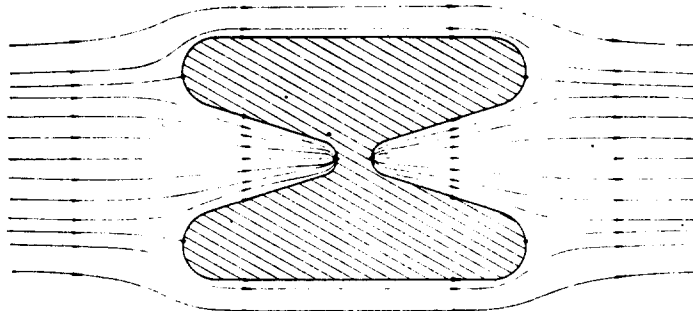

FIG. 65. Calculated streamlines in the plane containing the onset flow vector and the
body's symmetry axis for uniform cross flow about an axisymmetric yo-yo type
body.

was computed for the case of a uniform onset flow whose direction is from
left to right on the figure. Velocity components were evaluated at a large
number of points off the body surface, and streamlines were constructed by
the method of isoclines. The streamline pattern in the plane containing the
onset flow vector and the body's symmetry axis is shown in Fig. 65. On each
side of the body there are three stagnation points—one at the center of the
neck and one on each flange near the point of maximum body diameter. All
the streamlines between the two "dividing" streamlines that meet the body

at the stagnation points on the flanges come together at the windward stagnation point on the neck and travel around the neck as a single streamline, which branches into many streamlines at the leeward stagnation point on the neck. This behavior is essentially three-dimensional and cannot occur in two-dimensional or axisymmetric flows. The two "dividing" streamlines behave in a more familiar manner. Each one branches at a windward stagnation point into many streamlines, which traverse the body and join again at a leeward stagnation point.

An example of an interior flow field is shown in Fig. 66. The body is an axisymmetric duct in which a uniform flow in a circular pipe is diffused
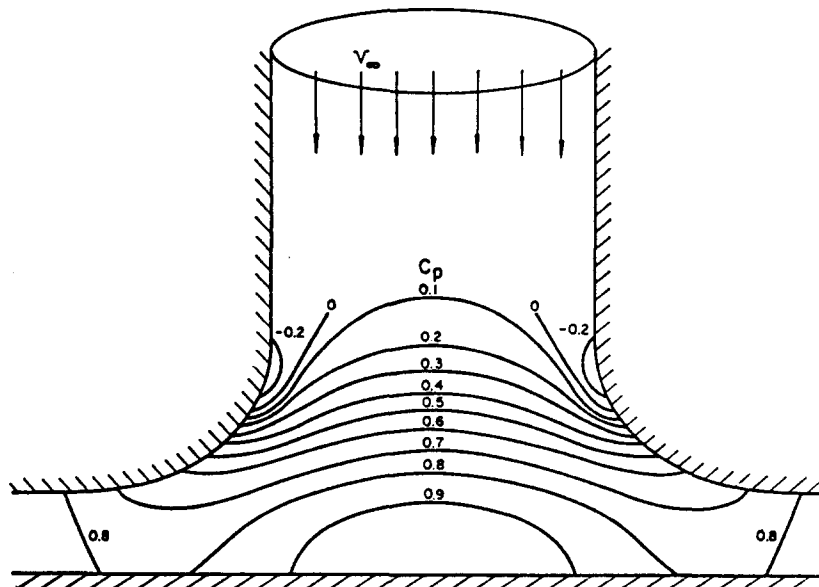

FIG. 66. Calculated isobars in a radial diffuser.

radially outward. The calculated isobars are shown in the figure. Although this flow was computed simply as an interesting example, the case of a radial diffuser has subsequently become a fairly common one in design applications. The problem is usually to shape the curved portion of the diffuser to obtain certain favorable flow properties.

A case that may have applications is a flush inlet in an infinite plane with a uniform onset flow parallel to the plane. The profile curve of the body is shown in Fig. 67. The inlet lips are polynomial curves that smoothly join the infinite plane to the straight parallel walls inside the inlet. The inlet was considered both as a two-dimensional body and as an axisymmetric body whose symmetry axis is the center line of the inlet. For each inlet two

fundamental solutions were calculated: the flow due to a uniform onset flow
from left to right for the case of zero flow far inside the inlet and the flow due
to a unit flow far inside the inlet with no onset flow. By combining these two
flows the flow for any ratio of inlet velocity to free-stream velocity can be
obtained. The velocity distributions shown in Fig. 67 are for the case when
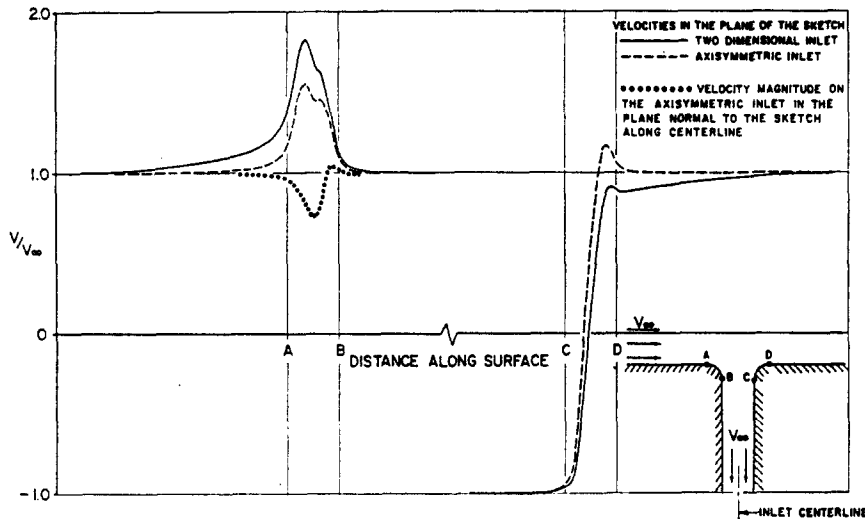
FIG. 67. Calculated velocity distributions on a two-dimensional and on an axi-
symmetric flush inlet for an inlet velocity equal to free-stream velocity.

the velocity far inside the inlet equals the velocity of the onset flow. The sign
convention for velocity is the one described in Section 3. The velocity is
positive if the flow field lies to the left with respect to the velocity vector, and
it is negative if the flow field lies to the right. Thus far inside the inlet the
velocity is positive on the left wall and negative on the right wall. For the
axisymmetric inlet velocity distributions in two planes are shown in the
figure. The first is the velocity in the plane containing the onset flow vector
and the inlet centerline (the plane of the sketch in the figure). Comparing this
velocity distribution with that for the two-dimensional case contrasts the
flow near a long slot inlet with that near a circular inlet. As expected the
approach to free-stream velocity along the infinite plane is more rapid for the
axisymmetric inlet than for the two-dimensional inlet. On the windward
side the velocity peak is higher for the two-dimensional inlet than for the
axisymmetric inlet, but this situation is reversed on the leeward side. The
"wiggles" near the windward velocity peaks are perhaps surprising, because
the surface is smooth in that vicinity. But the accuracy of the calculations is
such that they are apparently real. The variation of velocity is smooth for

both fundamental solutions for both inlets. The "wiggles" arise from adding two functions whose peaks are in different locations. The third curve shown in Fig. 67 gives the velocity magnitude for the axisymmetric inlet in the plane that contains the inlet centerline and is normal to the onset flow vector (the plane normal to the sketch in the figure). This distribution is shown only on one side of the inlet because it is symmetrical.

10. OTHER PHYSICAL PROBLEMS

10.1 *Types of Problems*

It is evident that the idea of reducing a boundary-value problem for a partial differential equation to an integral equation over the boundary surface can be applied to physical problems other than that of potential flow. This approach appears attractive for many linear problems governed by elliptic partial differential equations. In several applications the mathematical formulation describes the physical situation exactly, or nearly so, and experimental verification, such as that of Section 8, is not required. To date, two types of problems have received attention: those governed by Laplace's equation, with various boundary conditions, and those governed by the Helmholtz equation, which is the next simplest elliptic equation after Laplace's.

Laplace's equation with Dirichlet boundary conditions (the potential itself is specified on the boundary) governs certain problems of electrostatic potential and steady-state temperature distributions. Laplace's equation with Neumann boundary conditions (the normal derivative is specified on the boundary) has several applications outside of fluid dynamics. Mixed boundary conditions for Laplace's equation also have a variety of applications.

The Helmholtz equation is derived from the wave equation by assuming that all quantities have a harmonic dependence on time at a single frequency. Thus it governs problems of "steady" wave propagation, in particular propagation of acoustic waves. For the latter problem, the potential is proportional to the perturbation pressure in the fluid medium, and both it and the fluid velocity are complex. Boundary conditions for the Helmholtz equation may be Dirichlet, Neumann, or mixed.

The authors have modified the present method in several ways to make it applicable to different boundary conditions and different partial differential equations. These modifications are described briefly in Section 10.2. Several other investigators have applied integral equation techniques to the solution of various physical problems. Their work is described in Section 10.3. Since the present authors are not familiar with the literature of all fields, the investigations cited in Section 10.3 should be considered to be simply a group of examples.

10.2 *Extensions of the Present Method*

The present method has been modified by the authors to solve Laplace's equation with Dirichlet boundary conditions for both two-dimensional and axisymmetric boundaries. Both surface source distributions and surface dipole distributions have been employed. Use of the former leads to an integral equation of the first kind; use of the latter gives an integral equation of the second kind, which is quite similar to that obtained for the fluid-dynamics problem (Neumann boundary conditions) with a source distribution. A limited amount of experience indicates that it is preferable to use dipole distributions for interior problems and source distributions for exterior problems, but considerable study remains to be done before any result can be stated with confidence. A similar modification could be made for three-dimensional problems with Dirichlet boundary conditions, but it would be difficult to use a surface source distribution in a three-dimensional case. The coefficient matrix of the set of linear algebraic equations that approximate the resulting integral equation of the first kind does not have a dominant main diagonal, and the iterative solution methods, whose use is indicated by the large order of this matrix, would almost certainly not converge.

The present method is now being modified to calculate solutions of the three-dimensional Helmholtz equation with Neumann boundary conditions. The point source potential $1/r$ that is appropriate for Laplace's equation is replaced by the "point source" potential for the Helmholtz equation, which is

$$\varphi = \frac{e^{ikr}}{r} \tag{10.2.1}.$$

where the constant k is the wave number. All procedures used are logically similar to those used for the fluid dynamics problem. A complex Fredholm equation of the second kind for the surface source density is approximated by a set of linear algebraic equations for the values of source density on plane quadrilateral surface elements.

10.3 *Integral Equation Methods in the Literature*

10.3.1 *Laplace's equation.* A problem governed by Laplace's equation with Neumann boundary conditions is that of determining the magnetic field exterior to a superconducting body. Such a problem is considered by Bourke,[49] whose specific application is a magnetically-supported rotor. Since the mathematics is identical to that of the fluid dynamics problem, the present method is used without modification. Both axisymmetric and "cross flow" cases are considered.

Jaswon and Ponter[50] consider a two-dimensional problem with Neumann boundary conditions. They solve the St. Venant torsion problem, which is usually formulated with Dirichlet boundary conditions, and the principal

interest is in interior problems. Green's theorem is used to obtain an integral equation of the second kind for the warping function. A set of control points is used; the integral is evaluated by Simpson's rule (except for local effects); and the integral equation is approximated by a set of linear algebraic equations for the values of the warping function at the control points.

Cruise[51] investigates the axisymmetric case with Dirichlet boundary conditions. The specific problem of interest is that of the electric field about surfaces on which the potential is known, in particular conductors. The method of solution uses a surface distribution of source density, which in this case has physical significance, since it is the electric-charge density. Application of the boundary condition leads to an integral equation of the first kind. The body profile is approximated by straight-line elements, over each of which the source density is assumed to be constant. Integrations of the ring source formulas over the elements are performed numerically, and the boundary conditions are satisfied at the midpoints of the elements to give a set of linear algebraic equations for the values of surface source density. Thus the method of solution is exactly the same as the present method.

10.3.2 *Helmholtz equation.* Several authors have developed general methods for solving boundary-value problems governed by the Helmholtz equation based on the reduction of these problems to integral equations over the boundary surfaces. Banaugh and Goldsmith[52] solve the two-dimensional problem by using a specialization of Green's theorem known as Weber's equation, which expresses the potential as an integral over the boundary of a linear function of the potential and its normal derivative. The resulting integral equation is of the first kind for Dirichlet boundary conditions and of the second kind for Neumann boundary conditions. The integral is evaluated by the trapezoidal rule to give a set of linear algebraic equations for the values of the potential at control points on the profile curve of the body. As programmed, the method requires as input equations for the boundary location, slope, and curvature. The possibility of inputting only the coordinates of a set of points on the boundary is mentioned as one requiring numerical evaluation of the second derivatives.

Chertock[53] considers axisymmetric boundaries on which Neumann boundary conditions are prescribed. The boundary condition is not restricted to the axisymmetric case, but is only required to have a known Fourier series in the circumferential angle with coefficients depending on axial location. Each term of the Fourier series for the boundary condition gives rise to a term in the Fourier series for the solution with the same circumferential variation. (This situation causes the essential simplicity of the cross-flow case as treated by the present method.[2]) A solution is calculated for each separate term of the series for the boundary condition, and the results are linearly combined. Chertok's solution uses a specialization of Green's

theorem known as the Helmholtz integral, which for Neumann boundary conditions lead to an integral equation of the second kind for the pressure along the profile curve of the body. Integrations in the circumferential direction and along the profile curve are performed by quadrature formulas. The result is a set of linear algebraic equations for the values of pressure at control points on the profile curve. The equations are solved by iteration.

Chen and Schweikert[54] solve the three-dimensional Helmholtz equation. A source density distribution on the boundary is used to satisfy Neumann boundary conditions, and the result is an integral equation of the second kind. The boundary surface is approximated by plane triangular surface elements, over each of which the source density is assumed to be constant. The point source formulas are integrated numerically over the individual elements after a preliminary transformation. A set of linear algebraic equations is obtained for the values of the source density on the surface elements. Except for the numerical integration over the elements, this approach is conceptually identical to that of the present method. Chen and Schweikert also consider a more general problem whose solution accounts for the dynamic interaction between the boundary surface and the fluid in which it is immersed. The latter problem requires matrix multiplications of $N \times N$ matrices, where N is the number of surface elements used to approximate the boundary. Such a multiplication requires N^3 additions and multiplications (roughly three times the number required by a direct solution). Probably as a result of this, the maximum number of surface elements that can be used (unless the boundary has certain symmetries) is limited to approximately 100—a rather small number for a three-dimensional surface.

REFERENCES

1. A. M. O. SMITH and J. PIERCE, Exact solution of the Neumann problem. Calculation of plane and axially symmetric flows about or within arbitrary boundaries, Douglas Aircraft Company Report No. 26988 (April 1958). [A brief summary is contained in the *Proceedings of the Third U.S. National Congress of Applied Mechanics*, Brown University, (1958)].
2. J. L. HESS, Calculation of potential flow about bodies of revolution having axes perpendicular to the free-stream direction, *Journal of the Aerospace Sciences*, **29**, 726 (1962).
3. J. L. HESS and A. M. O. SMITH, Calculation of nonlifting potential flow about arbitrary three-dimensional bodies, *Journal of Ship Research*, **8**, No. 2, 22 (September 1964). [A somewhat expanded version is contained in Douglas Aircraft Company Report No. ES 40622 (March, 1962).]
4. J. P. GIESING, Extension of the Douglas Neumann program to problems of lifting infinite cascades, Douglas Aircraft Company Report No. LB 31653 (July 1964).
5. J. L. HESS, Extension of the Douglas-Neumann program for axisymmetric bodies to include calculation of potential, non-uniform cross flow, added mass, and conductor problems, Douglas Aircraft Company Report No. LB 31765 (September 1964).
6. S. FAULKNER, J. L. HESS and J. P. GIEISING, Comparison of experimental pressure distributions with those calculated by the Douglas Neumann program, Douglas Aircraft Company Report No. LB 31831 (December 1964).

7. J. P. GIESING and A. M. O. SMITH, Potential flow about two-dimensional hydrofoils, Douglas Aircraft Company Engineering Paper No. 3541 (1965). (To be published in Journal of Fluid Mechanics).

8. J. P. GIESING, Potential Flow about two-dimensional airfoils, Douglas Aircraft Company Report No. LB 31946 (1966).

9. H. LAMB, *Hydrodynamics*, Cambridge University Press, London (1932).

10. P. M. MORSE and H. FESHBACH, *Methods of Theoretical Physics*, McGraw-Hill, New York (1953).

11. P. MOON and D. E. SPENCER, *Field Theory for Engineers*, Van Nostrand, Princeton (1961).

12. B. THWAITES (Ed.), *Incompressible Aerodynamics, Fluid Motion Memoirs*, Oxford University Press (1960).

13. M. VAN DYKE, *Perturbation Methods in Fluid Dynamics*, Academic Press, New York (1964).

14. T. VON KÁRMÁN, Calculation of pressure distribution on airship hulls, NACA TM 574 (1930).

15. O. D. KELLOGG, *Foundations of Potential Theory*, Frederick Ungar Publishing Co., New York (1929). Chapter 11. [Also available from Dover Publications, Inc., New York.]

16. R. H. LEVY, Preliminary report on a proposed method of calculating pressure distributions over arbitrary bodies, Canadair Limited Report No. RAA-00-113 (October, 1959).

17. W. R. SEARS (Ed.), *General Theory of High Speed Aerodynamics*, Vol. VI of High Speed Aerodynamics and Jet Propulsion, Princeton University Press (1954), p. 79, p. 501.

18. I. LOTZ, Calculation of potential flow past airship bodies in yaw, NACA TM 675 (July 1932).

19. J. A. STRATTON, *Electromagnetic Theory*, McGraw-Hill, New York (1941), Chapter 3.

20. S. FLÜGGE (Ed.), *Encyclopedia of Physics*, Vol. IX, Fluid Dynamics, III. Section on surface waves, by J. V. Wehausen and E. V. Laitone, Springer-Verlag, Berlin (1960).

21. J. J. STOKER, *Water Waves*, Interscience, New York (1957).

22. N. E. KOCHIN, I. A. KIBEL and N. V. ROZE, *Theoretical Hydromechanics*, Interscience, New York (1964).

23. ANON., Tables of the exponential integral for complex arguments, Nat. Bur. of Stds., App. Math. Series 51, U.S. Govt. Printing Office (1958).

24. E. W. PURCELL, The vector method of solving simultaneous linear equations, *Journal of Math. Phys.*, 23, 180 (1953).

25. R. S. VARGA, *Matrix Iterative Analysis*, Prentice-Hall, Englewood Cliffs, New Jersey (1962).

26. G. E. FORSYTHE and W. R. WASOW, *Finite-Difference Methods for Partial Differential Equations*, John Wiley, New York (1960).

27. F. VANDREY, On the calculation of the transverse potential flow past a body of revolution with the aid of the method of Mrs. Flügge-Lotz, Astia AD-40 089.

28. F. VANDREY, A method for calculating the pressure distribution of a body of revolution moving in a circular path through a perfect incompressible fluid, Aeronautical Research Council R and M, No. 3139 (1960). See also: A direct iteration method for the calculation of the velocity distribution of bodies of revolution and symmetrical profiles. Aeronautical Research Council R and M No. 3374 (1964).

29. W. PRAGER, Die Druckverteilung an Körpern in ebener Potentialströmung, *Physik. Zeitschr.* XXIX, 865 (1928).

30. E. MARTENSEN, Berechnung der Druckverteilung an Gitterprofilen in ebener Potentialströmung mit einer Fredholmschen Integralgleichung, *Arch. Rat. Mech. and Analysis*, 3 No. 3 (1959), p. 235.

31. K. W. JACOB, Some programs for incompressible aerodynamic flow calculations, Calif. Inst. of Tech. Computing Center Tech. Rept. No. 122 (February 1964).

32. L. LANDWEBER, The axially symmetric potential flow about elongated bodies of revolution, David Taylor Model Basin Report No. 761 (August 1951).

33. L. LANDWEBER, Potential flow about bodies of revolution and symmetric two-dimensional forms, State University of Iowa Institute of Hydraulic Research (December 1959).
34. H. R. CHAPLIN, A method for numerical calculation of slipstream contraction of a shrouded impulse disk in the static case with application to other axisymmetric potential flow problems, David Taylor Model Basin Report No. 1857 (June 1964).
35. T. THEODORSEN, Theory of wing sections of arbitrary shape, NACA Report No. 411 (1932).
36. T. A. HARRIS and J. G. LOWRY, Pressure distribution over an NACA 23012 airfoil with a fixed slot and a slotted flap, NACA Report No. 732 (1942).
37. J. H. PRESTON and N. E. SWEETING, The experimental determination of the boundary layer wake characteristics of a simple Joukowski airfoil with particular reference to the trailing edge region, Aeronautical Research Council R and M, No. 1998 (March 1943).
38. B. R. PARKIN, B. PERRY and T. Y. WU, Pressure distribution on a hydrofoil running near the water surface, *Journal of Applied Physics*, 27 No. 3, 232 (March 1956).
39. J. L. HERRIG, J. C. EMERY and J. R. ERWIN, Systematic two-dimensional cascade tests of NACA 65-series compressor blades at low speeds, NACA TN 3916 (1957).
40. C. W. MATTHEWS, A comparison of the experimental subsonic pressure distributions about several bodies of revolution with pressure distributions computed by means of linearized theory, NACA RM L9F28 (September 1949).
41. A. D. YOUNG and P. R. OWEN, Simplified theory for streamline bodies of revolution and its application to the development of high-speed low-drag shapes, Aeronautical Research Council R and M, No. 2071 (July 1943).
42. M. S. CAHN, Shrouded propeller design analysis, Douglas Aircraft Company Engineering Paper No. 1394 (April 1962).
43. R. A. TAYLOR, Pressure distributions at transonic speeds for bumpy and indented midsections of a parabolic-arc body, NASA Memo 1-22-59A.
44. W. E. JOHNSON, Experimental investigation and correlation with theory of the surface pressure distribution on several sharp and blunted cones for incompressible flow, Master's Thesis, Department of Aeronautics and Astronautics, University of Washington (1963).
45. M. R. NICHOLS and A. L. KEITH, JR., Investigation of a systematic group of NACA 1-series cowlings with and without spinners, NACA Report 950(1949).
46. J. M. SWIHART and C. F. WHITCOMB, Pressure distributions on three bodies of revolution to determine the effect of Reynolds number up to and including the transonic speed range, NACA RM L53HO4 (October 1953).
47. D. M. NELSON, Hydrodynamic coefficient calculation using Douglas potential flow computer program, NAVWEPS Report No. 8799, NOTS TP 3905 (October 1965).
48. D. H. PECKHAM, Low-speed wind tunnel tests on a series of uncambered slender pointed wings with sharp edges, Aeronautical Research Council R and M, No. 3186 (1961).
49. R. D. BOURKE, A theoretical and experimental study of a superconducting magnetically-supported spinning body, Stanford University, Department of Aeronautics and Astronautics, SUDAER No. 189 (May 1964).
50. M. A. JASWON and A. R. PONTER, An integral equation solution of the torsion problem, *Proceedings of the Royal Society*, Series A, 273, No. 1353, 237 (May 1963).
51. D. R. CRUISE, A numerical method for the determination of an electric field about a complicated boundary, *Journal of Applied Physics*, 34, No. 12, 3477 (December 1963).
52. R. P. BANAUGH and W. GOLDSMITH, Diffraction of steady acoustic waves by surfaces of arbitrary shape, *Journal of the Acoustical Society of America*, 35, No. 10, 1590 (October 1963).
53. G. CHERTOCK, Sound radiation from vibrating surfaces, *Journal of the Acoustical Society of America*, 36, No. 7, 1305 (July 1964).
54. L. H. CHEN and D. G. SCHWEIKERT, Sound radiation from an arbitrary body, *Journal of the Acoustical Society of America*, 35, No. 10, 1626 (October 1963).